2021

A Comprehensive Study to Delineate the Role of an Extracellular Vesicle-Associated MicroRNA-29a in Chronic Methamphetamine Use Disorder

Subhash Chand

Austin Gowen

Mason Savine

Dalia Moore

Alexander Clark

See next page for additional authors

Authors

Subhash Chand, Austin Gowen, Mason Savine, Dalia Moore, Alexander Clark, Wendy Huynh, Niming Wu, Katherine Odegaard, Lucas Weyrich, Rick A. Bevins, Howard S. Fox, Gurudutt Pendyala, and Sowmya V. Yelamanchili

Received: 26 February 2021 | Revised: 27 October 2021 | Accepted: 25 November 2021

DOI: 10.1002/jev2.12177

RESEARCH ARTICLE

A comprehensive study to delineate the role of an extracellular vesicle-associated microRNA-29a in chronic methamphetamine use disorder

Subhash Chand[1] | **Austin Gowen**[1] | **Mason Savine**[1] | **Dalia Moore**[1] | **Alexander Clark**[1] | **Wendy Huynh**[2] | **Niming Wu**[3] | **Katherine Odegaard**[1] | **Lucas Weyrich**[4] | **Rick A. Bevins**[2] | **Howard S. Fox**[5] | **Gurudutt Pendyala**[1] | **Sowmya V. Yelamanchili**[1]

[1] Department of Anesthesiology, University of Nebraska Medical Center (UNMC), Omaha, Nebraska, USA

[2] Department of Psychology, University of Nebraska–Lincoln (UNL), Lincoln, Nebraska, USA

[3] Department of Pharmacology and Experimental Neuroscience, University of Nebraska Medical Center (UNMC), Omaha, Nebraska, USA

[4] Midland University, Omaha, Nebraska, USA

[5] Department of Neurological Sciences, University of Nebraska Medical Center (UNMC), Omaha, Nebraska, USA

Correspondence
Sowmya V. Yelamanchili, Department of Anesthesiology, University of Nebraska Medical Center (UNMC), Omaha, Nebraska, USA.
Email: syelamanchili@unmc.edu

Subhash Chand and Austin Gowen contributed equally to this work.

Funding information
NIDA, Grant/Award Numbers: R01DA042379, R21DA046855, R01DA046852

Abstract

Extracellular vesicles (EVs), which express a repertoire of cargo molecules (cf. proteins, microRNA, lipids, etc.), have been garnering a prominent role in the modulation of several cellular processes. Here, using both non-human primate and rodent model systems, we provide evidence that brain-derived EV (BDE) miRNA, miR-29a-3p (mir-29a), is significantly increased during chronic methamphetamine (MA) exposure. Further, miR-29a levels show significant increase both with drug-seeking and reinstatement in a rat MA self-administration model. We also show that EV-associated miR-29a is enriched in EV pool comprising of small EVs and exomeres and further plays a critical role in MA-induced inflammation and synaptodendritic damage. Furthermore, treatment with the anti-inflammatory drug ibudilast (AV411), which is known to reduce MA relapse, decreased the expression of miR-29a and subsequently attenuated inflammation and rescued synaptodendritic injury. Finally, using plasma from MUD subjects, we provide translational evidence that EV-miR29a could potentially serve as a biomarker to detect neuronal damage in humans diagnosed with MA use disorder (MUD). In summary, our work suggests that EV-associated miR-29a-3p plays a crucial role in MUD and might be used as a potential blood-based biomarker for detecting chronic inflammation and synaptic damage.

1 | INTRODUCTION

The abuse of methamphetamine (MA), a potent psychostimulant, poses a significant health and economic threat globally. Acute and chronic MA use is known to cause serious health problems leading to intense behavioural changes including paranoia, insomnia, agitation, hallucinations and delusions (Grant et al., 2012; Sacks et al., 2005). Neuroimaging studies have revealed that MA exposure can indeed cause neurodegenerative changes in the brains of human MA misusers (Aron & Paulus, 2007). These abnormalities include a persistent decrease in the levels of dopamine and serotonin transporters in the midbrain, subcortical and cortical regions of MA-dependent individuals (Mccann et al., 1998, Sekine et al., 2003; Volkow, Chang, Wang, Fowler, Ding, et al., 2001; Volkow, Chang, Wang, Fowler, Franceschi, et al., 2001).

Notably, a recent positron emission tomography (PET) study found prominent microglial activation in the midbrain, subcortical and cortical regions of MA misusers (Sekine et al., 2008). The levels of microglial activation correlated inversely with duration of MA abstinence, highlighting that glial cell responses persist during MA exposure (Sekine et al., 2008). Indeed, several studies have shown indirect and direct effects of MA on inflammation. For example, it has been postulated that MA exposure indirectly influences inflammation via the release of excessive glutamate (Glu) (Nash & Yamamoto, 1992; Stephans & Yamamoto, 1994). It has been previously shown that stimulation of Glu receptors increase microglial activation and blocking the receptors with antagonists reduced significant microglial activation indicating that Glu receptor stimulation can induce neuroinflammation (Thomas & Kuhn, 2005). Therefore, MA induced Glu release is thought to increase microglial activation, consequently leading to release of pro-inflammatory cytokines such as tumour necrosis factor-α (TNF-α), interleukin-1β (IL-1β), interleukin-6 (IL-6) and interleukin-8 (IL-8), contributing to neurotoxicity (Yamamoto et al., 2010). Further, direct MA exposure has also been shown to activate microglia (Fantegrossi et al., 2008; Lavoie et al., 2004; Sriram et al., 2006) and astrocytes (Miyatake et al., 2005; Shah et al., 2012) to release inflammatory cytokines in the brain. Chronic MA exposure can lead to sustained neuroinflammation that can lead to persistent MA-induced neuronal injury and neuropsychiatric impairments (Vandenbark et al., 2019). The underlying mechanism/s of chronic MA-induced inflammation and its effect on long-term damage to the brain is still unclear. Moreover, the specific role of glial cells, including their communication with neurons, in affecting overall brain function has not been well understood. One set of prominent and emerging players, extracellular vesicles (EVs), which include exosomes, microvesicles and apoptotic bodies, have been garnering increasing interest for their role in several neurodegenerative disorders (You & Ikezu, 2019). EVs are released by many cell types into the extracellular environment and are commonly found in biological fluids such as blood (Caby et al., 2005), urine (Pisitkun et al., 2004), saliva (Palanisamy et al., 2010), breast milk (Admyre et al., 2007), bronchoalveolar lavage fluid (Admyre et al., 2003) and semen (Frenette et al., 2010; Llorente et al., 2004; Madison et al., 2014; Renneberg et al., 2001; Renneberg et al., 1997; Ronquist et al., 2012; Sahlén et al., 2002; Skibinski et al., 1994; Stridsberg et al., 1996; Sullivan et al., 2005) and express various cargo molecules comprised of proteins, RNA, small RNAs such as microRNAs (miRNA), mRNA and lipids. Recent studies have shown that EVs play a major role in microbial pathogenesis and immune responses via intercellular communications, including activation of antiviral pathways or transfer of antiviral factors between different cells (Li et al., 2013; Madison et al., 2014; Madison et al., 2015; Näslund et al., 2014; Vojtech et al., 2014). In the brain, astrocytes (Taylor et al., 2007), microglia (Potolicchio et al., 2005) and neurons (Faure et al., 2006) have been shown to release EVs. In particular, EVs have been implicated to serve as carriers of toxic molecules to and from cells, thus making them attractive candidates to study the progression of disease pathogenesis (Gupta & Pulliam, 2014). While the role of EVs in cancer pathogenesis (Guo & Guo, 2015, Takahashi et al., 2017), neurodegenerative diseases and viral infections (Ellwanger et al., 2017; Raab-Traub & Dittmer, 2017) has been discussed extensively, the role of EVs in drug addiction is not yet clearly defined. Recently, our laboratory reported miRNA cargo of brain derived-EVs (BDE) produced in the brains of simian immunodeficiency virus (SIV)-infected macaques with central nervous system (CNS) disease (Yelamanchili et al., 2015), in mouse models of traumatic brain injury (Harrison et al., 2016), and in substance abuse related works (Hu et al., 2012; Koul et al., 2020; Shahjin et al., 2019). Importantly, we and others have shown that these EV-associated miRNAs can signal via binding to Toll-like receptors (TLRs) (Lehmann et al., 2012; Winkler et al., 2014; Yelamanchili et al., 2015). TLRs in the CNS can be activated by binding to endogenous ligands released by injured or stressed cells (Fang et al., 2014; Tsai et al., 2014). In the CNS, TLR7 is highly expressed in microglia but not commonly expressed in other cells including neurons, endothelial cells, astrocytes and oligodendrocytes (Michaelis et al., 2019). MiRNAs, which are single stranded RNA molecules, mimic viral RNA and therefore can bind directly to TLRs leading to activation of NF-$\kappa\beta$ signalling and secretion of pro-inflammatory cytokines (Fabbri et al., 2012). Therefore, it has been postulated that EV carrying miRNAs are signalling molecules with important functions in innate immunity and inflammation (Fabbri et al., 2013). Neuroinflammation, a key hallmark of several neurological disorders, including MA use disorder (Kim et al., 2020; Krasnova et al., 2016), is largely characterised by activation of microglia, pericytes and astrocytes as well as T-lymphocytes, macrophages and dendritic cells crossing the brain-blood barrier in the inflamed brain. Although, low level inflammation is considered to be beneficial to the brain, chronic inflammation causes neuronal injury (Shastri et al., 2013).

In the present study, we focus on the role of BDE associated miRNA, miR-29a-3p (miR-29a) whose expression was increased with chronic MA exposure. Using both in vivo and in vitro model systems, we provide novel evidence that miR-29a is localised to sEVs and exomeres. Further, we show a critical role in MA-induced inflammation and subsequent synaptodendritic damage. Treatment with the anti-inflammatory drug ibudilast, resulted in the reversal of this cascade.

2 | RESULTS

2.1 | Chronic MA exposure influences EV numbers, size and subtypes in brain

To study the effects of chronic MA exposure on EVs, we utilised two models; a well-established rhesus macaque model that was developed to mimic chronic MUD in people who go for periods with relatively high MA use followed by abstinence ('crashing')

for a few days (Madden et al., 2005; Marcondes et al., 2010) (see Figure S1 and Table S1 for animal data) and a self-administration rat model. Macaques that have chronic MA administration were necropsied at the end of 28 weeks. Brains were harvested and snap frozen for BDE isolation. BDE from both saline control and chronic MA-exposed brains were subjected to transmission electron microscopy (TEM) and nanoparticle tracking analysis (NTA). While BDE from saline controls displayed a size range between ~100 and 200 nm, the MA-treated animals revealed a wider range; we found a mix of heterogenous sizes from <50 nm to >500 nm (Figure 1a, see Figure S2A for wide field images). NTA also showed similar distribution in sizes (Figure 1b) and further revealed significantly higher concentrations of BDE in the MA group (Figure 1c). Based on the increase in number of BDE, we next assessed whether EV biogenesis was altered. EV biogenesis depends on several genes, including the endosomal sorting complexes required for transport (ESCRT)-dependent (Colombo et al., 2013; Juan & Fürthauer, 2018) and -independent pathways such as the ceramide synthesis pathway (Trajkovic et al., 2008). RNA isolated from macaque frontal grey tissue was subjected to qRT-PCR using an array-based format. Several genes involved in the ESCRT-dependent and -independent pathways were upregulated. Specifically, genes belonging to the families ESCRT-0: *HRS, STAM2*; ESCRT-I: *VPS28, TSG101*; ESCRT-III: *CHMP2B, CHMP4B, CHMP4C* and *CHMP5* and Disassembly complex: *ALIX, VPS4A* were significantly elevated in the MA group. We also found a significant upregulation of genes in ceramide synthesis pathway, such as *CERS2*, *CERS3* and *CERS6*, as well as the proinflammatory cytokine TNFα in the MA group (Figure 1d). These data indicate that the ESCRT and ceramide pathways were affected by chronic MA exposure.

Further, we assessed BDE isolated from rats that underwent a MA self-administration regimen. This model mimics closely humans who are diagnosed with MA use disorder. Rats were trained to self-administer MA over 25 days, after which these rats underwent extinction for 14 days (mimicking rehabilitation). Similar to what we saw with the monkey BDE, TEM (Figure 1e, Figure S2B and NTA (Figure 1f) analysis revealed heterogenous BDE sizes as well as increase in BDE concentration (Figure 1g). Since both the models showed a large heterogeneity in the EV populations, it is imperative to discern the kind of EV subtypes that are specifically released by chronic MA exposure. Recently, several groups have reported various vesicular and non-vesicular markers to identify specific EV subtypes (Jeppesen et al., 2019; Kowal et al., 2016; Zhang et al., 2019). Here, we used markers to distinguish small EVs (sEVs), large EVs (lEVs), nanovesicles and non-EVs. Specifically, Alix, TSG101, HSP70, CD63 and CD81 were used to detect sEVs; Annexin V (Anx V) for lEVs (microvesicles/apoptotic vesicles/apoptotic bodies); ApoE markers for detecting non-membranous vesicular markers such as lipoproteins and HSP90 for nanovesicles (exomeres). We also assessed the presence of miRNA biogenesis machinery such as Argonaute proteins (Ago1 and Ago2) and EV negative marker, GM130, in the BDE preparations. WB results indicate a significant increase in expression of sEV markers Alix, TSG101, HSP70 and CD63; lEV marker Anx V and exomere marker HSP90 in the MA groups when compared to the saline (SA) controls. Only CD 81 showed a significant decrease in MA group and no change in expression was observed for Flot 1. Other non-EV components such as ApoE, Ago1 and Ago2 were undetectable, indicating the BDE preparations were devoid of lipoproteins or miRNA biogenesis machinery, respectively (Figure 2). These data collectively not only indicates that chronic MA exposure influences size, concentration but also specific EV subtypes in the brain.

2.2 | Chronic MA exposure enhances BDE biogenesis and upregulates the expression of TLR7, activating miR-29a cargo

EV associated RNA cargo has gained significant interest in the field since their initial discovery (Skog et al., 2008; Valadi et al., 2007). We and others have found that miRNA cargo that contain specific GU-rich sequences can elicit inflammation as well as neuronal injury through binding to toll-like receptor (TLR) 7/8, similar to single stranded viral RNA molecules (Fabbri et al., 2012; Lehmann et al., 2012; Liu et al., 2013; Park et al., 2014; Yelamanchili et al., 2015). Chronic MA exposure causes neuroinflammation thereby leading to deleterious outcomes. We investigated the role of miRNA cargo in perpetuating inflammation and neuronal injury. Small RNA sequencing (seq) was performed on BDEs isolated from macaque brain (frontal grey). Results revealed six miRNAs above the average set of reads >635 that closely reached significance (Table S2). Intriguingly, all the miRNAs except miR-197 have GU motifs in the sequences. Out of the six miRNAs, hsa-miR-29a-3p_R1 (miR-29a) has the canonical GGUU sequence and has been shown previously to bind to TLR7 and elicit inflammation in macrophages (Fabbri et al., 2013). Similar to the previous findings, synthetic miR-29a is the only miRNA that strongly activated proinflammatory cytokine TNFα in two cell lines: TLR7-expressing RAW 264.7 monocyte-macrophages and immortalised wild type microglia (WT-MG) (Table S3). No TNFα secretion was seen with miR-29a treatments in TLR7$^{-/-}$ microglia (TLR$^{-/-}$-MG), confirming that the secretion was induced by binding. Although, miR-143-3p and miR-24-3p elicited TNFα response in RAW 264.7 macrophages, they failed to elicit response in WT-MG.

Next, post-validation of the RNA sequencing data was performed by targeted Taqman qRT-PCR assay. Due to the absence of a standard internal control for normalising miRNA in EVs, a standard curve was ran using synthetic miRNA oligonucleotides and miRNA copy numbers were estimated by qRT-PCR. Results indicate a significant increase in miR-29a copy number (Figure 3a, right panel). The other five miRNAs could not be post-validated (Figure S3). These data together suggest that BDE-miR29a is

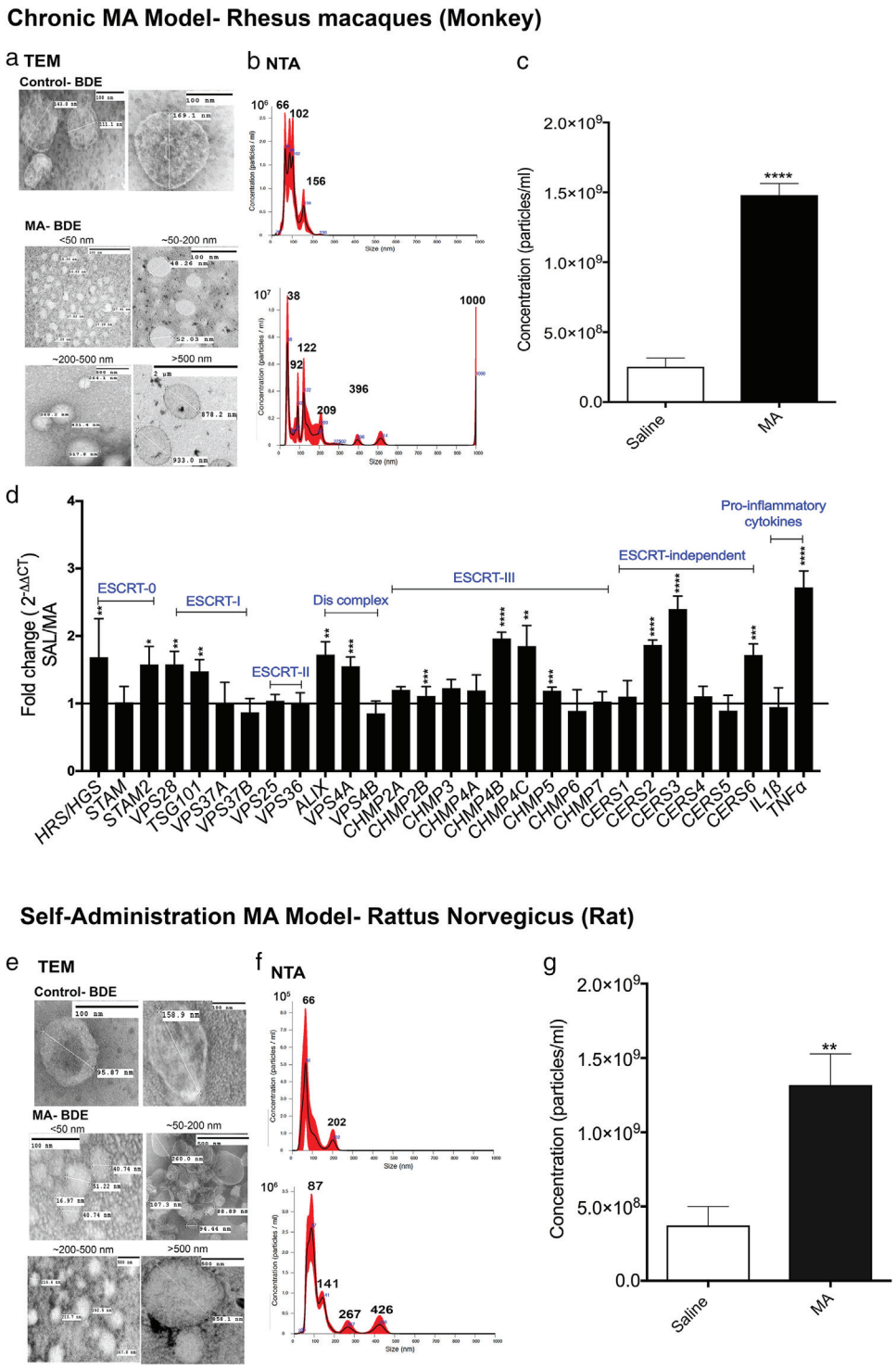

FIGURE 1 Chronic MA administration increases the number, size, and biogenesis of BDE. BDE were isolated from frontal grey and cortical tissue harvested from saline controls and MA-administered macaques and rats, respectively. (a, e) TEM reveals ~100–200 nm-sized vesicles in control-BDE samples, a significant range in vesicles ranging from small (<50 nm), medium (~50–200 nm), large (~200–500 nm) and very large (>500 nm) vesicles were seen in MA-BDE. (b and f) Similarly, NTA shows different size ranges in MA-BDE when compared to control-BDE and (c and g) reveals significant differences in BDE number between control and MA groups. Data represented as Mean ± SEM, $n = 5$ animals per group; $^{****}p < 0.0001$, Welch's t-test. (d) Custom qRT-PCR panel for EV biogenesis genes revealed several genes to be significantly upregulated in the frontal grey brain tissue such as *HRS*, *STAM2, VPS28, TSG101, ALIX, VPS4A, CHMP2B, CHMP4B, CHMP4C, CHMP5, CERS2, CERS3, CERS6* and proinflammatory cytokine *TNFα*. Data represented as Mean ± SEM, $n = 5$ animals per group, $^{****}p < 0.0001$, $^{***}p < 0.001$, $^{**}p < 0.005$, $^{*}p < 0.05$ (*Adjusted p value*), Multiple t-test followed by Holm-Sidak correction

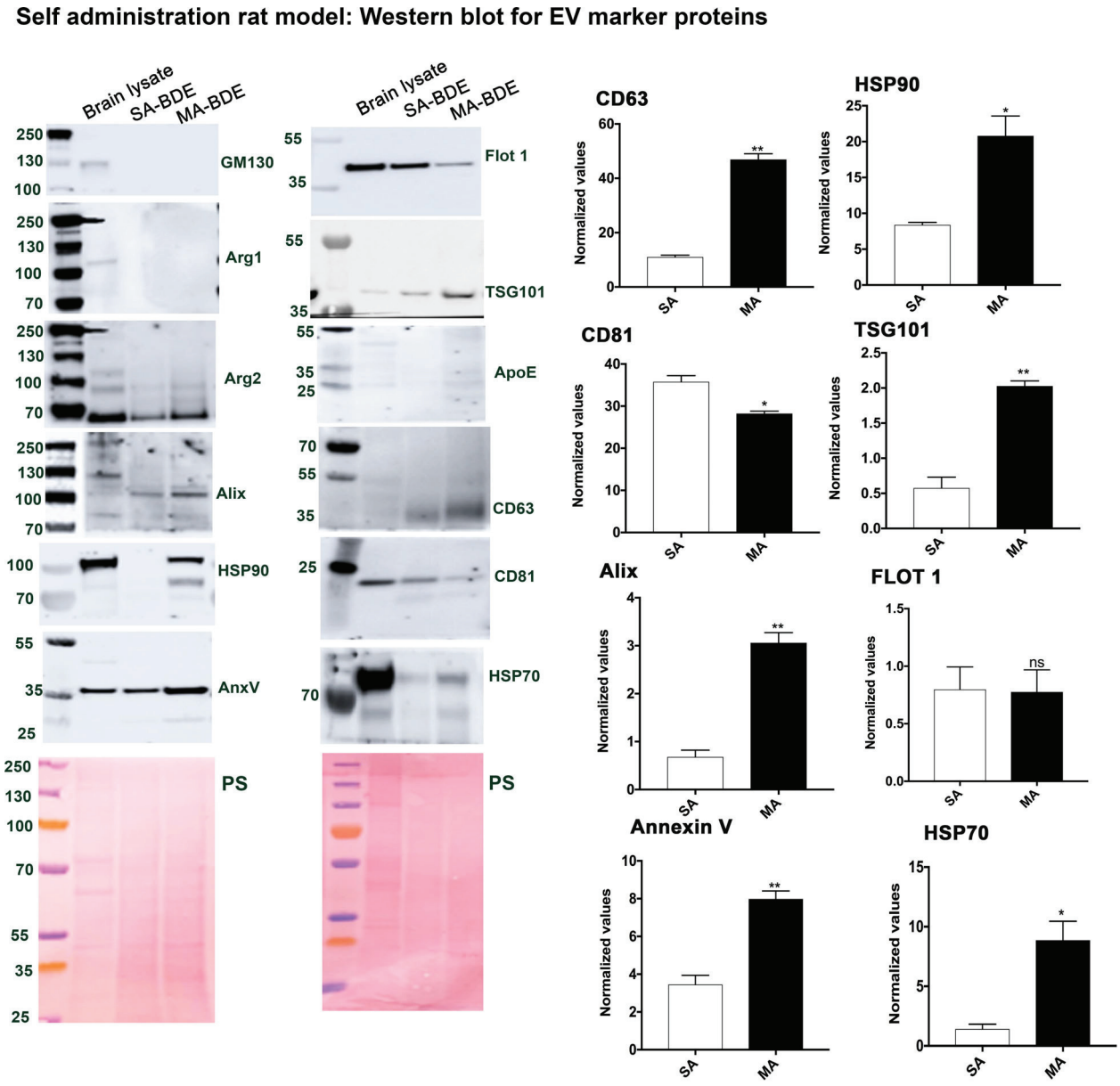

FIGURE 2 Comprehensive characterisation of EV markers on BDE. BDE were isolated from rat cortical tissues harvested from saline controls (SA-BDE) and MA treatments (MA-BDE). Western blotting was performed for Alix, TSG101, HSP70, CD63 and CD81 to detect sEVs; Annexin V (Anx V) for detecting lEVs (large EVs); ApoE for detecting lipoproteins and HSP90 for exomeres. MiRNA biogenesis machinery proteins such as Argonaute protein 1 (Ago1) and Argonaute protein 2 (Ago2) and EV negative marker, GM130, were also assessed in the BDE preparations. Ponceau stained (PS) bands were used for normalisation. Results indicate a significant increase in expression of sEV markers Alix, TSG101, HSP70 and CD63; lEV marker Anx V and exomere marker HSP90 in the MA groups when compared to the saline (SA) controls. Only CD 81 showed a significant decrease in MA group and no change in expression was observed for Flot 1. Other non-EV components such as ApoE, Ago1 and Ago2 were undetectable, indicating the BDE preparations was devoid of lipoproteins or miRNA biogenesis machinery, respectively. Negative marker GM130 was not detected. Data represented as Mean ± SEM, $n = 3$ animals per group, $^{**}p < 0.005$ and $^{*}p < 0.05$, Welch's unpaired t-test was performed

strongly associated with chronic MA exposure. Finally, to elucidate which specific cell type in the brain expressed miR-29a, in situ hybridisation (ISH) was performed on the frontal brain sections (macaques). Neurons (MAP2) and microglia (IBA1) expressed significantly higher miR-29a in the MA group (Figure 3b (i) and Figure 3c, left panel). Interestingly, we see that in MA brains, miR-29a-expressing microglia are in very close proximity to neighbouring neurons and the processes are in contact with neuronal cell bodies (Figure 3b (i), Zoom). An overall increase in IBA1-stained microglia, indicating increased activation of microglia in MA-exposed brains (Figure 3c, right panel; see also Figure S4). Alternatively, astrocytes (GFAP, red) showed minimal expression of miR-29a (Figure 3b (ii)).

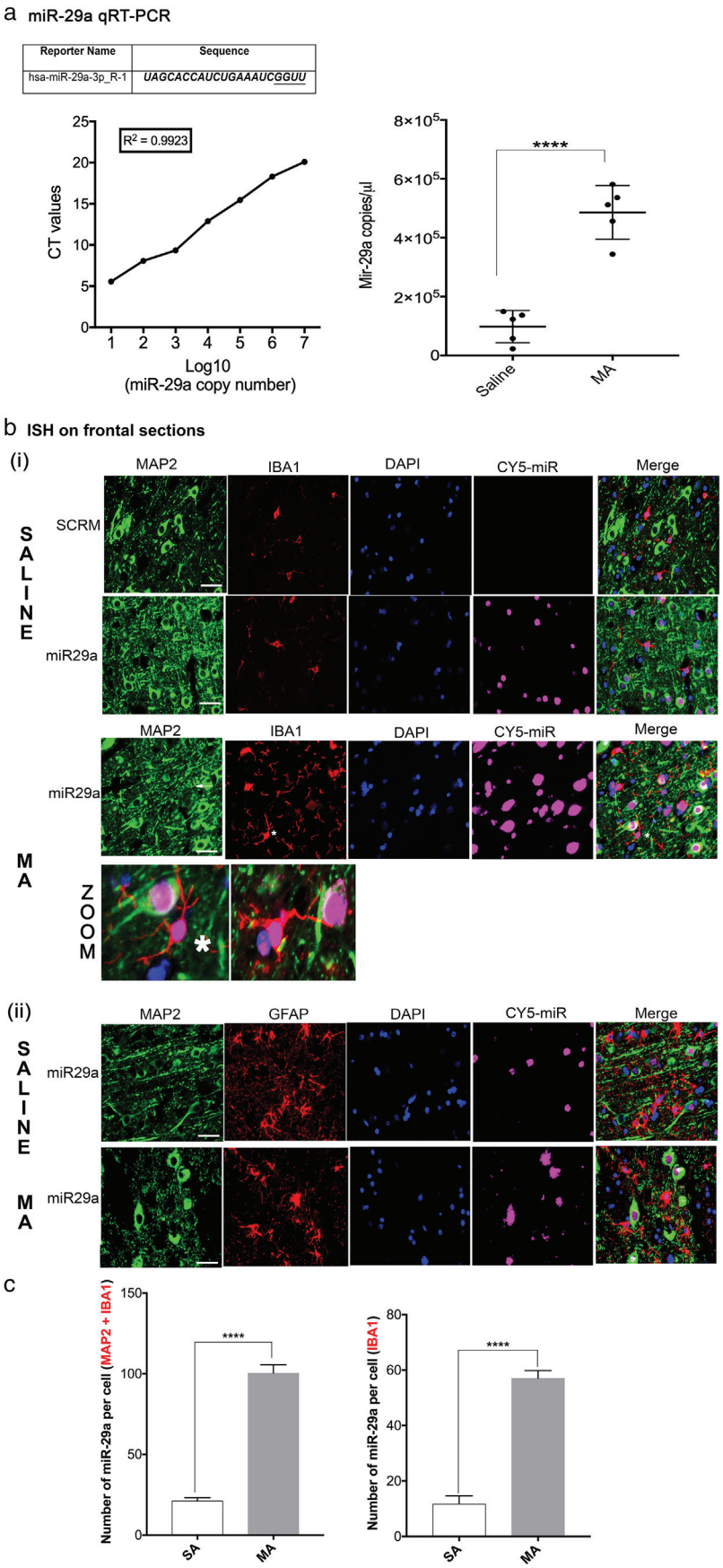

FIGURE 3 Chronic MA treatment increases the biogenesis and the expression of miR-29a-3p in BDE. (a) Post-validation by qRT-PCR analysis. Left panel: A standard curve for miR-29a-3p primer; right panel: qRT-PCR analysis reveals significant increase in miR-29a expression in MA group when compared to the saline controls. Data represented as Mean ± SEM, n = 5 animals per group, $^{****}p < 0.0001$, Two-tailed unpaired t-test. (b) (i) Top panels: Combined FISH and IF of frontal brain sections for Cy5-scrambled (SCRM), Cy5-miR-29, microglial marker IBA1 (red) and neuronal marker MAP2 (green). Increased expression of microglia (IBA1, red) and miR-29a (purple) is seen with chronic MA treatments when compared to saline treatments in rhesus macaques. ISH with SCRM probe do not show any non-specific reactivity. Zoom panels reveal close proximity of microglial cell processes (IBA1, red) with miR-29a (purple) expressed neurons (green). (ii) Bottom panels: No colocalisation was observed with GFAP (red), an astrocyte marker. DAPI (blue) was used to label nuclei. Scale bars = 20 μm for all panels except 5 μm for MA-zoom panels. (c) Quantifications for miR-29a number per cell revealed a significant increase in miR-29a not only in both neurons (MAP2) and microglia (IBA1) but also in only microglia (IBA1). A total of 100 cells obtained from 10 images from each animal ($n = 5$ per SA/MA) were used for analysis. Data represented as Mean ± SEM, $n = 100$, $^{****}p < 0.0001$, Welch's t-test

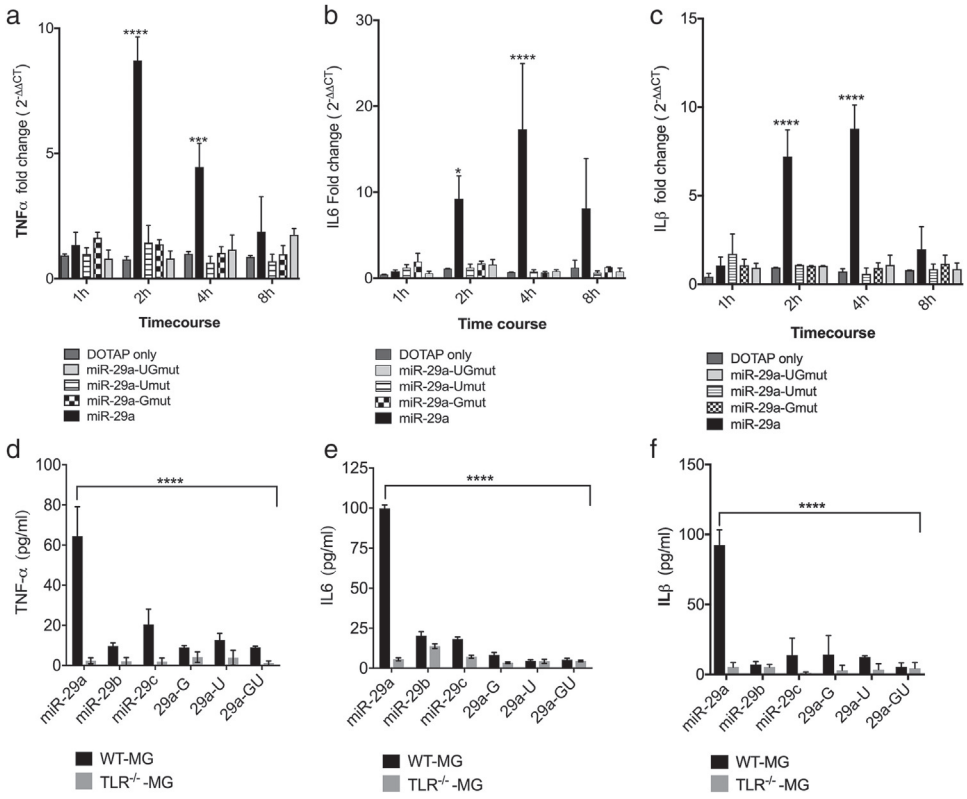

FIGURE 4 EV-miR29a enhances MA-induced microglial release of proinflammatory cytokines. (a–c) Immortalised wildtype microglia (WT-MG) were treated with synthetic DOTAP formulations generated for full-length miR-29a (miR-29a) along with TLR7 binding mutants: "G" (29a-G), "U" (29a-U) and "GU" (29a-GU). A time-dependent expression of (a) *TNFα* (b) *IL6* and (c) *IL1β* genes was measured by qRT-PCR. Results indicate a significant expression of *TNFα, IL6* and *IL1β* in 2 and 4 h, reaching a peak at 2 h for *TNFα* ; 4 h for *IL6 and IL1β*. No significant increase was observed when using either vehicle (DOTAP) control or miR-29a mutants. Data represented as Mean ± SEM, $n = 3$; ****$p < 0.0001$, ***$p < 0.001$. Two-way ANOVA with Dunnett's multiple comparison was performed. (d–f) ELISA assay conducted on media supernatants from immortalised wild-type microglia (WT-MG) and TLR7$^{-/-}$ microglia (TLR$^{-/-}$-MG)) treated with synthetic DOTAP formulations generated for full-length miR-29a (miR-29a) along with TLR7 binding mutants; "G" (29a-G), "U" (29a-U) and "GU" (29a-GU) and other miR-29 family members, miR-29b and miR-29c. Results indicate a significant increase in (d) TNFα (e) IL6 and (f) IL1β production in media supernatants from miR-29a-treated WT-MG when compared to non-detectable levels seen in media from either miR-29a mutants. Data represented as Mean ± SEM, $n = 4$; ****$p < 0.0001$, Two-way ANOVA with Sidak's multiple comparison was performed

2.3 | Artificial encapsulation of miR29a enhances microglial release of pro-inflammatory cytokines and induces synaptodendritic damage

To further investigate the role of EV-associated miR29a (EV-miR29a) on TLR7 signalling, inflammation and subsequent synaptic damage, we utilised immortalised microglial cells from WT and TLR7$^{-/-}$ mice. Wildtype miR-29a, along with mutants for 'G' (29a-G), 'U' (29a-U) and 'GU' (29a-GU) nucleotides to generate TLR7 signalling defective miR-29a, were synthesised. In parallel, miR-29b and miR-29c also belonging to miR-29 family were synthesised to corroborate the response is specific to miR-29a. The synthetic miRNAs were formulated with DOTAP and mouse immortalised WT microglial cultures (WT-MG) or TLR7$^{-/-}$ microglia (TLR$^{-/-}$-MG) were treated. Cells were collected at different timepoints (1, 2, 4 and 8 h) and media supernatants were taken after 24 h to check for the expression of proinflammatory cytokines (*TNFα, IL6* and *IL1β)* or their release into the media by ELISA. qRT-PCR results indicated a significant increase in expression of *TNFα, IL6* and *IL1β* after 2 and 4h, reaching peak expression at 2 h post-transfection for *TNFα* and at 4 h (Figure 4a) for *IL6* and *IL1β* (Figure 4b and c). However, no response was seen with either miR-29a mutant or when treated with DOTAP control. Media supernatants were collected after 24 h to measure the released cytokines. ELISA results indicated a significant increase in TNFα, IL6 and IL1β production in media supernatants from WT-MG when compared to non-detectable levels found in media from either miR-29a mutants or in media from TLR7$^{-/-}$ microglia (TLR$^{-/-}$-MG) (Figure 4d, e and f). These data collectively indicate that EV-miR29a can bind to the TLR7 receptor and activate the transcription of proinflammatory genes in microglia through activation of the TLR7 receptor.

Next, we examined the effects of EV-miR29a on synaptic integrity using primary neuronal cultures isolated from mouse cortex. WT and TLR7$^{-/-}$ mouse cortical neurons were cultured from P0 pups. At days in vitro (DIV) 13, neuronal cultures were treated with synthetic miRNA:DOTAP formulations for 24 h as described previously. For measuring the effects on synapses, neurons were fixed and stained with pre-synaptic marker VGLUT1, post-synaptic marker PSD95, and neuronal marker MAP2.

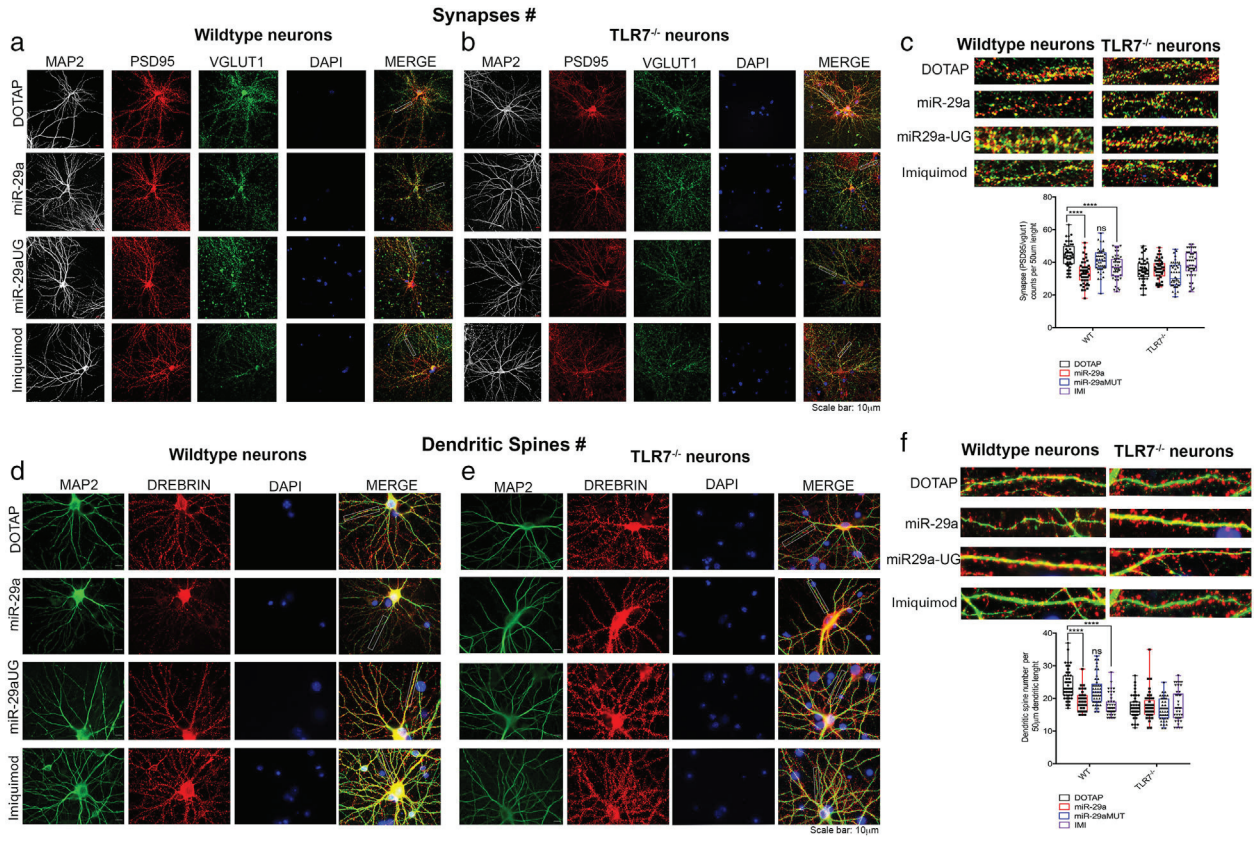

FIGURE 5 EV-miR29a causes synaptodendritic injury in primary cortical neurons. Wild-type (WT) and TLR7 knock out (TLR7$^{-/-}$) mouse cortical neurons were incubated with 1 μg of synthetic miRNAs; miR-29a, miR-29a containing a mutation in TLR7 binding site (miR29aUG) and a knownTLR7 agonist, Imiquimod, and DOTAP. Neurons were incubated for 24 h and then stained with MAP2 for neurons; PSD95 to mark the a post-synapse, VGLUT1 for pre-synapse and Drebrin for staining the dendritic spines. The number of PSD95/VGLUT1 co-localised puncta were counted and quantified in both (a) WT and (b) TLR7$^{-/-}$ neuronal cultures. (c) Quantification of the data from the WT cultures indicates a significant decrease in synapses as observed by a significant decrease in VGLUT1/PSD-95 puncta from miR-29a:DOTAP as well as in Imiquimod treated cultures when compared to miR29a-UG or vehicle (DOTAP) control. However, no such decrease was observed when TLR7$^{-/-}$ cultures were treated with either miR-29a or the other controls. Similarly, dendritic spine measurements were analyzed. Quantification of the dendritic spine number revealed a significant decrease in spines as observed by a decrease in drebrin-labelled spines in miR-29a:DOTAP as well as in Imiquimod-treated cultures when compared to miR29a-UG or vehicle (DOTAP) control. Again, we did not observe any differences in the spine numbers when TLR7$^{-/-}$ cultures were treated under similar conditions. All the experiments were performed in three replicates ($n = 3$) and a total of 10 neurons from each replicate were used for analysis. For the final compilation of the data, 50-μm dendrite segments and 45 dendrites per condition were used for the final analysis. Data represented as Mean ± SEM, ****$p < 0.0001$. Two-way ANOVA followed by Sidak multiple comparison was performed. Data are represented as box and whisker plot to display the median, lower and upper quartiles, and lower and upper extremes of a set of data

For measuring dendritic spine changes, neurons were immunostained with Drebrin, a dendritic spine marker. Compared to negative controls, miR-29aMUT (UG sequence when mutated to AA) and vehicle (DOTAP) control, miR-29a:DOTAP treatments resulted in a decrease in number of synapses as observed by a significant decrease in VGLUT1/PSD95 puncta (Figure 5a–c). A positive control for TLR7 activation, Imiquimod (IMI), displayed a similar decrease in synaptic puncta (Liu et al., 2013). Similarly, a significant decrease in dendritic spine numbers was observed with miR-29a:DOTAP treatments when compared to mutants or only DOTAP control (Figure 5d–f).

2.4 | Microglia exposed to chronic MA treatments release sEV-miR29a

ISH results showed an increased expression in miR-29a in microglial cells during MA exposure in the brain, therefore, to define the EV subtype origin for miR-29a, we utilised immortalised wild type microglial cells (WT-MG). Lactate dehydrogenase (LDH) assay was utilised to measure the cytotoxic effects of MA exposure on WT-MG. Dose response and time course assays indicated that a single treatment of 100 μM MA for 24 h or two treatments of MA over 48 h (once every 24 h) did not elicit toxicity when compared to three treatments over 72 h (Figure S5). Labeling with 1,2-dipalmitoyl-sn-glycero-3 phosphoethanolamine-N-[lissamine rhodamine B sulfonyl] (N-Rh-PE), a fluorescent phosphatidyl ethanolamine analogue that has been shown to be taken

up at the plasma membrane of cells, sorted to endosomes, and secreted in exosomes (Willem et al., 1990), showed an increase in plasma membrane blebbing and endocytotic vesicles after 24 h (Figure 6a). Further, MA-exposed microglial cultures were treated with a second dose of 100 μM MA or PBS (replicates an in vivo 'binge' scenario). TEM results show that most of the EVs after 1 H post MA treatments were lEVs, and EVs isolated after 24 h post MA treatments were majorly comprised of sEVs and nanoparticles which are <50 nm resembling exomeres, similar to what we observed with BDE (Figure 6b). Next, NTA analysis was performed on the microglia derived EVs to corroborate the TEM findings. Similar to TEM, we see that smaller particles sized (<50–100 nm) were significantly increased in the 24 h post MA and larger particles (~100–500 nm) were significantly more in the 1 h post MA treatments when compared to the control treatments (Figure 6c). Further, western blot indicated the presence of sEV marker, Alix and exomere marker, HSP90, after 24 h post MA treatments and lEV marker, Anx V after 1 h post MA treatments, confirming the NTA result (Figure 6d). Next, we investigated whether miR-29a is enriched in lEVs or sEVs by quantifying the expression levels of miR-29a at different timepoints after the second MA exposure on microglial cells. Results demonstrated that miR-29a is not expressed in the lEVs that are released immediately after MA exposure but only expressed significantly in sEVs that were collected after chronic 'binge' exposure (Figure 6e) indicating that miR-29a is localised to sEVs rather than lEVs. Finally, in order to confirm whether the EV biogenesis genes changed similar to the in vivo experiments, we ran qRT-PCR on total RNA isolated from WT-MG treated with 2× doses of MA over 48 h. Similar to the previous results, we saw differential regulation of several genes involved in the ESCRT-dependent and -independent pathways. Specifically, several overlapping genes, such as *HRS*, *VPS28, VPS25, ALIX, CERS2*, *CERS3, CERS6* and proinflammatory cytokine *TNFα*, were significantly upregulated. Additionally, in microglia, there is an increase in the expression of EV markers such as *CD9* and *FLOT2*; ESCRT-0: *STAM*; ESCRT-1: *VPS37B*; Disassembly complex: *VPS4A*; microglial receptors CCR5 and CXCR3 and proinflammatory cytokine *IL1β* (Figure 6f).

2.5 | sEV-miR29a induces synaptodendritic damage in primary neurons

Since we know that sEVs from microglial cells contain miR-29a cargo, we wanted to investigate their effects on neurons. sEVs were isolated from WT-MG cultures treated with saline (control), MA (2× doses) and from cultures that have been pre-treated with an sEV inhibitor, GW4869, prior to MA treatments. NTA analysis (Figure 7a) revealed an increase in release of EVs post MA treatments. Further, qRT-PCR on sEVs revealed increase in miR-29a copies (Figure 7b). Before evaluating the effect on neurons, WT-MG and TLR7$^{-/-}$-MG were treated with control- and MA-EVs. MA-EVs elicited a strong inflammatory response in WT-MG but not in TLR7$^{-/-}$-MG, confirming that MA-EVs can elicit an inflammatory response similar to the DOTAP complexed synthetic miR-29a oligo (Figure S6). Next, we evaluated the effect of WT microglial derived EVs (MG-EVs) on neurons. We first optimised the concentrations of MG-EVs to avoid non-specific toxicity. Concentrations of MG-EVs isolated from both control and MA-treated microglia were calculated by NTA. Primary mouse cortical cultures from WT (C57BL/6) mice were treated with various concentrations of serially diluted MG-EVs. First, toxicity was measured by quantifying LDH release in media supernatants. LDH assay indicated that a concentration of 1×10^9 particles/ml (25 μl EV volume) was non-toxic to neurons (Figure S7A). Neuronal cultures were treated with non-toxic concentrations of EVs followed by dendritic spine and synapse measurements after 24 h treatment. At this concentration, MA-EVs showed a significant effect on synaptodendritic architecture when compared to control-EVs (Figure S7B and C). Accordingly, primary cortical cultures from both WT and TLR7$^{-/-}$ mice were treated with 1×10^9 EVs, followed by the quantification of dendritic spine and synapse numbers. Results showed a reduction in dendritic spines (drebrin, red) (Figure 7c) synapse numbers (vglu1/psd95 puncta, yellow) (Figure 7d) in WT neurons treated with MA-EVs compared to the control-EVs. TLR7$^{-/-}$ neurons displayed no significant loss of spines or synapses (Figure 7e and f), indicating direct effects of synaptodendritic injury and TLR7 activation during MA insult. Quantifications are seen in Figure 7g and h.

2.6 | Drug reinstatement led to increase in BDE secretion, EV-miR29a expression and dendritic spine loss in primary neurons

In order to accurately understand the role miR-29a in MA use disorder, it is crucial to study relapse behaviours. We now know that chronic MA leads to increased EV biogenesis and secretion of EV-miR29a. In order to understand the role of miR-29a in MA use disorder, we utilised MA self-administered rats that underwent extinction and reinstatement regimen to mimic drug relapse in humans. During the self-administration and extinction sessions, the main effect on drug-seeking behaviour was seen with day [$F(38, 912) = 9.40$, $p < 0.001$]], IVSA (intravenous self-administration) drug [$F(1,24) = 91.56$, $p < 0.001$], and with day × drug interaction [$F(38,912) = 8.88$, $p < 0.001$] (Figure 8a). Post hoc tests examining the day x IVSA drug interaction revealed that total active lever presses for rats that received meth IVSA were greater than for rats that received saline IVSA for Days 1–30 and 32–34 ($p \leq 0.047$). There was no effect of IVSA drug for day 31 and days 35–39 ($p \geq 0.05002$). During reinstatement, there was a main effect of IVSA drug [$F(1,22) = 5.70$, $p = 0.026$] and reinstatement dose [$F(1,22) = 23.25$, $p < 0.001$]. We did not see any interaction effect [$F(1,22) = 2.20$, $p = 0.152$] (Figure 8b). Brain cortices were harvested immediately at the end of the reinstatement procedure and BDEs were isolated. NTA was performed to measure particle concentrations, and miR-29a levels were measured by

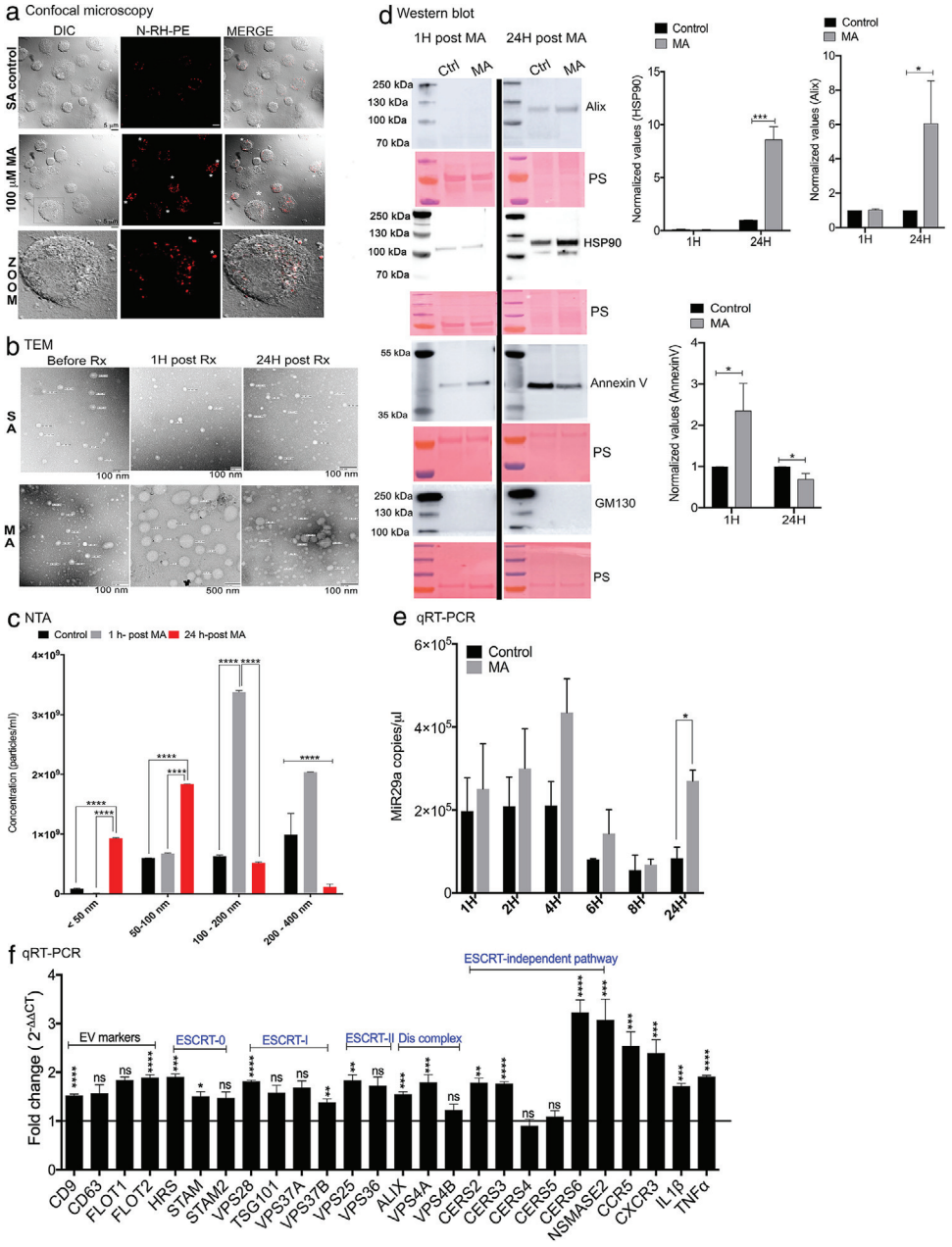

FIGURE 6 MA exposure induces release of different EV subtypes. (a) N-RH-PE labeled WT-MG were exposed to repeated doses (2x) of 100 μM MA or saline (SA control) for every 24 h. Post 24 h treatments (Rx), an increase in the expression of endocytotic vesicles and plasma membrane blebbing was observed in MA-exposed samples when compared to the SA controls. Scale bars = 5 μm. (b) TEM images of EVs; Left Panel: isolated from media supernatants of untreated controls (Control); Middle panel: isolated after 1 h second dose of 100 μM MA consisting of large EVs (1H postMA Rx- lEVs); Right panel: post 24 h after 1 h second dose of 100 μM MA consisting of mostly of small EVs (24H postMA Rx- sEVs). Scale bars = 100 nm. (c) NTA shows increase in sEVs and lEVs in 24 h (24 h-post MA) and 1 h (1 h- post MA) post MA treatment when compared to control groups, respectively. Data represented as Mean ± SEM, $n = 5$; ****$p < 0.0001$. Two-way ANOVA followed by Tukey's multiple comparisons. (d) Western blotting was performed on EVs isolated from media supernatants after 1 h and 24 h MA treatments. Results reveal a significant increase in expression of sEV marker- Alix, exomere marker- HSP90 and lEV marker- Anx V in the MA groups when compared to the controls (ctrl). Negative marker GM130 was not detected. Data represented as Mean ± SEM, $n = 3$, ***$p < 0.001$ and *$p < 0.05$, Welch's t-test. (e) qRT-PCR analysis for miR-29a expression after MA treatments reveal no difference in miR-29a after a single dose of MA treatments post 24H or at earlier timepoints after the second dose, however, a significant increase was seen only at 24 h post-second dose, indicating that miR-29a is released in small EVs rather than large EVs that were released during earlier timepoints. Data represented as Mean ± SEM, $n = 3$ experiments, *$p < 0.01$(*Adjusted p value*), Multiple t-test using Holm-Sidak multiple comparisons. (f) WT-MG cultures were treated with a vehicle control or 100 μM MA and qRT-PCR was performed. Results indicate several genes belonging to ESCRT pathway, EV markers (*CD9* and *FLOT2)*, chemokine receptors *(CCR5* and *CXCR3)* as well as proinflammatory cytokines *TNFα* and *IL1β* were upregulated. Data represented as Mean ± SEM; ****$p < 0.0001$, ***$p < 0.001$, **$p < 0.005$, *$p < 0.05$ (*Adjusted p value)*. Multiple t-test followed by Holm-Sidak method correction was performed

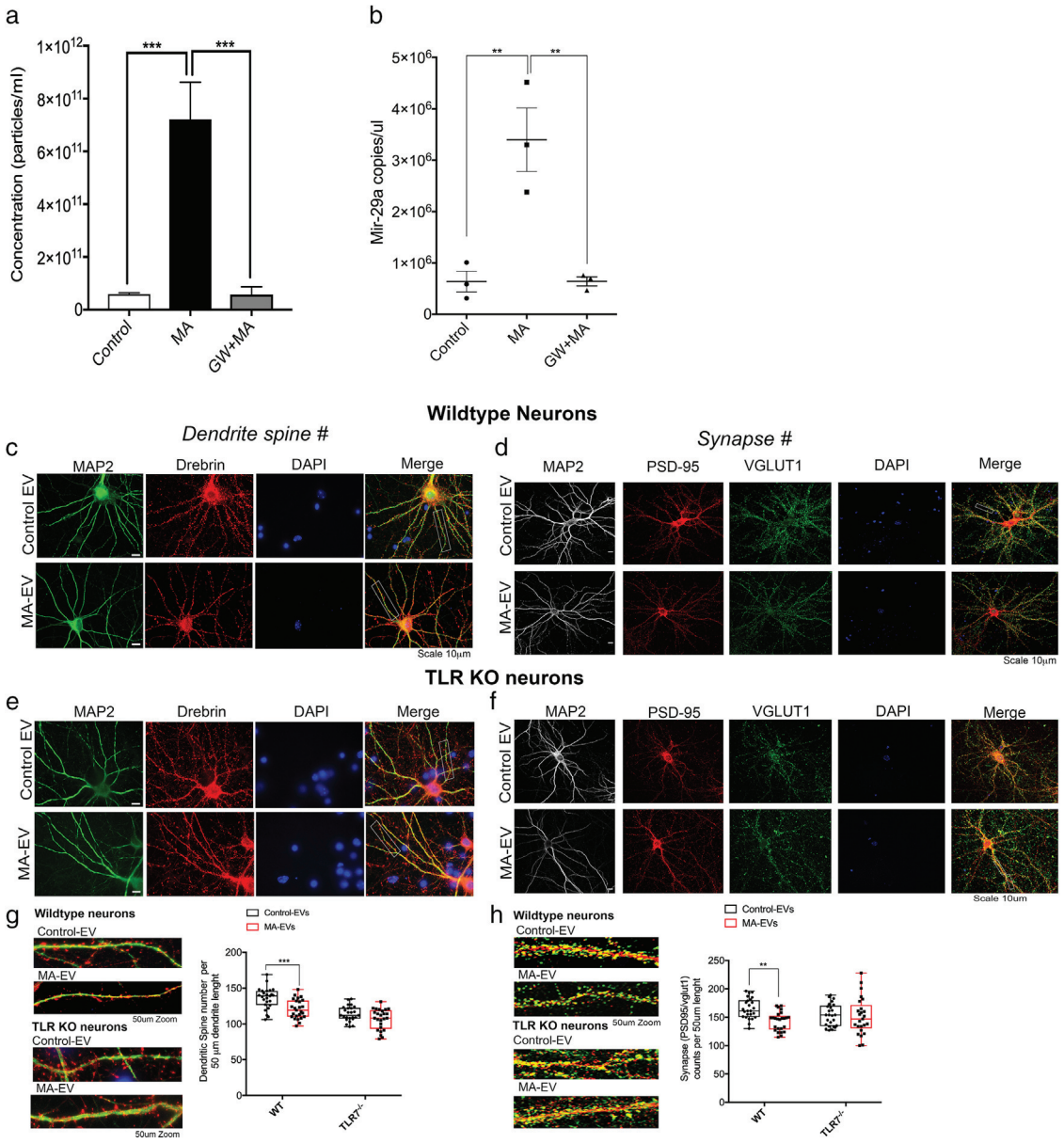

FIGURE 7 EVs released from MA-treated microglia cause synaptodendritic injury. Immortalised WT mouse microglia cultures (MG-WT) were treated with vehicle control, MA and pretreated with an EV inhibitor, GW4869, to confirm MA specific EV release. (a) NTA analysis revealed a significant increase in EV concentration in MA-treated microglia when compared to control or pretreated cultures with EV inhibitor, GW4869. Data represented as Mean ± SEM, $n = 3$, $^{***}p < 0.001$, One-way ANOVA followed by Tukey's multiple comparison. (b) QRT-PCR results revealed a significant increase in miR-29a copy number in EVs isolated from MA treated microglia when compared to control or pretreated cultures with GW4869. Data represented as Mean ± SEM, $n = 3$, $^{**}p < 0.005$, One-way ANOVA followed by Tukey's multiple comparison. Wildtype (WT) and TLR7 knock out (TLR7$^{-/-}$) mouse cortical neurons were incubated with 1x10^9 EV particles from control and MA treated microglia for 24 h and then stained with MAP2, PSD95, VGLUT1 and Drebrin. The number of PSD95/VGLUT1 colocalised puncta were counted and quantified in both (c and d) WT and (e and f) TLR7$^{-/-}$ neuronal cultures. (g, bottom panel) Quantification of the dendritic spine number reveal a significant decrease in spines as observed by a decrease in Drebrin labeled spines from cultures treated with MA-EVs when compared to control-EVs and no decrease was observed when TLR7$^{-/-}$ cultures were treated with either MA-EVs or control-EVs. (h, bottom panel) Results indicate that in WT cultures treated with MA-EVs a significant decrease in synapses is seen as indicated by a significant decrease in VGLUT1/PSD-95 puncta when compared to when treated with control-EVs. Data represented as Mean ± SEM, $n = 3$; $^{***}p < 0.001$, $^{**}p < 0.005$. Two-way ANOVA followed by Sidak multiple comparison was performed

qRT-PCR. As seen before with macaque brains, NTA showed a significant increase in particle count in MA-SA followed by extinction session (RS-SA) as well as with 0.5 mg/kg reinstatement dose (RS-0.5 MA) when compared to saline (SAL) groups. Interestingly, a single dose of MA in the saline (SAL) group did not show any increase in particle concentration (SAL/RS-0.5 MA). However, when MA groups that received reinstatement with saline (RS-SA) and MA (RS-0.5 MA) were compared, a significant increase in particle concentration was observed, indicating that reinstatement of MA (relapse) stimulates EV release in brain

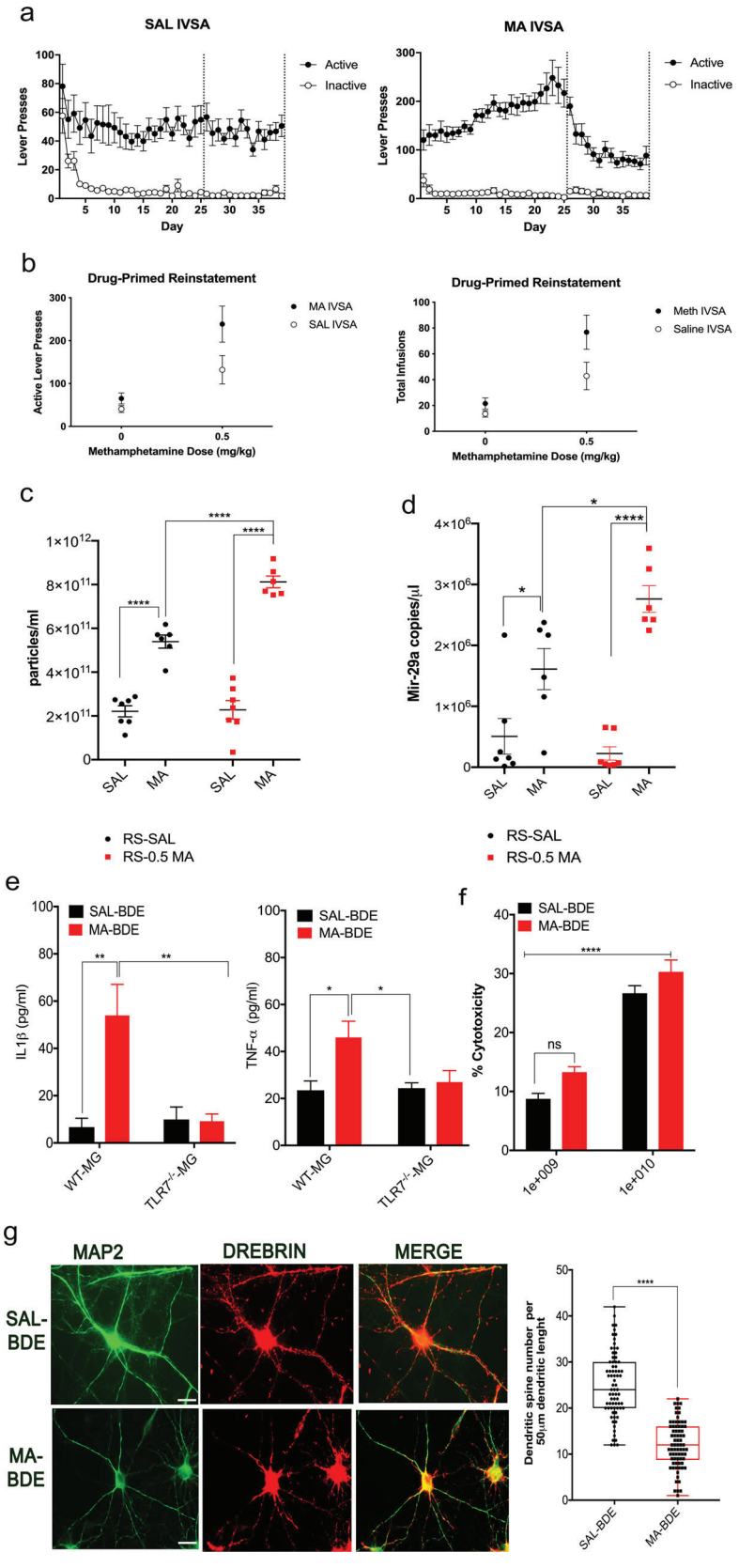

FIGURE 8 Drug reinstatement led to increase in BDE secretion, EV-miR29a expression and dendritic spine loss in primary neurons. (a) Active (closed circle) and inactive (open circle) lever presses (±SEM) are displayed for rats that received 0.05 mg/kg/infusion methamphetamine (MA) (right panel) or saline (SAL) (left panel) during self-administration sessions (Day 1–25). A dotted line depicts the transition between self-administration sessions and extinction (Day 26–39) sessions. The main effect on drug seeking behaviour was seen with day [$F(38, 912) = 9.40$, $p < 0.001$]], IVSA (intravenous self-administration) drug [$F(1,24) = 91.56$, $p < 0.001$], and with day x drug interaction [$F(38,912) = 8.88$, $p < 0.001$]. IVSA = intravenous self-administration; mg/kg = milligram per kilogram. (b) Rats that previously received MA (closed circle) or saline (open circle) intravenous self-administration (IVSA; Day 1-25) were intraperitoneally (IP) injected with 0 (saline) or 0.5 mg/kg MA 15 min before the start of the reinstatement session. Post hoc tests reveal that total active lever presses (left panel) for rats who received meth IVSA rats were greater than for rats that received saline IVSA for Day 1–30 and 32–34 (ps ≤ 0.047). No effect of IVSA drug for day 31 and days 35-39 ($p \geq 0.05002$) was observed. During drug-primed reinstatement, there was a main effect of IVSA drug [$F(1,22) = 5.70$, $p = 0.026$] and reinstatement dose [$F(1,22) = 23.25$, $p < 0.001$]. We did not see any interaction effect [$F(1,22) = 2.20$, $p = 0.152$]. Similarly, post-hoc tests revealed that total infusions for rats who received meth IVSA rats were greater than for rats that received saline IVSA (Day 1–30, 32–34). No effect of IVSA drug was seen for day 31 and days 35–39 ($p \geq 0.05002$). (c) NTA analysis on total particle number show a significant increase in particle concentration and (d) MiR-29a expression in BDEs after MA self-administration and saline reinstatement (RS-SAL), a further increase in both particle number and miR-29a expression was seen with MA reinstatement only in groups receiving 0.5 mg/kg but not in groups administering SAL. Data represented as Mean ± SEM, $n = 7$ animals for saline groups and $n = 6$ animals for MA groups. Two-way ANOVA followed by Tukey's multiple comparison test was performed. (e) Wildtype microglia (WT-MG) and TLR7$^{-/-}$ microglia (TLR7$^{-/-}$-MG) were treated with BDE isolated from saline (SAL-BDE) and MA (MA-BDE) groups. ELISA results show an increase in the release of both IL1β and TNFα in WT-MG. No response was seen with either SAL-BDE or with TLR7$^{-/-}$-MG. Data represented as Mean ± SEM, $n = 6$ per group; $^{**}p < 0.005$, $^{*}p < 0.05$. Two-way ANOVA with Tukey's multiple comparison test was used to determine the significance. (f) LDH assay on media supernatants of rat primary neuronal cultures treated with BDE. Results showed that a concentration of 1×10^9 particles/ml did not elicit any cell toxicity when compared to 1×10^{10} particles/ml. Data represented as Mean ± SEM, $n = 6$ per group: $^{****}p < 0.0001$. Two-way ANOVA with Tukey's multiple comparison test was used to determine the significance. (g) DIV 14 rat primary neuronal cultures were treated with SAL-BDE and MA-BDE and dendritic spines were analyzed. DIV 14 primary rat neuronal cultures were immunostained with neuronal marker MAP2 (green) and dendritic spine marker, Drebrin (red). Results show a significant decrease in spine number with MA-BDE when compared to SAL-BDE. In vitro experiments were performed in three replicates ($n = 3$) and a total of 24 neurons from each replicate was used for analysis. For the final compilation of the data, 50-μm dendrite segments from 306 dendrites for SAL-BDE or 369 dendrites for MA-BDE were used for the final analysis. Data represented as Mean ± SEM, $n = 3$ (Sal-BDE, 24.96 ± 0.8331, $n = 74$; MA-BDE, 12.03 ± 0.5827, $n = 74$). $^{****}p < 0.0001$. Welch's unpaired t-test was performed

(Figure 8c). When miR-29a levels were measured, we observed a similar increase in miR-29a copy numbers in MA groups (both extinction and reinstatement) when compared to saline (SAL). Similarly, we also see a further increase in miR-29a copy numbers in the MA reinstatement (RS-MA) group when compared to saline (RS-SA) (Figure 8d). Intriguingly, these results show that miR-29a-containing EVs were still being released even when the animals were in the drug extinction phase, which was further exacerbated during drug reinstatement. Together, these data confirm the release of EVs and EV-miR29a is not incidental during chronic MA seeking, but its increase during reinstatement period (relapse) further confirms that EV-miR29a is an important molecular target to be considered when studying MA use disorder.

We then wanted to investigate the effects of BDE isolated from MA reinstated animals on primary neurons. To address this, we used BDE isolated from prefrontal cortices of rats that were reinstated with either saline (SAL) or 0.5 mg/kg MA (MA) after extinction session. First, we wanted to investigate whether the BDE released from rats reinstated with MA induced pro-inflammatory cytokine release in microglia. Immortalised microglial cultures, from wildtype microglia (WT-MG) and TLR7$^{-/-}$ microglia (TLR7$^{-/-}$-MG), were treated with BDE isolated from SAL (SAL-BDE) and MA (MA-BDE) groups. ELISA on media supernatants revealed that MA-BDE induced the release of both IL1β and TNFα in WT-MG. However, in TLR7$^{-/-}$-MG, MA-BDE failed to elicit any responses indicating that cargo in MA-BDE indeed can activate TLR7, a similar phenomenon that we observed with EVs isolated from microglial cells (Figure 8e). Next, we wanted to investigate the effect of BDE on primary neuronal cultures. Since dose for treatment is a critical factor, we conducted LDH assay on media supernatants of rat primary neuronal cultures treated with BDE. Results showed that a concentration of 1×10^9 particles/ml did not elicit any cell toxicity and therefore could be safely used for the in vitro treatment experiments (Figure 8f). Next, DIV 14 rat primary neuronal cultures were treated with BDE isolated from SAL and MA groups and dendritic spines were analyzed. Since dendritic spines are the major sites for excitatory synaptic input and serve as functional markers for synaptic function, we conducted a comprehensive analysis on dendritic spines using the marker, drebrin. Results revealed that the spine number decreased significantly with MA-BDE when compared to SAL-BDE (Figure 8g). This data collectively indicates that MA-BDE is both pro-inflammatory and injurious to brain cells and is line with our in vitro data (Figure 7).

2.7 | Ibudilast (AV411), an anti-inflammatory drug, reduces EV biogenesis as well as the expression of EV-miR29a after MA treatments

We have previously shown that, by reducing inflammation using the anti-inflammatory drug Ibudilast (IBUD), or AV411, we were able to restore synaptic signalling and rescue drug-seeking behaviour in rats (Charntikov et al., 2015). IBUD is a phosphodiesterase (PDE) -4 and -10 inhibitor that has been extensively discussed to reduce glial activation (Suzumura et al., 2003; Suzumura et al., 1999) and attenuate prime and stress-induced MA reinstatement in rats (Beardsley et al., 2010). Here, we wanted to test whether IBUD can rescue EV-miR29a levels, thereby preventing synaptodendritic injury, using a rat self-administration model of MA-seeking. In order to test the efficacy of IBUD, brain RNA and blood plasma were isolated from a subset of SA rats that received either a low dose of 2.5 mg/kg (MA-2.5) or a high dose of 7.5 mg/kg (MA-7.5) IBUD during the extinction phase (Charntikov et al., 2015). QRT-PCR analysis on the brain RNA for microglial marker, *IBA1*, astrocyte marker, *GFAP*, and pro-inflammatory markers *TNFα and IL6* revealed a significant increase in gene expression in rats that self-administer MA, whereas IBUD treatments (either 2.5 or 7.5 mg/kg) clearly attenuated the expression of *IBA1, TNFα* and *IL6* (Figure 9a). Furthermore, TNFα and IL6 levels in blood plasma mirrored the effect seen in brain (Figure 9b). Next, we tested whether IBUD effects EV biogenesis and miR-29a secretion in brain. For BDE isolations, we chose only the low dose (2.5 mg/kg) IBUD group since both the concentrations reduced inflammation equally in rats. BDE were isolated and analysed by NTA and qRT-PCR. Results indicated that there is a significant reduction in the total number of particles in the IBUD group when compared to the MA groups (Figure 9c), which is also accompanied by significant reduction in miR-29a copies post-IBUD treatment (Figure 9d). In summary, we observed that anti-inflammatory drug, IBUD, was able to bring down both inflammation as well as miR-29a levels.

2.8 | Pretreatment with IBUD rescues synaptodendritic injury in primary neurons that were exposed to MA

Finally, we investigated whether IBUD pretreatments would rescue synaptic injury. Immortalised WT-MG cultures were pretreated with IBUD (100 μM) for 1 h before MA (100 μM) treatment. EVs were isolated from the media supernatants, followed by NTA and qRT-PCR analysis. Results indicated that IBUD pretreatment not only reduced the EV number but also decreased the miR-29a copy number in EVs isolated from microglial cells that were pretreated with IBUD (Figure 10a and b). Furthermore, we extracted RNA from the treated cultures and evaluated the expression of ESCRT-dependent and -independent genes responsible for EV biogenesis. QRT-PCR data revealed that IBUD pretreatment significantly decreased the expression of several genes that were elevated by MA, including ESCRT-dependent (ESCRT-0: *HRS/HGS* and *STAM2* ; ESCRT-I: *VPS28*; ESCRT-II: *VPS25, VPS36* and Disassembly (Dis) complex: *ALIX, VPS4A*), ESCRT-independent ceramide genes (*CERS2, CERS3, CERS4 and*

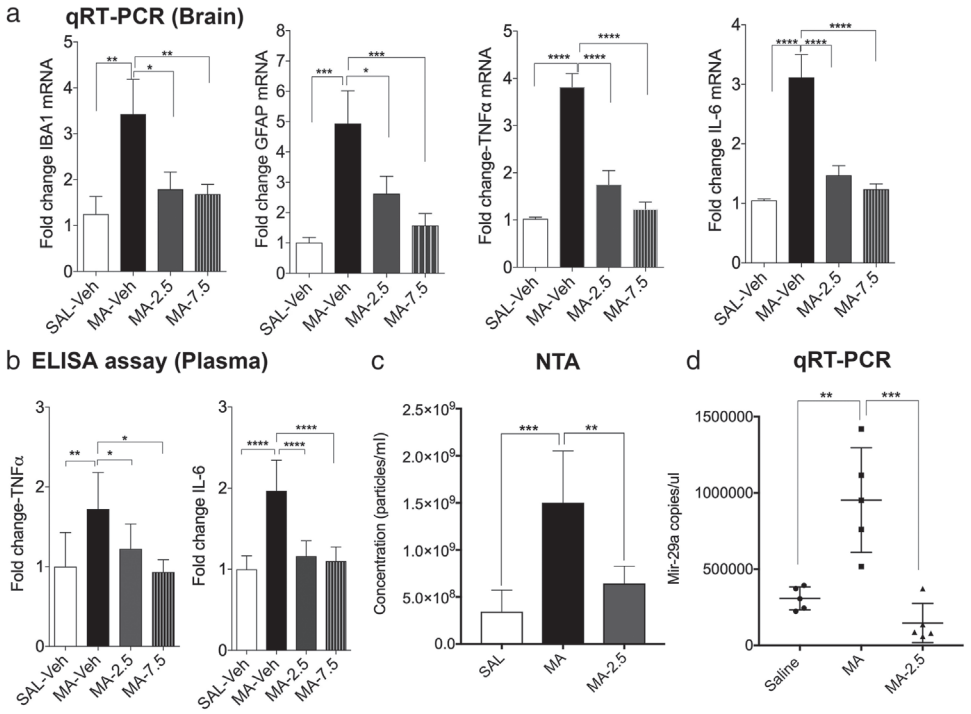

FIGURE 9 Ibudilast (IBUD), an anti-inflammatory drug, reduces EV biogenesis as well as the expression of EV-miR29a after MA treatments. (a) qRT-PCR analysis on brain mRNA showed a significant increase in the expression of the proinflammatory cytokines IL-6 and TNF-α by MA, which was attenuated by IBUD. Data represented as Mean ± SEM, $n = 3$ animals per group; $^{****}p < 0.0001$, $^{**}p < 0.005$, $^{*}p < 0.05$. One-way ANOVA with Tukey's multiple comparison test was used. (b) ELISA analysis on blood serum shows an increased expression of secretory IL6 and TNF-α by MA, attenuated by IBUD. Data represented as Mean ± SEM, $n = 6$ animals for saline (SAL-Veh) and $n = 8$ animals for MA, MA-2.5 and MA-7.5 groups; One-way ANOVA with Tukey's multiple comparison test was used to determine the significance. $^{****}p < 0.0001$, $^{**}p < 0.005$, $^{*}p < 0.05$ (c) NTA results indicate a significant increase in BDE concentration after administering MA, again reduced significantly by IBUD. Data represented as Mean ± SEM, $n = 5$ per group; $^{***}p < 0.001$, $^{**}p < 0.005$. One-way ANOVA with Tukey's multiple comparison test was used to determine the significance. (d) qRT-PCR on rat BDEs reveal increase in miR-29a copies with MA (MA) and a significant attenuation in miR-29a expression by administration of 2.5 mg/kg IBUD (MA-2.5) during the extinction phase. Data represented as Mean ± SEM, $n = 5$; $^{***}p < 0.001$, $^{**}p < 0.005$. One-way ANOVA with Tukey's multiple comparison test was used

NSMASE2) and proinflammatory cytokine *TNFα* (Figure 10c). Next, we isolated EVs from immortalised WT microglial cultures that were either treated with MA alone or pre-treated with IBUD and added to primary neuronal cultures. Neurons were imaged for spine and synapse changes, which demonstrated that pretreatment with IBUD rescued both the number of synapses (Figure 10d) as well as dendritic spine counts (Figure 10e), thus indicating a therapeutic potential of IBUD to revert synaptodendritic injury caused by EVs released by microglia during MA exposure. These data collectively indicate that IBUD not only decreases MA-induced microglia inflammation, but also can alleviate the effects of MA on EV biogenesis, expression of EV-miR29a and synaptodendritic injury.

2.9 | MA use increases plasma EV-miR29a in macaques and human

Several groups have shown that EVs isolated from peripheral biofluids, such as plasma, can serve as biomarkers to detect brain alterations (Athauda et al., 2019; Goetzl et al., 2016, 2018, Goetzl, Ledreux, et al., 2019, Goetzl, Peltz, et al., 2019; Karnati et al., 2019; Pulliam et al., 2019). To test whether peripheral EV-miR29a could serve as a potential marker to identify MA-induced neuronal injury; we utilised plasma samples from macaques that were on chronic MA regimen. Prior to quantification, the plasma was checked for haemolysis by visually scoring the samples as well as by determining the degree of haemolysis by spectrophotometry as described previously (Cripps, 1968; Yamada et al., 2014) (Figure 11a, left panel). Next, digital droplet-PCR (DDPCR) was performed on EV-RNA isolated from the plasma samples that showed no co-relation between the degree of haemolysis and the expression levels in the non-haemolysed samples (Figure 11a, middle panel). Accordingly, plasma EV from all the 10 animals (five each for saline and MA) were subjected to DDPCR that revealed significantly higher miR29a copies in the MA group (Figure 11a, right panel).

To corroborate the data from our preclinical samples into a translational relevance, we tested miR-29a levels in plasma from male human subjects diagnosed with MA use disorder (MUD) (see Table S4). Out of the original 21 samples from all the subjects

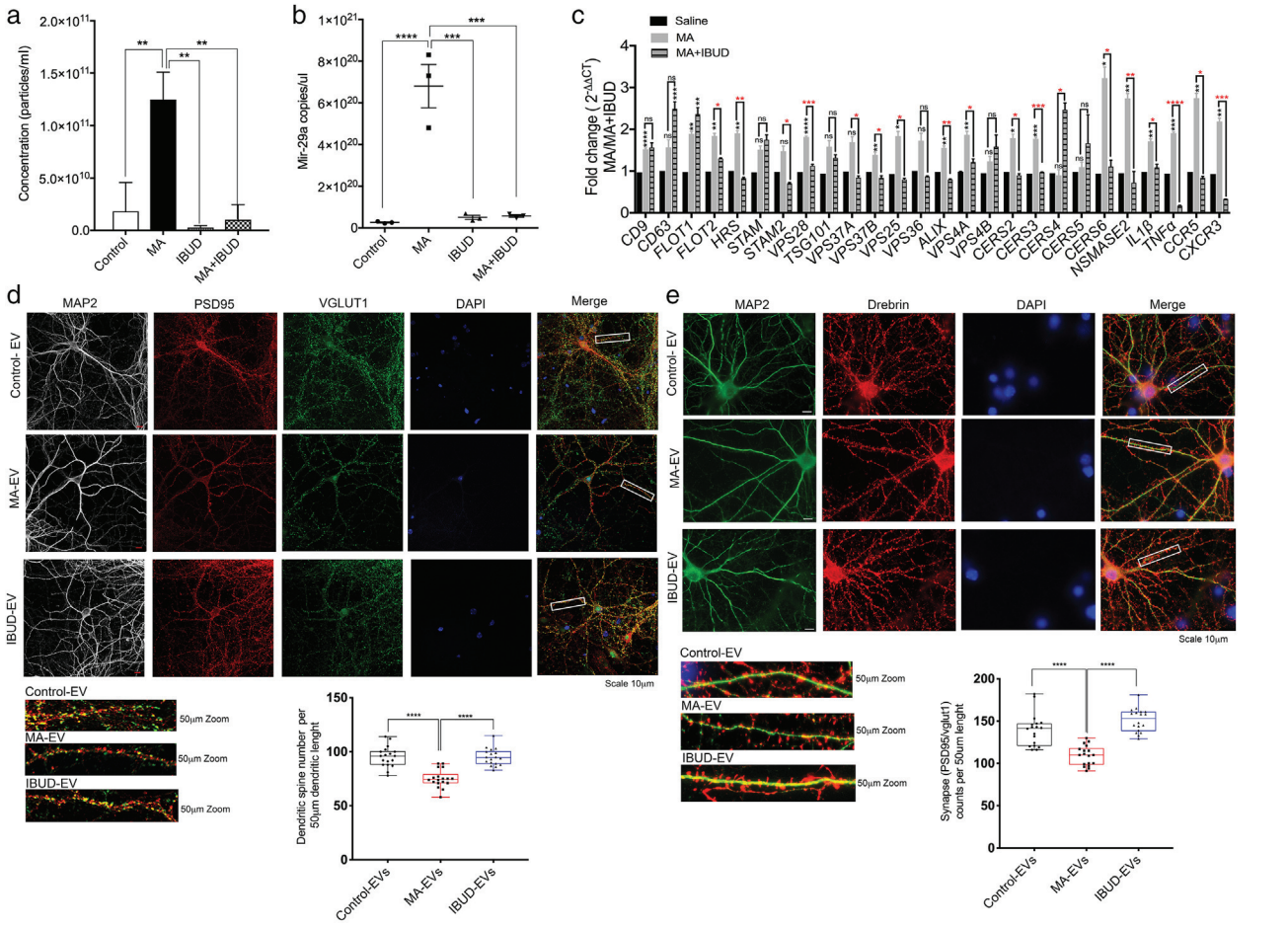

FIGURE 10 Pretreatment with IBUD rescues synaptodendritic injury in primary neurons that were exposed to MA. Immortalised WT mouse microglia (MG-WT) cultures were treated with vehicle control, MA, IBUD and IBUD+MA. (a) NTA analysis revealed that there is a significant increase in concentration and (b) qRT-PCR analysis revealed a significant increase in miR-29a copy number of the EVs released in MA-treated microglia when compared to control, whereas when treated with IBUD alone or pretreated with IBUD followed by MA, a significant decrease in concentration and miR-29a copy number was observed. (a and b) Data represented as Mean ± SEM, $n = 3$; $^{**}p < 0.01$. One-way ANOVA with Tukey's multiple comparison test was used. (c) Under similar conditions, qRT-PCR was performed to evaluate EV biogenesis genes. Results indicate genes belonging to ESCRT pathway and proinflammatory cytokines *IL1β* and *TNFα* were dramatically reduced. In addition, only one gene, *CERS4*, showed upregulation. Data represented as Mean ± SEM, $n = 3$, $^{****}p < 0.0001$, $^{***}p < 0.001$, $^{**}p < 0.005$, $^{*}p < 0.05$ *(Adjusted p value)*. Multiple t-test followed by Holm-Sidak method correction was performed. (d) WT mouse cortical neurons were incubated with 1×10^9 EV particles from control, MA-treated and IBUD+MA-treated microglia for 24 h followed by staining with MAP2, PSD95 and VGLUT1. The number of PSD95/VGLUT1 colocalised puncta were counted and quantified. Results indicate that WT cultures treated with MA-EVs show a significant decrease in VGLUT1/PSD-95 puncta when compared to control-EVs, whereas a pretreatment with IBUD showed a significant rescue in synaptic loss. (e) Similarly, a significant decrease in dendritic spine number as observed by a decrease in Drebrin-labelled spines from cultures treated with MA-EVs when compared to control-EVs, again a rescue in number was seen with pretreatment with IBUD. In vitro experiments were performed in three replicates ($n = 3$) and a total of six neurons from each replicate was used for analysis. For the final compilation of the data, 50-μm dendrite segments and 18 dendrites per condition were used for the final analysis. Data represented as Mean ± SEM, $n = 3$; $^{****}p < 0.0001$. One-way ANOVA followed by Tukey's multiple comparison was performed

(including controls), one sample showed high levels of haemolysis and therefore were discarded this from the final analysis of data (Figure 11b, left and middle panels). Finally, 20 samples (controls = 10; MA = 10) were analyzed by DDPCR. Results revealed a marked increase in the plasma miR-29a levels (Figure 11b, right panel), indicating that EV-miR29a could potentially serve as a plasma diagnostic marker to assess potential inflammation and neuronal injury in MUD.

3 | DISCUSSION

In this current study, we show for the first time how chronic MA exposure impacts EV release and biogenesis, including alterations in miRNA cargo that result in subsequent synaptodendritic damage.

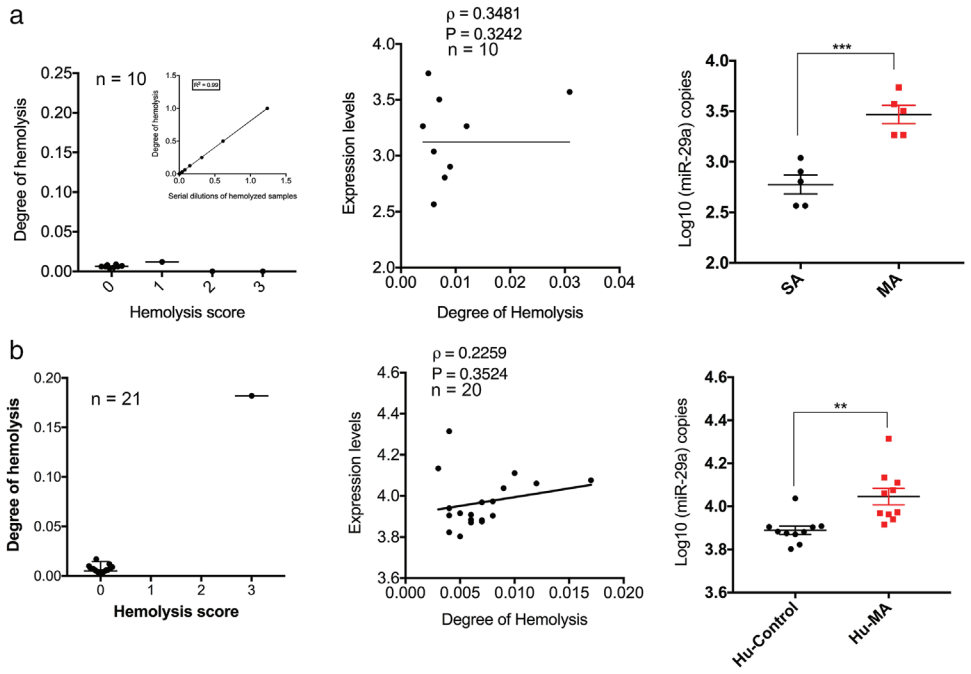

FIGURE 11 Chronic MA dependency increases plasma EV-miR29a in macaques and humans (a) Left graph; Blood plasma isolated from saline or chronic MA-administered male macaques was checked for haemolysis by visually scoring the samples as well as by determining the degree of haemolysis by spectrophotometry. Haemolysis was not detected in any of the samples; a standard curve of the haemolysed samples is shown as an insert. Middle graph; correlation analysis showed that miR-29a expression did not correlate with the degree of haemolysis. Right graph; Total EVs were isolated from plasma and miR-29a copies were quantified by DDPCR. Results indicate a significant increase in miR-29a copies in MA-treated animals. A total of ten male macaques were used for this study ($n = 5$ for saline; $n = 5$ for MA). Data represented as Mean ± SEM, $n = 5$, $^{***}p < 0.001$. Unpaired t-test. (b) Left graph; Haemolysis analysed for 21 human plasma samples revealed insignificant haemolysis for all except for one sample and therefore were eventually removed for further analysis. Middle graph; correlation analysis revealed that miR-29a expression did not correlate with the degree of haemolysis. Right graph; Total EVs were isolated from a total of 20 samples (controls = 10; MA = 10). MiR-29a copies were quantified by DDPCR. Results indicate a significant increase in miR-29a copies in the MUD cohort. Data represented as Mean ± SEM, $n = 10$, $^{***}p < 0.001$. Unpaired t-test with Welch's correction was performed

Our first observation was that chronic MA treatment in rhesus macaques caused an increase in BDE concentration and size (Figure 1). Further, we find the same phenomenon with in vitro microglial cells treated with MA (Figure 6) and with rat SA model (Figure 1). Previous studies have reported that MA causes vacuolation of endocytotic organelles (Cubells et al., 1994) and disrupts endosomal, lysosomal and autophagosomal pathways due to its ability to change pH gradient within subcellular organelles (Tallóczy et al., 2008). It has also shown to induce the formation of large electron-dense membranous whorls, multivesicular bodies and autophagic vacuoles (Larsen et al., 2002). It is well known that the aforementioned pathways are interrelated to EV biogenesis and secretion (Jeppesen et al., 2019). Therefore, we speculated whether MA could disrupt EV biogenesis and therefore release. A qRT-PCR analysis revealed changes in expression of ESCRT pathway genes such as *HRS, STAM1, VPS28, TGS101, ALIX, CHMP2A, CHMP4B, CHMP4C and VPS4B* (Figure 1d). All except for *VPS4B* gene were upregulated in MA-treated animals. Intriguingly, a previous study showed that knockdown of *HRS, STAM1* and *TSG101* decreased whereas, silencing of *VPS4B* increased the total exosome secretion (Colombo et al., 2013). Furthermore, they reported that *HRS* is responsible for the secretion of small EVs (<50 nm), whereas *STAM1/2* and *ALIX* are crucial for secretion of larger sized EVs (>100 nm). In our study, we saw a heterogenous population of BDE, indicating that similar pathways might be responsible for increased EV biogenesis during chronic MA treatment. *CHMP2A*, which belongs to the ESCRT-III family, has also been shown previously to play a crucial role in exosome secretion (Baietti et al., 2012), whereas *CHMP4B* and *CHMP4C* have been reported to play a crucial role in miRNA packaging and EV biogenesis in human stem cells (Iavello et al., 2016). The other ESCRT proteins, such as *VPS28* belonging to the ESCRT-I family, have not been previously discussed in EV biogenesis and hence for the first time we report their regulation in the brain after MA treatments.

Concomitant depletion of ESCRT subunits belonging to the four ESCRT complexes does not totally impair the formation of EVs, indicating that other mechanisms may operate in the formation of EVs (Stuffers et al., 2009). Ceramide biosynthesis is one of these pathways, and genes such as *CERS2, CERS4*, *CERS6* and *NSMASE2* have been previously shown to be involved in EV biogenesis and release (Trajkovic et al., 2008). Interestingly, a previous report has shown that acute MA exposure in rats can increase ceramide production in most tissues, including the brain, by increasing de novo ceramide biosynthesis genes such as *SPT1, SPT2, CERS2, CERS4* and *CERS6* (Astarita et al., 2015). Here, we see an increased expression of *CERS2* and *CERS6* genes

that might indicate their role in secretion of EVs in macaques. Altogether, our data shows dysregulation in ESCRT-dependent and -independent genes.

Since we observed that heterogenous populations of BDEs were released after chronic and repeated MA treatments, we wanted to further characterise in what EV subtype miR-29a is localised. To further explore this question, we utilised BDE from saline and MA self-administered rats. MA exposure in the brain led to release of different sizes of BDE, including really small (<50 nm) to very large sizes (>500 nm). Absence of classical exosome markers has been reported in recent works that explored the heterogeneity of EVs, including non-membranous structures referred to as 'exomere' nanoparticles (Jeppesen et al., 2019; Kowal et al., 2016; Zhang et al., 2019). Specifically, it was shown that many abundant miRNAs are localised to the non-vesicular fractions that contain exomeres. To distinguish the EV subtypes in BDE, we used markers to distinguish sEVs, lEVs and non-membranous nanovesicles or exomeres. Western blotting on BDE protein showed an increase in classical sEV markers such as Alix, TSG101, HSP70 and CD63 indicating that chronic MA exposure led to increased exosome biogenesis, also, corroborating our qRT-PCR data. Further, we surprisingly see an increase in HSP90 (Zhang et al., 2018) expression in MA-BDE indicating that chronic MA induces the release of exomeres. This is a novel observation in our study. It has been shown previously that exomeres are highly enriched in metabolic enzymes, nucleic acids and lipids (Zhang et al., 2018). It has also been shown that exomeres are also enriched in miRNA biogenesis machinery such as Ago proteins (Jeppesen et al., 2019; Zhang et al., 2019). We did not detect any Ago proteins in our BDE preparations. It could be speculated that exomeres isolated from brain BDE are different in composition than other cell types. A high-resolution purification of the specific EV types would probably help to delineate brain derived exomere specific cargo. Other non-vesicular structures such as lipoproteins were undetectable in the BDE, indicating that the preparations were devoid of any protein aggregates, a common contaminant found in plasma (Sódar et al., 2016). Furthermore, we also found an increase lEV marker, Anx V, which is usually localised to EV secreted from apoptotic cells. It has been shown previously that MA causes apoptosis of neurons in the brain, therefore, detection of Anx V^+ EVs could be a strong indicator of cell death pathway activation. These data collectively not only indicate that chronic MA exposure influences size, concentration but also specific EV subtypes in the brain. Most, importantly, we for first time report exomeres as possible carriers of miR-29a, although more works need to be done to further elucidate the function of exomeres in the brain and in substance use disorders.

Next, we investigated whether chronic MA exposure influences the miRNA cargo in BDE. A recent report showed evidence that plasma EV-miRNA profile is altered in active MA users (Sandau et al., 2020). However, the tissue origin of plasma EV-miRNAs is unclear. To gain more insight in the BDE-miRNA cargo, we ran small RNA sequencing. A total of six miRNAs were found to be upregulated in chronic MA group when compared to saline controls. Out of the six miRNAs, hsa-miR-29a-3p_R1 (miR-29a) has the canonical GGUU sequence, and which has been identified earlier as a TLR7 ligand (Fabbri et al., 2012). Using synthetic oligos, we found that miR-29a treated WT macrophages (RAW 264.7) and microglia (WT-MG) cells secreted significant amounts of TNFα when compared to other miRNAs. Failure in TNFα secretion was observed when TLR7 deficient microglial cells were used confirming that the secretion was induced by binding. Interestingly, binding of miR-29a to TLR7 is not incidental because mutant forms of miR-29a were unable to bind to TLR7 or stimulate immune response (Fabbri et al., 2012). Other miRNAs, miR-143-3p and miR-24-3p elicited TNFα response in RAW 264.7 macrophages, however, they failed to elicit any response in WT-MG. Intracellular localisation of TLR7 has been shown to influence its functional response to ligand binding. For example, it has been reported that in cortical and hippocampal neurons where TLR7 is localised to the endosomes, stimulation with let-7b, another TLR7 ligand, led to apoptosis (Lehmann et al., 2012), whereas in sensory neurons where TLR7 is localised to the plasma membrane, let-7b binding led to stimulation of the cation channel transient receptor potential A1 (TRPA1) (Park et al., 2014). Similarly, TLR7 is expressed on both cell surface and endosomes in macrophages (Mielcarska et al., 2020), however it is exclusively present in endosomes in microglia (Kumar, 2019), therefore it is likely to see differences in ligand binding response between RAW 264.7 cells and WT-MG.

Further, a qRT-PCR post validation confirmed that miR-29a is indeed significantly increased in BDE isolated from chronic MA treatments. Other miRNAs from the RNA sequencing screen failed to show any differences indicating that miR-29a is predominantly upregulated in BDE isolated from chronically MA exposed monkeys. Interestingly, miR-29a expression was seen strongly in microglia and neurons but minimally in astrocytes. It is well known that MA causes chronic neuroinflammation and microglial activation in the brain, responsible for relapse-like behaviours in humans (Krasnova et al., 2016; Sekine et al., 2008). However, it is still unknown whether MA-induced neuroinflammation perpetuates neurodegeneration and unclear whether it contributes to MA-induced neurotoxicity. To investigate whether miR-29a could potentially cause such damage, we examined the effects on microglia and neurons. First, to test the effect on microglia, synthetic miRNA oligonucleotides complexed with DOTAP and WT or $TLR7^{-/-}$ microglia were treated with the complexes. An increased expression of *TNFα* and *IL6* genes at 2 and 4 h post-treatments in response to EV-miR29a was observed, indicating a valid transcription event in response to binding of miR29a:DOTAP to TLR7. Further, a significant increase in the expression of TNFα and IL6 cytokines in media supernatants from WT microglia was seen when compared to other miR-29 family members or miR-29a mutants or while using $TLR7^{-/-}$ microglia. Activation of microglia appears to precede MA-induced damage to striatal dopaminergic terminals in rodents (Lavoie et al., 2004; Thomas & Kuhn, 2005; Thomas et al., 2004). Another study has shown the attenuation of MA-induced neurotoxicity in interleukin-6-null mice, further supporting a potential role of activated microglia in the toxic effects of the drug (Ladenheim et al., 2000). While the binding of EV-miR29a to TLR7/8 has been only shown in peripheral immune cells such as peritoneal

macrophages (Fabbri et al., 2012) or dendritic cells (Ranganathan et al., 2017), we are first to report its binding in microglial cells. Together, the data clearly indicate that MA, via the release of miR-29a in EVs, triggers inflammation in the brain. MA causes long-term synaptic damage as well as induces changes in synaptic protein expression that persist even after long periods of drug abstinence (Bosch et al., 2015; Charntikov et al., 2015; Faure et al., 2009). However, exact mechanisms by which MA causes synaptic deficits are still unknown. Here, we investigated whether EV-miR29a elicits synaptic deficits in neurons. Both WT and TLR7$^{-/-}$ mouse primary neurons were treated with DOTAP complexes that indicated a significant decrease in both synapses and spines in miR29a:DOTAP-treated WT cultures but not in TLR7$^{-/-}$ cultures or when treated with miR-29a mutants. An overall decrease in synapse and spine counts was seen in the TLR7$^{-/-}$ groups, this difference could be attributed to technical variations in the primary culture preparations.

Since we now know that EV-miR29a could potentially elicit inflammation and cause neuronal damage, we questioned which EV subtype is responsible for miR-29a cargo secretion. To explore this question, an in vitro method was employed. WT-MG were exposed to repeated doses (2×) of 100 μM MA for 48 h to mimic chronic in vitro exposure. After 24 h treatments, we observed an increase in the expression of endocytotic vesicles and plasma membrane blebbing (Figure 6a). Further, a second dose of MA treatment for one hour initiated the immediate release of lEVs into the media, whereas media collected after another 24 h comprised mostly of sEVs and particles <50 nm, as measured by TEM and NTA (Figure 6b and c). Interestingly, plasma membrane blebbing and large vesicle release have been observed before in microglial cells upon activation with ATP (Prada et al., 2013); large EVs (0.1–1 μM in diametre), were seen to bleb from the cell surface. These results suggest that acute MA exposure could elicit the release of lEVs from the plasma membrane, and repeated chronic exposure stimulated the release of sEVs from multi-vesicular bodies (MVBs). Furthermore, to corroborate the in vivo BDE data, expression for markers to distinguish sEVs, lEVs and exomeres revealed a significant increase in Alix (sEV) and HSP90 (exomere) were significantly increased in the sEVs (secreted after 24 h treatment of the second dose) and Anx V (lEV) was upregulated in the 1 h post treatment groups. These results nicely corelate with the in vivo experiment (Figure 6). Further, miR-29a expression was seen to be upregulated in the sEVs and exomere pool (secreted after 24 h treatment of the second dose). These data indicate further confirm that miR-29a is localised mainly to the sEVs and exomeres rather than lEVs. Previous studies have described selective (Tosar et al., 2015) and non-selective (Santangelo et al., 2016; Shurtleff et al., 2016; Villarroya-Beltri et al., 2013) sorting of miRNAs within lEVs or sEVs. Specifically, studies in cancer (Temoche-Diaz et al., 2019; Tosar et al., 2015) found that non-selective miRNA sorting occurs in lEVs, whereas a selective mechanism of sorting occurs in sEVs. Several studies have mentioned various RNA binding proteins (RBPs) such as hnRNPA2B1, Ago2, YBX-1, MEX3C, MVP and the La protein that help sort miRNAs into EVs; however, the specific mechanisms are still unclear (Thomas & Kuhn, 2005). Similarly, certain membrane proteins such as Cav-1, nSMase2 and Vps4A have been implicated in EV biogenesis and in the process have been shown to selectively shuttle miRNAs (Groot & Lee, 2020). Intriguingly, we see that there is an increase in the expression of both Vps4A and nSMase2 in microglial cultures (Figure 6f). However, the purpose of selective sorting is still not completely understood. Whether the cell secretes specific miRNAs as a means of eliminating unnecessary RNAs, including miRNAs, or for a specific signalling mechanism is challenging to determine at this point. It has been reported by others that miR-29a can bind to RBPs such as YBX1 and TRIM71 (Treiber et al., 2017). Hence, a similar mechanism of miR-29a sorting into EVs could be possible for miR-29a sorting as a result of inflammation during chronic MA exposure. More mechanistic studies along these lines will be needed in the future to understand these complex processes.

Furthermore, we wanted to determine whether EVs isolated from WT microglia treated with MA would induce similar deficits. EV characterisation from WT microglia treated with MA revealed a significant increase in EV-miR29a expression. As expected, we see a decrease in synapse and spine numbers in cultures treated with EVs isolated from WT microglia treated with MA when compared to EVs isolated from non-treated controls. Again, no effect was observed on neurons isolated from TLR7$^{-/-}$ animals (Figure 7). These data confirm that chronic MA treatment on microglia released EVs containing neuro-damaging cargo leading to synaptodendritic injury. Interestingly, differential expression of TLR7 in various cell types largely affects the activation of different signalling mechanisms. For example, a previous study showed that both miR-21 and miR-29a bind and activate TLR7 in macrophages, stimulating NFκB pathway and producing an inflammatory response (Fabbri et al., 2012). In a previous study from our group, we revealed that miR-21 failed to activate the canonical TLR7 signalling in neurons but initiated a novel cell death pathway, necroptosis, leading to neuronal cell death (Yelamanchili et al., 2015). Similarly, other studies have shown that yet another TLR7/8 binding miRNA, Let-7b, could activate TLR7 and induce apoptosis of cortical neurons via activation of myeloid differentiation factor 88 (MyD88)-dependent signalling pathways (Lehmann et al., 2012). However, when Let-7b is applied extracellularly, it induces neuronal activation and the excitation of the nociceptor dorsal root ganglion (DRG) neurons via the TLR7/TRPA1 interaction on the surface, therefore eluding the intracellular (e.g., MyD88, PKA, PKC, PLC and MAPK) signalling (Park et al., 2014). These data clearly conclude that EV-miRNAs can have pleotropic effects and therefore the downstream mechanisms could largely vary and depend on cell-type, such as immune cells or neurons. These data collectively reveal that EV-miR29a could be responsible for the induction of synaptodendritic injury during MA misuse.

While the effects of EV-miR29a were identified in the in vitro model, the larger and more challenging question to answer is whether there is a direct relationship among chronic inflammation, EV-miR29a and drug-seeking behaviour. To understand this relationship, we used the SA rat model. This model mimics the three phases of addiction: active drug-seeking, extinction (abstinence) and reinstatement (relapse). Behaviour analysis clearly showed that rats receiving MA were more actively seeking

the drug than the saline group. When BDEs were isolated from the brain cortices and EV number and miR-29a expression were measured, the results showed that there was a sustained increase in EV number and miR-29a expression after extinction, and a further increase was seen after MA reinstatement only in animals that self-administered MA (Figure 8c and d). These results clearly indicate that chronic exposure to MA caused perturbations in EV biogenesis, thereby leading to increased secretion of EVs and their associated miR-29a cargo. A surprising effect was the higher expression of miR-29a even after drug extinction indicating that chronic inflammation could be driving these effects. This is supported by our previous works where we showed that chronic drug-seeking enhanced neuroinflammation (Charntikov et al., 2015). Moreover, drug reinstatement further reinforced these effects, indicating that the increase in EV secretion and its associated miR29a is a direct effect of MA-induced changes to the EV biogenesis pathway. Interestingly, a recent study showed that active MA use could potentially increase plasma EV number (Sandau et al., 2020). To further delineate the role of MA-BDE on neuronal function, we conducted a comprehensive functional study on primary neuronal cultures that have been treated with BDE isolated from rats that were reinstated with either SAL or MA. Results indicated that MA-BDE elicited both pro-inflammatory as well as injurious responses and specifically we were able to show that MA-BDE can elicit inflammatory response via TLR7 (Figure 8e–g). Dendritic spine density in prefrontal neurons have a direct relationship to synaptic plasticity and behaviour in primates as well as rodents (Kolb & Gibb, 2015). It is well known that alterations in spine density could lead to perturbations in neuronal circuit functioning (Kolb & Gibb, 2015). Our results show a significant decrease in spines indicating that MA-BDE could potentially cause damage to the neural circuits. Previous studies showed that repeated MA exposure increased as well as decreased spine density in different areas of dorsal striatum (Jedynak et al., 2007). There are no studies describing the same in SA models or in models of relapse. Our studies for the first time show that the chronic effects of MA toxicity in the brain could be a result of BDE carrying neurotoxic cargo which could possibly exacerbate neuronal injury during relapse. Although EVs and their associated miRNA cargo have been discussed as potential tools for investigating neuronal health and as novel drug targets in drug addiction (Rao et al., 2018), so far there are no reports directly correlating the effects of EVs, miRNAs and addiction behaviours. Our data for the first time shows such a direct correlation between EV-miRNA and MA addiction using the SA model system.

To delineate the role of inflammation, we investigated whether ameliorating inflammation would reduce EV secretion and subsequently affect EV-miR29a levels and therefore rescue synaptodendritic injury. Recent studies support the potential use of anti-inflammatory drugs to ameliorate the behavioural and cognitive consequences of addiction (Kohno et al., 2019). One such drug, Ibudilast (IBUD) or AV411, a phosphodiesterase inhibitor has shown promising results in animal models of MA addiction (Charntikov et al., 2015). IBUD can easily cross the blood brain barrier (BBB), and clinical trials in MS patients have shown that the drug is well tolerated and safe to be used in humans (Kolahdouzan et al., 2019). Intriguingly, phosphodiesterases are important enzymes that not only act as secondary messengers but are also involved in ceramide biosynthesis which, in turn, regulates EV biogenesis. A significant amount of work has been shown regarding sphingolipid phosphodiesterases as inhibitors of EV biogenesis and release (Trajkovic et al., 2008). Similar to the chronic MA administration in macaques, EV biogenesis and miR-29a expression were significantly enhanced in rats which were under a SA regimen. MA also significantly increased the expression of IBA1, microglial marker, as well as proinflammatory cytokines TNFα and IL6 in both brain and blood (Figure 9a and b). These data clearly indicate that MA contributes to both brain and peripheral inflammation. Surprisingly, administering IBUD after MA regimen significantly rescued inflammation as seen from decreased expression of IBA1 as well as proinflammatory cytokines. Several studies of Human Immunodeficiency Virus-1(HIV) Tat-Mediated activation of microglial cells (Kiebala & Maggirwar, 2011), MPTP model of Parkinson's Disease (Schwenkgrub et al., 2017), experimental arthritis (Clanchy & Williams, 2019) and Multiple Sclerosis (MS) (Fiedler et al., 2017) have also shown a similar anti-inflammatory effect of IBUD. Furthermore, we see that IBUD treatment reduces the BDE number as well as miR-29a levels in MA rats (Figure 9c and d). Therefore, we wanted to investigate whether IBUD can rescue EV biogenesis. To test this, we pretreated microglial cells with IBUD before treating with MA. QRT-PCR data clearly revealed a decrease in many ESCRT-dependent and -independent genes that went up with MA treatment. EV marker proteins, *FLOT2* and *ALIX*, and ESCRT genes such as *HRS, STAM2, VPS28, VPS37A, VPS37B* and *VPS25* were decreased by pretreatment with IBUD. Surprisingly, an increase in *CD63* and *FLOT1* was seen with IBUD treatments, indicating a probable increase in EV release; however, this result directly contradicts our NTA data where we showed a decreased secretion of EVs after IBUD treatment. A plausible explanation for this discrepancy comes from recent studies that highlighted a synergistic relationship between autophagy and EV biogenesis pathways (Salimi et al., 2020). Intriguingly, a recent study showed that IBUD increases autophagosomal synthesis, indicating that the autophagic clearance pathway might be its target of action (Chen et al., 2020). Emerging evidence clearly indicates a direct link between autophagy and EV biogenesis through shared molecular machinery or organelles (Xu et al., 2018). It has also been shown that CD63 bridges autophagy and endosomal pathways (Hurwitz et al., 2018). Therefore, increase in intracellular *CD63* is not a direct indication of increased EV biogenesis but could result from potential activation of autophagic pathways by IBUD to protect cells from the harmful effects of MA. It is well known that autophagy plays a fundamental role in regulating immunity and inflammation (Matsuzawa-Ishimoto et al., 2018) and therefore could be the most likely explanation for IBUD action on EV biogenesis in MA-treated cells. On the other hand, it is unclear why an increase in *FLOT1* and a decrease in *FLOT2* expression was seen with IBUD. Both FLOT1 & 2 are expressed in small EVs and are enriched in lipid raft domains, whether IBUD influences such lipid domains is still unclear at this point. More detailed investigation would be required to understand these effects. These are novel observations and have never been reported

earlier. Although, several studies considered the role of EVs in perpetuating inflammation (Console et al., 2019), here, for the first time we report the direct effect of an anti-inflammatory agent on EV biogenesis.

Finally, to explore the translational relevance of these works, we evaluated the expression of plasma miR-29a as a potential biomarker for MA use disorder. Although, there are reports of plasma EV protein or RNA as biomarkers for disease progression and pathogenesis in several disorders, there have been few reports in addiction field, specifically, only in alcohol abuse (Kodidela et al., 2019). EV-miRNA cargoes have several advantages over protein cargoes, due to their extreme stability in the plasma (Ge et al., 2014). Hence, plasma EVs and their miRNA cargo can serve as perfect windows into brain disorders. Here, we evaluated the presence of miR-29a in plasma EVs from the chronic macaque model as well as from human male MA users using DDPCR that clearly revealed the upregulation of EV-miR29a copies in plasma EVs from MA groups in the two species. These data collectively suggest that EV-miR29a from plasma could be used as a potential marker to indicate neuronal damage in human MA misusers. A recent study on plasma-derived EVs from a population ($n = 10$) of MA active female users showed that there is increased EV biogenesis in users that actively misused MA throughout their lifetime when compared to non-MA users, further supporting our observation with BDE (Sandau et al., 2020). The authors further claim that they saw an overall reduction in the miRNA content in the plasma EVs. Our RNA sequencing results from BDE also revealed very few upregulated miRNAs compared to the larger portion of the downregulated miRNAs in the BDEs. Intriguingly, the authors also reported downregulation of miR-29a in the plasma EVs from female MA users who were classified as active smokers when compared to users that did not smoke, indicating that smoking influenced the miRNA expression profile in plasma. The study did not show an increased expression of miR-29a in EVs when compared to non-MA users. Interestingly, our cohort consists of only males, and only one male MA user has reported as an active smoker. It is highly likely that an interesting sex-specific difference exists, and these data needs to be evaluated in future works.

In summary, using both in vivo and in vitro model systems, we provide novel evidence on the role of a brain-derived EV (BDE) miRNA, miR-29a, to play a critical role in MA use disorder. Specifically, we show that chronic MA exposure leads to secretion of different EV subtypes and that miR-29a is localised to the EV pool enriched in sEVs and exomeres. We also provide a therapeutic relevance of the anti-inflammatory drug, IBUD, which was shown to rescue EV biogenesis, reduce the secretion of miR-29a, and rescue synaptodendritic injury. Our data further support the use of IBUD as a therapeutic intervention for MA use disorder. Finally, we show that miR-29a is upregulated in plasma obtained from male participants identified with MA use disorder, indicating a possible role as a potential biomarker for therapeutic interventions.

4 | METHODS

4.1 | Ethics

Nonhuman primate (*Macaca mulatta*) specimens used in these studies were from previous animal studies performed under Institutional Animal Care and Use Committee approval (Protocol #: 11-032-05FC) at the University of Nebraska Medical Center. Animal welfare was maintained by following the National Institutes of Health Guide for the Care and Use of Laboratory Animals (National Research Council of the US National Academy of Sciences) and US Department of Agriculture policies by trained veterinary staff and researchers under Association for Assessment and Accreditation of Laboratory Animal Care certification, insuring standards for housing, health care, nutrition, environmental enrichment and psychological well-being. Conditions met or exceeded those set forth in the Guide for the Care and Use of Laboratory Animals from the National Research Council of the US National Academy of Sciences. Following saline or MA administration, as described in the text, animals were sacrificed following deep anesthesia by intracardiac perfusion with sterile PBS containing 1 U/ml heparin. Tissues were removed and dissected, and specimens placed in formalin for paraffin embedding as well as frozen and stored at -80° until use.

4.2 | Animal samples, and methamphetamine treatment

MA treatments was performed as described previously (Niu et al., 2020). Briefly, male macaques were acclimated to the drug using an escalating protocol, where the concentration of MA was slowly increased over a month-long period (0.1–2.5 mg/kg of MA dissolved in sterile saline, delivered intramuscularly; Sigma Aldrich, St. Louis, MO, USA). After the ramp-up phase, animals were maintained at 2.5 mg/kg using a five-day on and 2-day off paradigm for the entire study period (28 weeks). Untreated animals were injected with saline following the same injection regime. Blood samples were taken after 56 days of maintenance for assessment. Necropsies were performed as determined by the animal protocol. At necropsy, deeply anesthetised animals were perfused intracardially with sterile PBS containing 1 U/ml of heparin to clear blood including blood-borne cells from the brains, and brains harvested for histopathology, viral determination and further experimental studies. Drug regimen and animal details are provided in Figure S1 and Table S1.

4.3 | Rat MA self-administration

Experimental protocols were approved by the University of Nebraska–Lincoln Institutional Animal Care and Use Committee.

4.3.1 | Subjects

Twenty-six Sprague Dawley rats (17 M, 9 F) were obtained at 9-weeks old from Envigo (Indianapolis, IN, USA). Rats were handled by experimenters for 3 days upon arrival to allow for acclimation to the temperature- and humidity-controlled colony room. Following acclimation, rats were food restricted to a target weight of 90% of their free-feeding weight; target weights were increased by 2 g each month to allow for typical growth. Water was available ad libitum in the home cage throughout the experiment. Experiments were conducted during the light phase of a 12-h light-dark cycle (6AM-6PM). The protocols for this study were approved by the University of Nebraska-Lincoln Institutional Animal Care and Use Committee.

4.3.2 | Apparatus

Experimental sessions were conducted in ten standard conditioning chambers (ENV-008CT; Med Associates IV, Georgia, VT, USA). Chambers (30.5 cm × 24.1 cm × 21 cm; l × w × h) were light- and sound-attenuating with aluminum sidewalls, metal rod floors, and clear polycarbonate ceiling, front, and back walls. The dipper receptacle was mounted on the right aluminum sidewall occupying a 5.2 × 5.2 × 3.8 cm (l × w × h) recessed space. Here, a dipper arm with an attached 0.1-ml cup was raised to provide access to a solution inside the chamber. An infrared beam located within the dipper receptacle recorded the number of dipper entries. A variable-speed syringe pump (PMH-100VS; Med-Associates) was located outside each cubicle. Tygon tubing was attached to the pump syringe, threaded through a metal spring leash, and into the ceiling of the chamber where it was to be attached to the catheter port on the back of the rat. Two retractable levers were located on each side of the receptacle. A white cue light (2.54-cm diameter; 28 V, 100-mA) was mounted 7 cm above each lever. A house light (two white 28 V, 100-mA lamps) was located in the cubicle, 10 cm above the chamber ceiling. Med Associates interface and software (Med-PC for Windows, version IV) were used to collect data and present programmed events. All Med-PC programs are available upon request.

4.3.3 | Drugs

(+)-Methamphetamine hydrochloride obtained from Sigma–Aldrich (St. Louis, MO, USA) was dissolved in 0.9% sterile saline. Meth was infused intravenously at 35.74 ul over 1 s at 0.05 mg/kg/infusion. For the drug-primed reinstatement session, 0.5 mg/kg meth was injected intraperitoneally (IP) 15-min before the chamber placement. Dose for self-administration and drug-primed reinstatement were based on previous research (Pittenger, Barrett, Chou et al., 2016). All doses are expressed in the salt form.

4.3.4 | Lever training

Following colony acclimation, all rats received 5 days of sucrose-reinforced lever training using a fixed ratio 1 (FR1) schedule of reinforcement. Training sessions began with the insertion of one of the two levers into the chamber and house light illumination. Following one lever press or a lapse of 15 s, the lever retracted, liquid sucrose (26% v/v) was presented in the dipper receptacle for 4 s, the house light was extinguished and a time-out period occurred (duration ranged between 30 and 89 s). Following the time-out period, the opposite lever was inserted into the chamber. All rats received equal presentations of both levers (60 lever presentations total). Sessions were completed when the rat received 60 sucrose presentations; session duration varied based on individual performance (65–80 min).

4.3.5 | Surgery

Rats were implanted with an indwelling catheter into the right jugular vein (cf. Pittenger, Barret, Chou et al., 2016). Rats received a 1 ml/kg intramuscular injection of 2:1 ratio cocktail of ketamine HCL (100 mg/ml) and xylazine HCL (20 mg/ml) to anesthetise the animal. After surgery, rats were injected with 0.1 mg/kg buprenorphine to manage pain and 0.5 mg/kg atipamezole to terminate anesthesia. Buprenorphine was administered a second time 24-hr after surgery. Rats were allowed to recover for 7 to 8 days during which their catheters were flushed with 0.2 ml of a baytril (5 mg/ml) and heparin (30 U/ml) solution. On the final day of

self-administration (day 25), rats underwent a catheter patency check by intravenous infusion of 0.05 ml xylazine (20 mg/ml). Rats that displayed motor ataxia within 20 s of infusion were considered to have patent catheters.

4.3.6 | Post-surgery training

Following recovery, rats received three days of post-surgery lever training with sucrose. During each 1-h session, 4-s sucrose reinforcement was available following a variable ratio 3 (VR3) schedule of reinforcement. Each lever was presented individually and alternated between sucrose presentation to prevent lever preference. Training produced robust lever pressing on both levers such that all rats earned more than 80% of the 60 available sucrose reinforcers.

4.3.7 | Self-administration

Rats received 25 days of self-administration in which they received group-specific intravenous infusions of either 0.05 mg/kg/infusion meth ($n = 12$) or saline ($n = 14$). Self-administration sessions were conducted for 2 h per day, 7 days per week. Rats were randomly assigned which lever was designated as the active lever (meth or saline infusion) versus the inactive lever. Before each session, rats were flushed with 0.2 ml of heparinised saline (30 U/ml). During each session, both levers were inserted into the chamber. Completion of a VR3 schedule of reinforcement on the designated active lever resulted in an infusion of 0.05 mg/kg/infusion meth or saline, retraction of both levers, illumination of the house light, and a 20-s time-out. Following each time out, both levers were inserted back into the chamber and the house light was extinguished. Inactive lever responses were recorded but had no programmed consequence. At the end of each session, rats were flushed with 0.2 ml of a cocktail comprised of baytril (5 mg/ml) and heparinised saline (30 U/ml).

4.3.8 | Extinction

Extinction sessions were procedurally identical to self-administration sessions with the exception that the completion of a VR3 on the active lever resulted in the same cue presentations (i.e., lever retraction, house light illumination) but infusions of meth or saline were not delivered. Rats underwent 14 days of extinction.

4.3.9 | Reinstatement

Following extinction, rats received one drug-primed reinstatement session. Rats were randomly assigned to receive an intraperitoneal injection of either 1 mg/ml saline ($n = 13$) or 0.5 mg/ml meth ($n = 13$) 15 min before the 2-h session. The reinstatement session was procedurally identical to extinction sessions in which intravenous infusions of meth or saline were withheld.

Archived rat brains used for this study were a part of the previously published works by Charnitkov et al. (2015).

4.4 | Reagents and drugs

Synthetic miRNAs with phosphorothioate or phosphodiester linkages were synthesised, desalted and purified by reverse-phase cartridge by Sigma-Aldrich (St. Louis, MO, USA). The sequences are: miR-29a-3p (5′-UAGCACCAUCUGAAAUCGGUUA-3′), 29 Gmut (5′ UAGCACCAUCUGAAAUCAAUUA -3′), 29 Umut (5′-UAGCACCAUCUGAAAUCGGCCA -3′), 29 GUmut (5′ UAGCACCAUCUGAAAUCAACCA -3′). For in vitro studies, (+)-Methamphetamine hydrochloride (Sigma, St. Louis, MO) was dissolved in sterile PBS and Ibudilast (Sigma) was dissolved in distilled water.

4.5 | Mice, rats and cell lines

Tlr7$^{-/-}$ mice were purchased from Jackson Laboratories (Bar Harbor, Maine) and bred in the UNMC animal facility. Pregnant wildtype (WT) mice and Sprague Dawley rats were purchased from Charles River (Wilmington, MA, USA). RAW 264.7 macrophages (American Type Culture Collection, Manassus, VA, USA) were cultured in Dulbecco's modified eagle's medium (DMEM) (Invitrogen, CA, USA) supplemented with 10% fetal bovine serum (FBS) (Invitrogen) and penicillin-streptomycin. The NR-9460 microglial cell line, derived from wild-type mice (WT-MG), and the NR-19980 microglial cell line, derived from toll-like receptor 7 (TLR7) knockout mice (denoted TLR$^{-/-}$-MG) (BEI Resources, Manassus, VA, USA), were cultured in DMEM

supplemented with 10% FBS, 2 mM L-glutamine, 1 mM sodium pyruvate and 10 μg/ml ciprofloxacin. Cells were grown to confluence at 37°C in humidified air with 5% CO_2. Details for the cell lines are provided in supplemental files S1&S2.

4.6 | Human biobank plasma samples

The office of Regulatory Affairs has determined that this study does not constitute human subject research as defined at 45CFR46.102(f). Plasma samples acquired from the Nebraska Biobank are collected from the Nebraska Medicine Clinical Laboratory from patients who have consented to donate their leftover clinical samples to the biorepository for research. Excess blood, serum or plasma collected solely for clinical purposes is stripped of identifiers prior to entry into the biorepository. These samples are linked via one-way hashing using an industry standard 128-character code and Secure Hash Algorithm (SHA-128) to a subset of clinical data which itself contains no identifying information. This link allows addition of subsequent, non-identifiable clinical information to the database, but it is not possible to infer or compute the medical record number that generated the string.

Blood samples are collected into lithium heparin tubes (green top vacutainer tubes with gel separator). Plasma samples are spun in the clinical laboratory and stored at 4°C in the Nebraska Medicine Clinical Laboratory until their release (up to 5 days) to the Nebraska Biobank. Donor consent is checked for these released samples using a TECAN EVO Freedom 100 liquid handling robot programmed to accept only consented and unique samples, that is, duplicate tubes from the same donor are not accrued. Consented samples are aliquoted into 2D bar-coded tubes for long-term storage using a TECAN EVO Freedom 200 liquid handling robot. Bar-code and tube location data are imported into Dataworks Development Inc. 'Freezerworks,' a 21 CFR Part 11 compliant LIMS and linked to the de-identified database. Repository samples are stored in dedicated, secured, -80°C ultralow freezers equipped with CO_2 back-up, temperature surveillance and alarm notification systems. Sample search was performed against the Nebraska BioBank Database by generating SQL queries for cases and controls separately as per the inclusion (MA use disorder/MA addiction) and exclusion criteria (No HIV or polydrug use). The complete demographics for the individual donors are now made available in the Table S4.

4.7 | ELISA assays

Cells were prepared as above and stimulated for 16 h with 6 mg/ml of miRNAs complexed to the transfection agent N-[1-(2,3-Dioleoyloxy)propyl]-N,N,Ntrimethylammonium methylsulfate (DOTAP) (1811177; Roche, Basel, Switzerland). Conditioned medium was collected and analysed by TNF-α, IL1β and IL6 ELISA kit as per manufacturer's instructions (eBioscience, San Diego, CA, USA). Final cytokine concentrations were calculated based on a standard curve constructed in each independent experiment. Values <8 and >1000 were recorded as 8 and 1000, respectively.

4.8 | Fluorescent in situ hybridisation (FISH) and immunofluorescent (IF) labelling

FISH and IF were performed as described previously (Chaudhuri et al., 2013). First, formalin-fixed paraffin-embedded sections were deparaffinised. For combined FISH and IF, this was followed by antigen retrieval using 0.01 M citrate buffer and postfixation using 0.16 M l-ethyl-3-(3-dimethylaminopropyl) carbodiimide (EDC; Sigma–Aldrich, St. Louis, MO, USA) to prevent loss of small RNAs. The sections were incubated with hybridisation buffer (50% formamide; 10 mM Tris-HCl, pH 8.0; 200 μg/ml yeast tRNA; 1× Denhardt's solution; 600 mM NaCl; 0.25% SDS; 1 mM EDTA; and 10% dextran sulfate) for 1 h at 37°C in a humidified chamber for prehybridisation. They were then incubated overnight at 37°C with locked nucleic acid (LNA)-modified DNA probes, all labelled with digoxigenin at the 5′- and 3′-termini (Exiqon, Woburn, MA, USA). Probes were used at a concentration of 4 pmol of probe per 100 μl of hybridisation buffer. The sequences of the probes are; U6: 5′-CAC GAA TTT GCG TGT CAT CCT-3′ ; miR-29a: 5′-UAG CAC CAU CU GAA AUC GGUU A -3′. Stringency washes were performed with 2× and 0.2× SSC (Invitrogen, Carlsbad, CA, USA) at 42°C. The hybridisation and wash temperatures were optimised in preliminary experiments. The sections were then blocked with a solution of 1% BSA, 3% normal goat serum in 1× PBS for 1 h at room temperature, followed by incubation with anti-digoxigenin peroxidase antibody (1:100 in blocking buffer; Roche Applied Science, Mannheim, Germany) overnight at 4°C. For combined FISH and IF, co-incubation with either anti-IBA1 (1:1000; Wako, Mountain View, CA, USA) or anti-glial fibrillary acidic protein (GFAP; 1:2000; Dako, Glostrup, Denmark) was performed at this step. The following secondary antibodies were used: 568 donkey anti-rabbit and 488 goat anti-mouse IgG (1:400; Invitrogen). This was followed by signal amplification using tyramide signal amplification Cy5 kit (Perkin Elmer, Waltham, MA, USA) according to the manufacturer's protocol. The slides were mounted in Prolong gold antifade reagent with DAPI (Invitrogen). The sections were imaged in Zeiss Observer.Z1 microscope equipped with a monochromatic Axiocam MRm camera using Axiovision 40 v.4.8.0.0 software (Carl Zeiss, Oberkochen, Germany). The following colours were assigned to the fluorescent signals using the Axiovision software: Green for MAP2, Red for GFAP/IBA1, Magenta for Cy5-MiR, Blue for DAPI. ImageJ software was used to quantify the ISH

images according to the previously published protocol (Lu & Tsourkas, 2011). Briefly, all images were processed to binary images and total number of isolated signals within single cells was calculated in ImageJ using the particle analysis counter programme as described in the protocol. A total of 100 cells per group were obtained from 10 images from each animal ($n = 5$ per SA/MA) were used for analysis.

4.9 | MA 'binge' treatments, N-RH-PE labelling and EV isolations

The NR-9460 microglial cell line, derived from wild-type mice (WT-MG) (BEI Resources, Manassas, VA, USA), were cultured in DMEM supplemented with 10% FBS, 2 mM L-glutamine, 1 mM sodium pyruvate and 10 μg/ml ciprofloxacin. Cells maintained at 37°C in humidified air with 5% CO_2. For dose response assay, cells were treated with increasing concentrations of MA (50–500 μM) or saline for 24 h followed by toxicity assay. For the time course assay, cells were treated with a single dose (1×) of 100 μM MA for 24 h or 2× doses of MA over 48 h (once every 24 h) or 3× doses of MA over 72 h. Before treating the cells with the second dose, EVs were isolated from media, which served as control (please see section below for EV isolation from media). The cells were supplemented with fresh media with the second dose of 100 μM MA or PBS, and EVs were isolated immediately after 1 h. Fresh media was replaced again and EVs were re-isolated after 24 h of repeated MA treatments. For labelling experiments, microglia were labelled with 1,2-dipalmitoyl-sn-glycero-3 phosphoethanolamine-N-[lissamine rhodamine B sulfonyl] (N-Rh-PE), a fluorescent phosphatidyl ethanolamine analogue that has been shown to be taken up at the plasma membrane of cells, sorted to endosomes, and secreted in exosomes (Willem et al., 1990). Cells were incubated with 1 μM N-RH-PE at 4°C for 60 min, followed by washing three times with PBS. Post-labelling, the media was replaced with growth medium containing either 100 μM MA or saline for 24 h at 37°C. Finally, the cells were fixed in 4% PFA for confocal microscopy.

4.10 | EV isolations from media supernatants

The NR-9460 microglial cell line, derived from wild-type mice (denoted WT microglia), and the NR-19980 microglial cell line, derived from TLR7 knockout mice (denoted $TLR7^{-/-}$ microglia) (BEI Resources, Manassas, VA, USA), were cultured in DMEM supplemented with 10% FBS, 2 mM L-glutamine, 1 mM sodium pyruvate and 10 μg/ml ciprofloxacin. To isolate EVs from media, ~ 20–25 × 10^6 cells were plated per T75 flask (three flasks per condition) and grown in EV-free complete media. To prepare the EV-free complete media, DMEM supplemented with 10% FBS was spun at 200,000 × g at 4°C for 1 h. Cells were grown in EV-free media and grown to confluence at 37° C in humidified air with 5% CO_2. EVs were prepared from the media supernatants of immortalised microglial cells by differential centrifugations. Conditioned media were harvested, centrifuged at 1000 × g for 10 min to eliminate cells, and again spun at 10,000 × g for 30 min, followed by filtration through a 0.22-μm filter to remove cell debris. EVs were pelleted by ultracentrifugation ((Beckman Coulter SW32Ti rotor; Beckman Coulter, Brea, CA, USA) at 100,000 × g (adjusted *k-factor* = 624.65; rotor SW32Ti) for 70 min. EVs were assessed for their protein content using a BCA Protein Assay Kit (Pierce, Rockford, IL, USA). TSG101 and CD63 were detected by Western blot as exosome markers. EVs were further quantified by TEM and NTA. For treatments on neurons, 1 × 10^9 particles (~25 μl volume) were used.

4.11 | EV isolations from brain tissue

EV isolations from the brains were carried out as described previously with modifications (Chand et al., 2020, Perez-Gonzalez et al., 2012). Previously dissected and frozen macaque (frontal grey) or rat brain tissues (prefrontal cortices) (weighing approximately 450 mg each) were dissected and treated with 20 U/ml papain (Worthington, Lakewood, NJ) in Hibernate A solution (5 ml/hemi-brain; BrainBits, Springfield, IL, USA) and rocked for 15 min at 37°C. In our modified protocol, we preferred using Hibernate A for adult tissues instead of Hiberate E which is recommended for embryonic tissues as described in the original protocol (Perez-Gonzalez et al., 2012).The brain tissue was gently homogenised in 10 ml/brain of cold Hibernate A solution. The brain homogenate was sequentially filtered through a 40 μm mesh filter (BD Biosciences, San Jose, CA), and a 0.2 μm syringe filter (Corning Incorporated (catalog # 431219), Corning, distributed by Thermo Scientific, Waltham, MA). EVs were isolated from the filtrate as described previously (Lopez-Verrilli & Court, 2012; Perez-Gonzalez et al., 2012). Briefly, the filtrate was sequentially centrifuged at 300 × g for 10 min at 4°C, 2000 × g for 10 min at 4°C, and 10,000 × g for 30 min at 4°C to discard cells, membranes, and debris. The supernatant was put in Beckman Coulter Centrifuge Tube (# 344058) and was centrifuged at 100,000 × g (adjusted *k-factor* = 624.65; rotor SW32Ti) for 60 min at 4°C to pellet EVs. The EV pellet was resuspended in 37 ml of cold PBS (Thermo Scientific, Waltham, MA), and the EV solution was centrifuged at 100,000 × g (adjusted k-factor = 624.65; rotor SW32Ti) for 60 min at 4°C. The washed EV pellet was resuspended in 2 ml of 0.95 M sucrose solution and inserted inside a sucrose step gradient column (six 2-ml steps starting from 2.0 M sucrose down to 0.25 M sucrose in 0.35 M increments, with the

0.95 M sucrose step containing the EVs). The sucrose step gradient was centrifuged at 200,000 × *g* (adjusted *k-factor* = 256.65; rotor SW41Ti), 7 acceleration and 7 deceleration for 16 h at 4°C. A 1-ml fraction was collected from the top of the gradient and discarded, and 6 ml of the gradient were collected in the EV rich layers containing material with a density higher than 1.07 (0.60 M sucrose layer) and lower than 1.17 (1.30 M sucrose layer) (Perez-Gonzalez et al., 2012). Pooled fractions were diluted to 30 ml with cold PBS. and centrifuged at 100,000 × *g* (adjusted *k-factor* = 624.65; rotor SW32Ti) at 4°C for 60 min. PBS was pipetted off the pellet. Pellet was suspended in 50 to 100 μl of PBS depending on pellet size and was used for RNA extraction and Western blot studies.

4.12 | Electron microscopy

For transmission electron microscope (TEM), a 10 μl drop of EV sample was placed on the grid (200 mesh copper grids coated with Formvar and silicon monoxide) and allowed to sit for 2 min. The excess solution was drawn off by filter paper, and the remaining thin film of sample was allowed to dry for 2 min. A drop of NanoVan negative stain was placed on the grid for 1 min. The excess negative stain was then drawn off by filter paper and allowed to dry for at least 1 min before being placed in the TEM. Grids were examined on a Tecnai G2 Transmission Electron Microscope (built by FEI, Hillsboro, Oregon, USA) operated at 80 Kv.

4.13 | Nanoparticle tracking analysis (NTA)

EV size distribution curves and concentration measurements were carried out by NTA using a Nanosight NS300TM (Malvern Instruments, UK). For NTA analysis, EV pellets were resuspended in 100 μl of particle free PBS (PBS spun at 100,000 × *g* for 1 h to remove salts and other particulates), following which 10 μl of the sample was diluted to 1:100 to 1:1000 in PBS prior to measurements. All samples were loaded with the laser module outside the instrument. As the sample was loaded, care was taken to avoid air pockets. The machine was equipped with a 488 nm laser and a syringe pump system, with a pump infusion speed of 20. The standard measurement option was selected for the scripted workflow to capture videos. The number and duration of captures were set to 5 and 60 s, respectively. The base filename and location were selected prior to starting the run. The camera level was set at 11. Background measurements were performed with particle free filtered PBS, which revealed the absence of any kind of particles. Five video recordings were carried out for each EV preparation with a duration of 60 s with frame rates of 25 frames/s. Once the videos were recorded, the NTA 3.1 software version was used to analyse the sample videos. For analysis, the screen gain was set to 1.0, and the detection threshold was adjusted to set the minimum brightness of pixels to be considered. At the end of the analyses, the dilution factor for the samples was updated before data export.

4.14 | RNA isolation and qRT-PCR (BDEs, media derived EVs and tissues)

Total RNA for miRNA sequencing isolated from both monkey and rat BDE and media derived EV samples was performed using the miRVANA miRNA kit (Thermo Scientific, Rockford, IL, USA) as per the manufacturer's instructions. Briefly, EV pellets are lysed in mirVana lysis buffer and incubated for 10 min on ice. Organic extraction was performed by addition of one-tenth volume of miR homogenate additive, followed by incubation for 10 min. Acid-Phenol:Chloroform was added, briefly vortexed and centrifuged at 10,000 x *g* for 5 min to separate the aqueous and organic phase. For total RNA isolation, 1.25 volumes of 100% ethanol were added to the separated aqueous phase and passed through filter cartridge. The filter was washed with the wash solutions provided in the kit and the RNA was eluted using pre-heated nuclease free water. Preheated nuclease free water passed through column to recover RNA. Nano Drop Spectrophotometer was used to quantify RNA. For quantification of miRNA in EVs by qRT-PCR, TaqMan mature miR assays (Applied Biosystems, Carlsbad, CA, USA) for miR-29a-3p (Assay ID: 002112); miR-24-3p (Assay ID: 000402); miR-143-3p (Assay ID: 000466); miR-191-5p (Assay ID: 002299) and miR-126 (Assay ID: 002228) were used according to the manufacturer's protocol. The relative amount of miRs was determined by comparison to a standard dilution curve, made from known standards (copy number) created from synthetic miRs (Sigma–Aldrich, St. Louis, MO, USA). The Ct values of the samples were extrapolated into the standard curve to calculate the miR-29a copies/μl. We used the formula [RNA/DNA] = 10^Ct-b/m (where Ct = threshold Ct value, b = Y-intercept and m = slope) to calculate the amount of miRNA in each sample.

Total RNA from brain tissues were isolated using the Direct-Zol RNA kit (Zymo Research, Irvine, CA, USA) based on the manufacturer's protocol. Nano Drop Spectrophotometer was used to quantify RNA. cDNA was prepared from the respective samples using the Superscript IV kit (Invitrogen, Waltham, MA, USA), and thereafter RT-PCR was performed using TaqMan Custom Array Plates for genes involved with the endosomal sorting complexes required for transport (ESCRT) pathways (Applied

Biosystems, Carlsbad, CA, USA), see Table S5 for details on primers. The Delta-delta Ct method was used to calculate fold change. Data normalisation was performed using 18S and GAPDH as internal controls. Details for taqman primers are provide in Table S5.

4.15 | RNA sequencing

Small RNAseq was performed by LC Sciences (Houston, TX, USA). Quality check was performed by running the RNA on bioanalyzer before sequencing. Using the RNA isolated from EVs, a small RNA library was generated using the Illumina Truseq Small RNA Preparation kit following the manufacturer's guidelines. The cDNA library was purified and used for cluster generation on Illumina's Cluster Station and then sequenced on the Illumina GAIIx (Ilumina, San Diego, CA). Raw sequencing reads were obtained using Illumina's Sequencing Control Studio software (version 2.8) following real-time sequencing image analyses and base-calling by Illumina's Real-Time Analysis (version 1.8.70). A pipeline script, ACGT101-miR v4.2 (LC Sciences), was used for sequencing data analyses (Li et al., 2010, Meyer et al., 2011, Wei et al., 2011). Sequences were then mapped to miRbase (version 20.0) (Kozomara & Griffiths-Jones, 2014). 774 unique sequences mapped to both *Macaca mullata* mirs in miRbase and the *Macaca mullata* genome. Many of these had very low normalised counts; thus, only those with >635 counts in any one group (comprising 109 mirs) were chosen for statistical analyses. Normalisation of the miRNAs was performed by selecting a set of miRNAs that show similar expression across all the samples and re-calculating the library size parameter as described previously (Anders & Huber, 2010). To assess differences between the groups, normalised sequence counts were subjected to a Bayes-regularised one-way ANOVA using analysis conducted using the Cyber-T web server (http://cybert.ics.uci.edu) (Baldi & Long, 2001, Kayala & Baldi, 2012). The sliding window size was set at 101, the Bayesian confidence value was 11, and analysis was performed on the natural logarithm of the values. Significant changes were assigned if the Bonferroni corrected p value was < 0.05.

4.16 | Digital droplet PCR (DDPCR)

Droplet DD PCR was performed to quantify EV-miR29a from healthy and MA-addicted individuals. PCR mix reaction consisted of 20 μl volume, containing 4.25 μl of diluted cDNA, 10 μl of 2x Eva green super mix, 0.75 μl of 20x miR29a RT primer and 5 μl of nuclease free water. The master mix is then transferred to a 96 well reaction plate and run on a QX200 Automatic Droplet Generator (Bio-Rad). The droplet generator generates each reaction which is partitioned into 20,000 nanoliter-sized droplets, which are transferred to 96 well PCR plate, which is kept in C1000 Touch thermal cycler. PCR reaction was performed according to the manufacturer's instructions. The sealed 96-well plate was then transferred to a plate holder of the QX200 Droplet Reader. QuantaSoft software v1.7 was used to analyze the droplets in each well as well as to count copy number of miRNA in each sample.

4.17 | Isolation of EVs and total RNA from blood plasma

EVs and total RNA was isolated from blood plasma using the ExoRNeasy serum/plasma Midi kit (Qiagen, 77044) as described in previously published protocol (Alexander et al., 2021).

4.18 | Western blotting

To prepare BDE/EV, same amount of starting material was always chosen. BDE/EV lysates were prepared using RIPA buffer (50 mM Tris/HCl, pH 8; 150 mM NaCl; 1% Nonidet P-40; 0.5% sodium deoxycholate; and 0.1% SDS), and protein quantification was carried out using Pierce BCA protein assay (Thermo Scientific, Rockford, IL, USA). We used equal concentrations of particles for rat tissues as measured by NTA. All the BDE pellets were resuspended in equal volumes of particle free PBS. BDE protein was loaded in each lane of NuPAGE 4%–12% Bis-Tris gels (Invitrogen, Carlsbad, CA, USA). Separated proteins were transferred onto nitrocellulose membranes using iBlot 2 (Invitrogen, Carlsbad, CA, USA). The membranes were first stained with Ponceau stain (PS) to visualise equal loading, followed by washing with 1x PBS and blocking in SuperBlock (TBS) blocking buffer (Thermo Scientific). Membranes were then incubated overnight at 4°C with primary antibody followed by secondary antibody (see table below). Blots were developed with 1:1 solution of Radiance Chemiluminescent Substrate and Luminol/Enhancer (Azure Biosystems, Dublin, CA, USA). A c300 imaging system (Azure Biosystems) was used to visualise the blots, and images acquired were quantified using the ImageJ software version 1.52a. Ponceau stained blots were used for normalisation as published previously (Sander et al., 2019). Lanes were manually fit to each lane and strongly stained bands were quantified. Band intensities were totaled for each lane and used for normalisation. The following table described the running conditions, primary and secondary antibodies used in this study.

Antibody	Company	Cat#	Running condition	Host	Reactivity	MW (kDa)	1^0 Ab dilution	2^0 Ab	2^0 Ab dilution
TSG101	Abcam	ab133586	Reducing	Rabbit	mouse, rat, human	44	1:1000	HRP-conjugated goat anti-Rabbit	1:10000
CD9	SBI	EXOABCD9A-1	Non-reducing	Rabbit	human, mouse, r	28	1:500	HRP-conjugated goat anti-Rabbit	1:10000
Calreticulin	Cell signalling	2891S	Reducing	Rabbit	mouse, rat, human	55	1:1000	HRP-conjugated goat anti-Rabbit	1:10000
Hsp-90	Cell signalling	C45G5	Reducing	Rabbit	human, mouse, rat, monkey	90	1:1000	HRP-conjugated goat anti-Rabbit	1:10000
Flotillin-1	Abcam	ab41927	Reducing	Rabbit	human, mouse, rat, dog	47	1:1000	HRP-conjugated goat anti-Rabbit	1:10000
Alix	Santa Cruz Biotechnology	sc-99010 (h-270)	Reducing	Rabbit	human, mouse, rat, dog, horse, pig, bovine	95	1:1000	HRP-conjugated goat anti-Rabbit	1:10000
ANXA5	Abcam	ab14196	Reducing	Rabbit	human, mouse, rat,	36.8	1:1000	HRP-conjugated goat anti-Rabbit	1:10000
Arg-1	Cell signalling	D84G10	Reducing	Rabbit	human, mouse, rat, monkey	97	1:1000	HRP-conjugated goat anti-Rabbit	1:10000
Arg-2	Abcam	ab186733	Reducing	Rabbit	human, mouse, rat	97	1:1000	HRP-conjugated goat anti-Rabbit	1:10000
CD81	BIO-RAD	MCA1846	Non-reducing	Hamster	rat	~26	1:500	HRP-conjugated goat anti-Hamster	1:10000
CD63	BD Biosciences	BD551458	Non-reducing	Mouse	human, rat	30-60	1:500	HRP-conjugated rabbit anti-mouse IgG	1:10000
GAPDH	ThermoFisher	MA5-15738	Reducing	Mouse	bacteria, dog, chicken, hamster, human, insect, mouse, rabbit, rat, yeast	37	1:5000	HRP-conjugated rabbit anti-mouse IgG	1:10000
Apo-E	Santa Cruz Biotechnology	SC-390925 (F-9)	Reducing	Mouse	mouse, rat, human	36	1:1000	HRP-conjugated rabbit anti-mouse IgG	1:10000
GM130	BD Biosciences	610822	Reducing	Mouse	human, mouse, dog	130	1:1000	HRP-conjugated rabbit anti-mouse IgG	1:10000
Hsp-70	Millipore Sigma	SAB4200714	Reducing	Mouse	bovine, monkey, sea urchin, dog, human, insect, fish, chicken, mouse, rat, rabbit, plant	~70	1:1000	HRP-conjugated rabbit anti-mouse IgG	1:10000

(Continues)

Antibody	Company	Cat#	Running condition	Host	Reactivity	MW (kDa)	1^0 Ab dilution	2^0 Ab	2^0 Ab dilution
Alix	Biolegend	634501	Reducing	Mouse	mouse, human	96	1:1000	HRP-conjugated rabbit anti-mouse IgG	1:10000
VDAC1	Abcam	ab14734	Reducing	Mouse	mouse, rat, sheep, goat, cat, dog, human, pig, drosophila melanogaster, fish, quail, common marmoset, dogfish, catshark	39	1:1000	HRP-conjugated rabbit anti-mouse IgG	1:10000

4.19 | Primary neuronal isolation

Primary cortical cultures were isolated from postnatal P0/P1 mice or embryonic day 18 (E18) rat pups as described previously (Beaudoin et al., 2012). In brief, cortices were dissected and washed 3x with ice-cold calcium–magnesium-free Hanks' balanced salt solution followed by incubation with 0.25% trypsin for 20 min in a 37°C water bath. Followed by subsequent washes with HBSS and complete neuronal media (neurobasal medium containing 0.5 mM l-glutamine and B27 supplement (Life Technologies, Grand Island, NY)). Individual cells were mechanically isolated by trituration in complete neuronal media with a fire-polished glass pipette. The cells were plated on poly-d-lysine-coated coverslips/plates and cultured in at 37°C in a humidified atmosphere of 5% CO_2 incubator till DIV 14.

4.20 | DOTAP treatments on immortalised microglial and neuronal cultures

DOTAP treatments were performed as described previously (Yelamanchili et al., 2015). Synthetic miRNAs were complexed with DOTAP, which is capable of protecting as well as delivering miRNAs to the endosome (Sioud, 2005), to mimic miRNA delivery by EVs. Synthetic miRNAs were diluted in HBS buffer (20 mM HEPES, 150 mM NaCl, pH 7.4) or mixed with lipofection reagent N-[1-(2,3-Dioleoyloxy)propyl]-N,N,Ntrimethylammonium methylsulfate (DOTAP) (1811177; Roche, Basel, Switzerland). DOTAP was first diluted in HBS- for 5 min before mixing with an equal volume of HBS containing the RNA. The resulting mix was incubated for 20 min and 50 μl were added per well of a 24-well plate, resulting in a final volume of 200 μl. Transfections were conducted in triplicate in all experiments. The ratio of DOTAP to ssRNA was 3:1 (3 μl DOTAP to 1 μg RNA). After stimulation, conditioned medium was collected and TNFα ELISA was performed.

To treat cultures, reagents were added to cell cultures for 24 h. For EV toxicity (LDH) assay EV/BDE preparations (1 x 10^9 particles/ml) were added to either days in vitro 14 (DIV 14) differentiated primary neurons or to immortalised microglial cultures plated at a density of 2×10^5 cells/well in a 24 well plate. Control cultures were incubated with phosphate-buffered saline. After 24 h, LDH assay was conducted on the media according to the manufacturer's instructions (Cytotoxicity detection kit (LDH), Roche, Basel, Switzerland). Briefly, 100 μL of culture medium were transferred to a new 96-well plate. Hundred microlitres of the reaction solution from the kit, containing the detection dye and the catalyst, were then added; absorption was measured after 30 min at 490 nm with 655 nm as reference wavelength. A positive control, 2% triton was used leading to 100% cytotoxicity by lysing the cells completely. The background values from wells without cells were subtracted and average values for the triplicates calculated. Cytotoxicity was then calculated according to the following equation: Cytotoxicity (%) = (experimental value – media control)/(positive control – media control) × 100.

4.21 | Immunocytochemistry

After DOTAP treatments, DIV 14 neurons were fixed in 4% Paraformaldehyde (Thermo Scientific) in 1x PBS for 15 minutes at room temperature. Neurons were washed three times with 1x PBS. Neurons were then permeabilised with 0.25% Tween-20 (Thermo Scientific) in 1x PBS for 15 min. Cells were blocked in 0.5% Normal Goat Serum (Vector Labs Burlingame, CA), 0.25%

Tween-20, and 1% Bovine Serum Albumin (Millipore) in 1x PBS for 1 h at room temperature. Primary antibodies were diluted in 1% Normal Goat Serum, 0.25% Tween-20, and 1% Bovine Serum Albumin in 1x PBS. Primary antibodies were applied overnight at 4°C. Coverslips were washed three times with 1x PBS. Secondary antibodies and DAPI (Life Technologies) were diluted in the same buffer as primary, and coverslips were incubated in secondary for 1 h at room temperature. Cells were washed thrice in 1x PBS and once with de-ionised water then mounted with ProLong Gold antifade (Invitrogen) on Superfrost Plus charged microscope slides (Thermo Scientific). The following antibodies were used for ICC:

1° Antibody	Dilution	Company	Animal Host	2° Antibody	Dilution	Animal Host
MAP2	1:200	Thermo Scientific, (Rockford, IL, USA) PA5-17646	Rabbit	Alexa 488	1:500	Chicken-Anti-Rabbit
Drebrin	1:1000	MBL (Woburn, MA) D029-3	Mouse	Alexa 568	1:500	Donkey-Anti-Mouse
VGLUT1	1:200	Millipore (Burlington, MA) ab5905	Guinea Pig	Alexa 647	1:500	Goat-Anti-Guinea Pig
PSD95	1:300	Invitrogen (Carlsbad, CA) MA1-045	Mouse	Alexa 568	1:500	Donkey-Anti-Mouse

4.22 | Confocal imaging of spines and synapses

All experiments were randomised and performed by a blinded independent researcher.

Confocal imaging was performed and synaptic puncta as well as dendritic spines were imaged using the IMARIS software. *Z*-Stack images (pixel size 0.4143 μm with a 0.2 μm *Z* step) were acquired with a Nikon A1R Confocal microscope or with EVOS M5000 (60x oil objective, NA 1.50) 16-Stacked images were then compressed together in ImageJ using the *ZProjection* function. Synapse colocalisation of PSD95 and VGLUT1 was analyzed along 50 μm dendrite segments using the NeuronJ and SynapCountJ plugins for imageJ according to Mata et al. (2021). Secondary dendrites were chosen for spine measurements. Dendritic 'spines' were defined as dendritic protrusions at roughly right angles from the dendrite and had no further branches and were distinct from dendritic branches or growth cones. Dendritic spine marker Drebrin was used for immunostaining. For dendritic spine analysis, *Z*-Stack images (pixel size 0.1 μm with a 0.1 μm *Z* Step) were acquired with a Zeiss Observer Z1 fluorescent microscope with ApoTome (63x oil objective, NA 1.40). A 10-Stacked images were then compressed together in ImageJ using the *ZProjection* function. All three-color channels were then merged together into a flattened image. A total of 50 μm dendrite segments were selected from soma were selected and measured for spine analysis using ImageJ. All the segments selected were randomised from three separate experiments.

4.23 | Preparation of serially diluted haemolysed controls

Blood from a healthy volunteer was drawn into a K2 EDTA tube. A stock solution of haemolysis controls was made by adding 0.2 ml of whole blood from a K2 EDTA tube into 10 ml of distilled water to lyse the blood cells. PBS was added to the stock solution to generate serial dilutions of this sample.

4.24 | Assessment of the degree of haemolysis

Blood plasma samples were visually inspected, and the haemolysis score was determined as follows: 0, no sign of haemolysis; 1, slight haemolysis that cannot be ruled out due to dark yellow discolouring; 2, haemolysis is strongly suspected by orange to pink discoloring; 3, evident haemolysis with dark pink to red discolouring. Absorbance of plasma samples was measured at 560, 576 and 592 nm by spectrophotometry (Infinite M200 PRO, Tecan, Ma¨nnedorf, Switzerland), and the degree of haemolysis was determined by the following formula: estimated haemoglobin level = 2*OD576 nm–OD560 nm–OD592 nm (Cripps, 1968).

4.25 | Statistical analysis

Data was analyzed with GraphPad Prism software using unpaired two-tailed Student's t or one-way ANOVA or two-way ANOVA test where required. For synapse and spine analysis, box and whisker plots were made to include distribution variability. Error

bars in figures indicate ± SEM. A p value < 0.05 was considered statistically significant; $^{*}p < 0.05$, $^{**}p < 0.005$, $^{***}p < 0.001$ and $^{****}p < 0.0001$.

ACKNOWLEDGEMENTS

The authors thank Tom Barger and Nicolas Conoan with excellent technical assistance with TEM analysis. This study is supported by NIDA grants R01DA042379, R21DA046855 awarded to SVY and R01DA046852 awarded to GP and SVY.

CONFLICT OF INTEREST

The authors declare no competing interests.

AUTHORS' CONTRIBUTIONS

Subhash Chand, Austin Gowen, Dalia Moore, Alexander Clark, Wendy Huynh, Niming Wu, Lucas Weyrich and Katherine Odegaard performed experiments, collected data and are responsible for data analysis. Rick A. Bevins and Gurudutt Pendyala contributed to rat self-administration experiments. Howard S. Fox provided the resources for the Rhesus Macaque study. Sowmya V. Yelamanchili conceptualized, supervised, designed, interpreted and wrote the manuscript.

REFERENCES

Admyre, C., Grunewald, J., Thyberg, J., Gripenbäck, S., Tornling, G., Eklund, A., Scheynius, A., & Gabrielsson, S. (2003). Exosomes with major histocompatibility complex class II and co-stimulatory molecules are present in human BAL fluid. *European Respiratory Journal*, *22*, 578–583. https://doi.org/10.1183/09031936.03.00041703

Admyre, C., Johansson, S. M., Qazi, K. R., Filén, J.-J., Lahesmaa, R., Norman, M., Neve, E. P. A., Scheynius, A., & Gabrielsson, S. (2007). Exosomes with immune modulatory features are present in human breast milk. *Journal of Immunology*, *179*, 1969–1978. https://doi.org/10.4049/jimmunol.179.3.1969

Alexander, R. P., Balaj, L., Filant, J., Nejad, P., Paul, A., Simonson, B., Srinivasan, S., Zhang, X., Breakefield, X. O., Das, S., Gandhi, R., Laurent, L. C., & Sood, A. K. (2021). Isolation of exosomal RNA from serum or plasma using the Qiagen ExoRNeasy Midi kit. *Protocol Exchange*. https://doi.org/10.1038/protex.2017.073

Anders, S., & Huber, W. (2010). Differential expression analysis for sequence count data. *Genome Biology*, *11*, R106. https://doi.org/10.1186/gb-2010-11-10-r106

Aron, J. L., & Paulus, M. P. (2007). Location, location: using functional magnetic resonance imaging to pinpoint brain differences relevant to stimulant use. *Addiction*, *102*(1), 33–43. https://doi.org/10.1111/j.1360-0443.2006.01778.x

Astarita, G., Avanesian, A., Grimaldi, B., Realini, N., Justinova, Z., Panlilio, L. V., Basit, A., Goldberg, S. R., & Piomelli, D. (2015). Methamphetamine accelerates cellular senescence through stimulation of de novo ceramide biosynthesis. *PLoS ONE*, *10*, e0116961. https://doi.org/10.1371/journal.pone.0116961

Athauda, D., Gulyani, S., Karnati, H. K., Li, Y., Tweedie, D., Mustapic, M., Chawla, S., Chowdhury, K., Skene, S. S., Greig, N. H., Kapogiannis, D., & Foltynie, T. (2019). Utility of neuronal-derived exosomes to examine molecular mechanisms that affect motor function in patients with Parkinson disease: A secondary analysis of the Exenatide-PD trial. *JAMA Neurology*, *76*, 420–429. https://doi.org/10.1001/jamaneurol.2018.4304

Baietti, M. F., Zhang, Z., Mortier, E., Melchior, A., Degeest, G., Geeraerts, A., Ivarsson, Y., Depoortere, F., Coomans, C., Vermeiren, E., Zimmermann, P., & David, G. (2012). Syndecan-syntenin-ALIX regulates the biogenesis of exosomes. *Nature Cell Biology*, *14*, 677–685. https://doi.org/10.1038/ncb2502

Baldi, P., & Long, A. D. (2001). A Bayesian framework for the analysis of microarray expression data: Regularized t-test and statistical inferences of gene changes. *Bioinformatics*, *17*, 509–519.

Beardsley, P. M., Shelton, K. L., Hendrick, E., & Johnson, K. W. (2010). The glial cell modulator and phosphodiesterase inhibitor, AV411 (ibudilast), attenuates prime- and stress-induced methamphetamine relapse. *European Journal of Pharmacology*, *637*, 102–108. https://doi.org/10.1016/j.ejphar.2010.04.010

Beaudoin, G. M. J., Lee, S.-H., Singh, D., Yuan, Y., Ng, Yu-G, Reichardt, L. F., & Arikkath, J. (2012). Culturing pyramidal neurons from the early postnatal mouse hippocampus and cortex. *Nature Protocols*, *7*, 1741–1754. https://doi.org/10.1038/nprot.2012.099

Bosch, P. J., Peng, L., & Kivell, B. M. (2015). Proteomics analysis of dorsal striatum reveals changes in synaptosomal proteins following methamphetamine self-administration in rats. *PLoS ONE*, *10*, e0139829. https://doi.org/10.1371/journal.pone.0139829

Caby, M.-P., Lankar, D., Vincendeau-Scherrer, C., Raposo, G., & Bonnerot, C. (2005). Exosomal-like vesicles are present in human blood plasma. *International Immunology*, *17*, 879–887. https://doi.org/10.1093/intimm/dxh267

Chand, S., Jo, A., Vellichirammal, N. N., Gowen, A., Guda, C., Schaal, V., Odegaard, K., Lee, H., Pendyala, G., & Yelamanchili, S. V. (2020). Comprehensive characterization of nanosized extracellular vesicles from central and peripheral organs: Implications for preclinical and clinical applications. *ACS Applied Nano Materials*, *3*, 8906–8919. https://doi.org/10.1021/acsanm.0c01654

Charntikov, S., Pittenger, S. T., Thapa, I., Bastola, D. R., Bevins, R. A., & Pendyala, G. (2015). Ibudilast reverses the decrease in the synaptic signaling protein phosphatidylethanolamine-binding protein 1 (PEBP1) produced by chronic methamphetamine intake in rats. *Drug and Alcohol Dependence*, *152*, 15–23. https://doi.org/10.1016/j.drugalcdep.2015.04.012

Chaudhuri, A. D., Yelamanchili, S. V., & Fox, H. S.(2013). Combined fluorescent in situ hybridization for detection of microRNAs and immunofluorescent labeling for cell-type markers. *Frontiers in Cellular Neuroscience*, *7*, 160. https://doi.org/10.3389/fncel.2013.00160

Chen, Y., Wang, H., Ying, Z., & Gao, Q. (2020). Ibudilast enhances the clearance of SOD1 and TDP-43 aggregates through TFEB-mediated autophagy and lysosomal biogenesis: The new molecular mechanism of ibudilast and its implication for neuroprotective therapy. *Biochemical and Biophysical Research Communications*, *526*, 231–238. https://doi.org/10.1016/j.bbrc.2020.03.051

Clanchy, F. I. L., & Williams, R. O. (2019). Ibudilast inhibits chemokine expression in rheumatoid arthritis synovial fibroblasts and exhibits immunomodulatory activity in experimental arthritis. *Arthritis & Rheumatology*, *71*, 703–711. https://doi.org/10.1002/art.40787

Colombo, M., Moita, C., Van Niel, G., Kowal, J., Vigneron, J., Benaroch, P., Manel, N., Moita, L. F., Théry, C., & Raposo, G. (2013). Analysis of ESCRT functions in exosome biogenesis, composition and secretion highlights the heterogeneity of extracellular vesicles. *Journal of Cell Science*, *126*, 5553–5565. https://doi.org/10.1242/jcs.128868

Console, L., Scalise, M., & Indiveri, C. (2019). Exosomes in inflammation and role as biomarkers. *Clinica Chimica Acta*, *488*, 165–171. https://doi.org/10.1016/j.cca.2018.11.009

Cripps, C. M. (1968). Rapid method for the estimation of plasma haemoglobin levels. *Journal of Clinical Pathology*, *21*, 110–112. https://doi.org/10.1136/jcp.21.1.110

Cubells, Jf, Rayport, S., Rajendran, G., & Sulzer, D. (1994). Methamphetamine neurotoxicity involves vacuolation of endocytic organelles and dopamine-dependent intracellular oxidative stress. *Journal of Neuroscience*, *14*, 2260–2271.

Ellwanger, J. H., Veit, T. D., & Chies, J. A. B. (2017). Exosomes in HIV infection: A review and critical look. *Infection, Genetics and Evolution*, *53*, 146–154. https://doi.org/10.1016/j.meegid.2017.05.021

Fabbri, M., Paone, A., Calore, F., Galli, R., & Croce, C. M. (2013). A new role for microRNAs, as ligands of Toll-like receptors. *RNA Biology*, *10*, 169–174. https://doi.org/10.4161/rna.23144

Fabbri, M., Paone, A., Calore, F., Galli, R., Gaudio, E., Santhanam, R., Lovat, F., Fadda, P., Mao, C., Nuovo, G. J., Zanesi, N., Crawford, M., Ozer, G. H., Wernicke, D., Alder, H., Caligiuri, M. A., Nana-Sinkam, P., Perrotti, D., & Croce, C. M. (2012). MicroRNAs bind to Toll-like receptors to induce prometastatic inflammatory response. *PNAS*, *109*, E2110–E2116. https://doi.org/10.1073/pnas.1209414109

Fang, H., Ang, B., Xu, X., Huang, X., Wu, Y., Sun, Y., Wang, W., Li, N., Cao, X., & Wan, T. (2014). TLR4 is essential for dendritic cell activation and anti-tumor T-cell response enhancement by DAMPs released from chemically stressed cancer cells. *Cellular & Molecular Immunology*, *11*, 150–159. https://doi.org/10.1038/cmi.2013.59

Fantegrossi, W. E., Ciullo, J. R., Wakabayashi, K. T., De La Garza, R., Traynor, J. R., & Woods, J. H. (2008). A comparison of the physiological, behavioral, neurochemical and microglial effects of methamphetamine and 3,4-methylenedioxymethamphetamine in the mouse. *Neuroscience*, *151*, 533–543. https://doi.org/10.1016/j.neuroscience.2007.11.007

Faure, J. J., Hattingh, S. M., Stein, D. J., & Daniels, W. M. (2009). Proteomic analysis reveals differentially expressed proteins in the rat frontal cortex after methamphetamine treatment. *Metabolic Brain Disease*, *24*(4), 685–700. https://doi.org/10.1007/s11011-009-9167-0

Faure, J., Lachenal, G., Court, M., Hirrlinger, J., Chatellard-Causse, C., Blot, B., Grange, J., Schoehn, G., Goldberg, Y., Boyer, V., Kirchhoff, F., Raposo, G., Garin, J., & Sadoul, R. (2006). Exosomes are released by cultured cortical neurones. *Molecular and Cellular Neuroscience*, *31*, 642–648. S1044-7431(05)00302-7 [pii] https://doi.org/10.1016/j.mcn.2005.12.003

Fiedler, S. E., George, J. D., Love, H. N., Kim, E., Spain, R., Bourdette, D., & Salinthone, S. (2017). Analysis of IL-6, IL-1beta and TNF-alpha production in monocytes isolated from multiple sclerosis patients treated with disease modifying drugs. *Journal of Systems and Integrative Neuroscience*, *3*. https://doi.org/10.15761/JSIN.1000166

Frenette, G., Girouard, J., D'amours, O., Allard, N., Tessier, L., & Sullivan, R. (2010). Characterization of two distinct populations of epididymosomes collected in the intraluminal compartment of the bovine cauda epididymis. *Biology of Reproduction*, *83*, 473–480. https://doi.org/10.1095/biolreprod.109.082438

Ge, Q., Zhou, Y., Lu, J., Bai, Y., Xie, X., & Lu, Z. (2014). miRNA in plasma exosome is stable under different storage conditions. *Molecules (Basel, Switzerland)*, *19*, 1568–1575. https://doi.org/10.3390/molecules19021568

Goetzl, E. J., Kapogiannis, D., Schwartz, J. B., Lobach, I. V., Goetzl, L., Abner, E. L., Jicha, G. A., Karydas, A. M., Boxer, A., & Miller, B. L. (2016). Decreased synaptic proteins in neuronal exosomes of frontotemporal dementia and Alzheimer's disease. *Faseb Journal*, *30*, 4141–4148. https://doi.org/10.1096/fj.201600816R

Goetzl, E. J., Ledreux, A., Granholm, A.-C., Elahi, F. M., Goetzl, L., Hiramoto, J., & Kapogiannis, D. (2019). Neuron-derived exosome proteins may contribute to progression from repetitive mild traumatic brain injuries to chronic traumatic encephalopathy. *Frontiers in Neuroscience*, *13*, 452. https://doi.org/10.3389/fnins.2019.00452

Goetzl, E. J., Peltz, C. B., Mustapic, M., Kapogiannis, D., & Yaffe, K. (2019). Neuron-derived plasma exosome proteins after remote traumatic brain injury. *Journal of Neurotrauma*, 382–388. https://doi.org/10.1089/neu.2019.6711

Goetzl, E. J., Schwartz, J. B., Abner, E. L., Jicha, G. A., & Kapogiannis, D. (2018). High complement levels in astrocyte-derived exosomes of Alzheimer disease. *Annals of Neurology*, *83*, 544–552. https://doi.org/10.1002/ana.25172

Grant, K. M., Levan, T. D., Wells, S. M., Li, M., Stoltenberg, S. F., Gendelman, H. E., Carlo, G., & Bevins, R. A. (2012). Methamphetamine-associated psychosis. *Journal of Neuroimmune Pharmacology*, *7*, 113–139. https://doi.org/10.1007/s11481-011-9288-1

Groot, M., & Lee, H. (2020). Sorting mechanisms for MicroRNAs into extracellular vesicles and their associated diseases. *Cells*, *9*, 1044. https://doi.org/10.3390/cells9041044

Guo, L., & Guo, N. (2015). Exosomes: Potent regulators of tumor malignancy and potential bio-tools in clinical application. *Critical Reviews in Oncology/Hematology*, *95*, 346–358. https://doi.org/10.1016/j.critrevonc.2015.04.002

Gupta, A., & Pulliam, L. (2014). Exosomes as mediators of neuroinflammation. *Journal of Neuroinflammation*, *11*, 68. 10.1186/1742-2094-11-68

Harrison, E. B., Hochfelder, C. G., Lamberty, B. G., Meays, B. M., Morsey, B. M., Kelso, M. L., Fox, H. S., & Yelamanchili, S. V. (2016). Traumatic brain injury increases levels of miR-21 in extracellular vesicles: implications for neuroinflammation. *FEBS Open Bio*, *6*, 835–846. https://doi.org/10.1002/2211-5463.12092

Hu, G., Yao, H., Chaudhuri, A. D., Duan, M., Yelamanchili, S. V., Wen, H., Cheney, P. D., Fox, H. S., & Buch, S. (2012). Exosome-mediated shuttling of microRNA-29 regulates HIV Tat and morphine-mediated neuronal dysfunction. *Cell Death & Disease*, *3*, e381. https://doi.org/10.1038/cddis.2012.114

Hurwitz, S. N., Cheerathodi, M. R., Nkosi, D., York, S. B., & Meckes, D. G. (2018). Tetraspanin CD63 Bridges autophagic and endosomal processes to regulate exosomal secretion and intracellular signaling of Epstein-Barr virus LMP1. *Journal of Virology*, *92*(5), https://doi.org/10.1128/JVI.01969-17

Iavello, A., Frech, V. S. L., Gai, C., Deregibus, M. C., Quesenberry, P. J., & Camussi, G. (2016). Role of Alix in miRNA packaging during extracellular vesicle biogenesis. *International Journal of Molecular Medicine*, *37*, 958–966. https://doi.org/10.3892/ijmm.2016.2488

Jedynak, J. P., Uslaner, J. M., Esteban, J. A., & Robinson, T. E. (2007). Methamphetamine-induced structural plasticity in the dorsal striatum. *European Journal of Neuroscience*, *25*, 847–853. https://doi.org/10.1111/j.1460-9568.2007.05316.x

Jeppesen, D. K., Fenix, A. M., Franklin, J. L., Higginbotham, J. N., Zhang, Q., Zimmerman, L. J., Liebler, D. C., Ping, J., Liu, Qi, Evans, R., Fissell, W. H., Patton, J. G., Rome, L. H., Burnette, D. T., & Coffey, R. J. (2019). Reassessment of exosome composition. *Cell*, *177*, 428–445.e18 e418. https://doi.org/10.1016/j.cell.2019.02.029

Juan, T., & Fürthauer, M. (2018). Biogenesis and function of ESCRT-dependent extracellular vesicles. *Seminars in Cell & Developmental Biology*, *74*, 66–77. https://doi.org/10.1016/j.semcdb.2017.08.022

Karnati, H. K., Garcia, J. H., Tweedie, D., Becker, R. E., Kapogiannis, D., & Greig, N. H. (2019). Neuronal enriched extracellular vesicle proteins as biomarkers for traumatic brain injury. *Journal of Neurotrauma*, *36*, 975–987. https://doi.org/10.1089/neu.2018.5898

Kayala, M. A., & Baldi, P. (2012). Cyber-T web server: differential analysis of high-throughput data. *Nucleic Acids Research*, *40*, W553–W559. https://doi.org/10.1093/nar/gks420

Kiebala, M., & Maggirwar, S. B. (2011). Ibudilast, a pharmacologic phosphodiesterase inhibitor, prevents human immunodeficiency virus-1 Tat-mediated activation of microglial cells. *PLoS ONE*, *6*, e18633. https://doi.org/10.1371/journal.pone.0018633

Kim, B., Yun, J., & Park, B. (2020). Methamphetamine-induced neuronal damage: Neurotoxicity and neuroinflammation. *Biomolecules and Therapeutics (Seoul)*, *28*, 381–388. https://doi.org/10.4062/biomolther.2020.044

Kodidela, S., Wang, Y., Patters, B. J., Gong, Y., Sinha, N., Ranjit, S., Gerth, K., Haque, S., Cory, T., Mcarthur, C., Kumar, A., Wan, J. Y., & Kumar, S. (2019). Proteomic profiling of exosomes derived from plasma of HIV-infected alcohol drinkers and cigarette smokers. *Journal of Neuroimmune Pharmacology*, *15*(3), 501–519. https://doi.org/10.1007/s11481-019-09853-2

Kohno, M., Link, J., Dennis, L. E., Mccready, H., Huckans, M., Hoffman, W. F., & Loftis, J. M. (2019). Neuroinflammation in addiction: A review of neuroimaging studies and potential immunotherapies. *Pharmacology, Biochemistry and Behavior*, *179*, 34–42. https://doi.org/10.1016/j.pbb.2019.01.007

Kolahdouzan, M., Futhey, N. C., Kieran, N. W., & Healy, L. M. (2019). Novel molecular leads for the prevention of damage and the promotion of repair in neuroimmunological disease. *Frontiers in Immunology*, *10*, 1657. https://doi.org/10.3389/fimmu.2019.01657

Kolb, B., & Gibb, R. (2015). Plasticity in the prefrontal cortex of adult rats. *Frontiers in Cellular Neuroscience*, *9*, 15. https://doi.org/10.3389/fncel.2015.00015

Koul, S., Schaal, V. L., Chand, S., Pittenger, S. T., Nanoth Vellichirammal, N., Kumar, V., Guda, C., Bevins, R. A., Yelamanchili, S. V., & Pendyala, G. (2020). Role of brain derived extracellular vesicles in decoding sex differences associated with nicotine self-administration. *Cells*, *9*, 1883. https://doi.org/10.3390/cells9081883

Kowal, J., Arras, G., Colombo, M., Jouve, M., Morath, J. P., Primdal-Bengtson, B., Dingli, F., Loew, D., Tkach, M., & Théry, C. (2016). Proteomic comparison defines novel markers to characterize heterogeneous populations of extracellular vesicle subtypes. *PNAS*, *113*, E968–E977. https://doi.org/10.1073/pnas.1521230113

Kozomara, A., & Griffiths-Jones, S. (2014). miRBase: Annotating high confidence microRNAs using deep sequencing data. *Nucleic Acids Research*, *42*, D68–D73. https://doi.org/10.1093/nar/gkt1181

Krasnova, I. N., Justinova, Z., & Cadet, J. L. (2016). Methamphetamine addiction: Involvement of CREB and neuroinflammatory signaling pathways. *Psychopharmacology*, *233*, 1945–1962. https://doi.org/10.1007/s00213-016-4235-8

Kumar, V. (2019). Toll-like receptors in the pathogenesis of neuroinflammation. *Journal of Neuroimmunology*, *332*, 16–30. https://doi.org/10.1016/j.jneuroim.2019.03.012

Ladenheim, B., Krasnova, I. N., Deng, X., Oyler, J. M., Polettini, A., Moran, T. H., Huestis, M. A., & Cadet, J. L. (2000). Methamphetamine-induced neurotoxicity is attenuated in transgenic mice with a null mutation for interleukin-6. *Molecular Pharmacology*, *58*, 1247–1256. https://doi.org/10.1124/mol.58.6.1247

Larsen, K. E., Fon, E. A., Hastings, T. G., Edwards, R. H., & Sulzer, D. (2002). Methamphetamine-induced degeneration of dopaminergic neurons involves autophagy and upregulation of dopamine synthesis. *Journal of Neuroscience*, *22*, 8951–8960.

Lavoie, M. J., Card, J. P., & Hastings, T. G. (2004). Microglial activation precedes dopamine terminal pathology in methamphetamine-induced neurotoxicity. *Experimental Neurology*, *187*, 47–57. https://doi.org/10.1016/j.expneurol.2004.01.010

Lehmann, S. M., Krüger, C., Park, B., Derkow, K., Rosenberger, K., Baumgart, J., Trimbuch, T., Eom, G., Hinz, M., Kaul, D., Habbel, P., Kälin, R., Franzoni, E., Rybak, A., Nguyen, D., Veh, R., Ninnemann, O., Peters, O., Nitsch, R., … Lehnardt, S. (2012). An unconventional role for miRNA: let-7 activates Toll-like receptor 7 and causes neurodegeneration. *Nature Neuroscience*, *15*, 827–835. https://doi.org/10.1038/nn.3113

Li, J., Liu, K., Liu, Y., Xu, Y., Zhang, F., Yang, H., Liu, J., Pan, T., Chen, J., Wu, M., Zhou, X., & Yuan, Z. (2013). Exosomes mediate the cell-to-cell transmission of IFN-alpha-induced antiviral activity. *Nature Immunology*, *14*, 793–803. https://doi.org/10.1038/ni.2647

Li, M., Xia, Y., Gu, Y., Zhang, K., Lang, Q., Chen, L., Guan, J., Luo, Z., Chen, H., Li, Y., Li, Q., Li, X., Jiang, A.-A., Shuai, S., Wang, J., Zhu, Q., Zhou, X., Gao, X., & Li, X. (2010). MicroRNAome of porcine pre- and postnatal development. *PLoS ONE*, *5*, e11541. https://doi.org/10.1371/journal.pone.0011541

Liu, H.-Y., Hong, Y.-F., Huang, C.-M., Chen, C.-Y., Huang, T.-N., & Hsueh, Y.-P. (2013). TLR7 negatively regulates dendrite outgrowth through the Myd88-c-Fos-IL-6 pathway. *Journal of Neuroscience*, *33*, 11479–11493. https://doi.org/10.1523/JNEUROSCI.5566-12.2013

Llorente, A., de Marco, M. C., & Alonso, M. A. (2004). Caveolin-1 and MAL are located on prostasomes secreted by the prostate cancer PC-3 cell line. *Journal of Cell Science*, *117*, 5343–5351. https://doi.org/10.1242/jcs.01420

Lopez-Verrilli, M. A., & Court, F. A. (2012). Transfer of vesicles from Schwann cells to axons: A novel mechanism of communication in the peripheral nervous system. *Frontiers in Physiology*, *3*, 205. https://doi.org/10.3389/fphys.2012.00205

Lu, J., & Tsourkas, A. (2011). In K. Shah (Ed.), *Molecular imaging: Methods and protocols* (pp. 77–88). Humana Press.

Madden, L. J., Flynn, C. T., Zandonatti, M. A., May, M., Parsons, L. H., Katner, S. N., Henriksen, S. J., & Fox, H. S. (2005). Modeling human methamphetamine exposure in nonhuman primates: Chronic dosing in the rhesus macaque leads to behavioral and physiological abnormalities. *Neuropsychopharmacology*, *30*, 350–359. https://doi.org/10.1038/sj.npp.1300575

Madison, M. N., Jones, P. H., & Okeoma, C. M. (2015). Exosomes in human semen restrict HIV-1 transmission by vaginal cells and block intravaginal replication of LP-BM5 murine AIDS virus complex. *Virology*, *482*, 189–201. https://doi.org/10.1016/j.virol.2015.03.040

Madison, M. N., Roller, R. J., & Okeoma, C. M. (2014). Human semen contains exosomes with potent anti-HIV-1 activity. *Retrovirology*, *11*, 102. https://doi.org/10.1186/s12977-014-0102-z

Marcondes, M. C. G., Flynn, C., Watry, D. D., Zandonatti, M., & Fox, H. S. (2010). Methamphetamine increases brain viral load and activates natural killer cells in simian immunodeficiency virus-infected monkeys. *American Journal of Pathology*, *177*, 355–361. https://doi.org/10.2353/ajpath.2010.090953

Mata, G., Cuesto, G., Heras, J., Morales, M., Romero, A., Rubio, J. (Eds.), *SynapCountJ: A Validated Tool for Analyzing Synaptic Densities in Neurons2017*; (pp. 41–55) Cham: Springer International Publishing.

Matsuzawa-Ishimoto, Y., Hwang, S., Cadwell, K. (2018). Autophagy and inflammation. *Annual Review of Immunology*, *36*, 73–101. https://doi.org/10.1146/annurev-immunol-042617-053253

Mccann, U. D., Wong, D. F., Yokoi, F., Villemagne, V., Dannals, R. F., & Ricaurte, G. A. (1998). Reduced striatal dopamine transporter density in abstinent methamphetamine and methcathinone users: evidence from positron emission tomography studies with [11C]WIN-35,428. *Journal of Neuroscience*, *18*, 8417–8422.

Meyer, C., Grey, F., Kreklywich, C. N., Andoh, T. F., Tirabassi, R. S., Orloff, S. L., & Streblow, D. N. (2011). Cytomegalovirus microRNA expression is tissue specific and is associated with persistence. *Journal of Virology*, *85*, 378–389. https://doi.org/10.1128/JVI.01900-10

Michaelis, K. A., Norgard, M. A., Levasseur, P. R., Olson, B., Burfeind, K. G., Buenafe, A. C., Zhu, X., Jeng, S., Mcweeney, S. K., & Marks, D. L. (2019). Persistent Toll-like receptor 7 stimulation induces behavioral and molecular innate immune tolerance. *Brain, Behavior, and Immunity*, *82*, 338–353. https://doi.org/10.1016/j.bbi.2019.09.004

Mielcarska, M. B., Bossowska-Nowicka, M., & Toka, F. N. (2020). Cell surface expression of endosomal toll-like receptors-A necessity or a superfluous duplication? *Frontiers in Immunology*, *11*, 620972. https://doi.org/10.3389/fimmu.2020.620972

Miyatake, M., Narita, M., Shibasaki, M., Nakamura, A., & Suzuki, T. (2005). Glutamatergic neurotransmission and protein kinase C play a role in neuron-glia communication during the development of methamphetamine-induced psychological dependence. *European Journal of Neuroscience*, *22*, 1476–1488. https://doi.org/10.1111/j.1460-9568.2005.04325.x

Nash, J. F., & Yamamoto, B. K. (1992). Methamphetamine neurotoxicity and striatal glutamate release: Comparison to 3,4-methylenedioxymethamphetamine. *Brain Research*, *581*, 237–243. https://doi.org/10.1016/0006-8993(92)90713-j

Näslund, T. I., Paquin-Proulx, D., Paredes, P. T., Vallhov, H., Sandberg, J. K., & Gabrielsson, S. (2014). Exosomes from breast milk inhibit HIV-1 infection of dendritic cells and subsequent viral transfer to CD4+ T cells. *Aids*, *28*, 171–180. https://doi.org/10.1097/QAD.0000000000000159

Niu, M., Morsey, B., Lamberty, B. G., Emanuel, K., Yu, F., León-Rivera, R., Berman, J. W., Gaskill, P. J., Matt, S. M., Ciborowski, P. S., & Fox, H. S. (2020). Methamphetamine increases the proportion of SIV-infected Microglia/Macrophages, alters metabolic pathways, and elevates cell death pathways: A single-cell analysis. *Viruses*, *12*, 1297. https://doi.org/10.3390/v12111297

Palanisamy, V., Sharma, S., Deshpande, A., Zhou, H., Gimzewski, J., & Wong, D. T. (2010). Nanostructural and transcriptomic analyses of human saliva derived exosomes. *PLoS ONE*, *5*, e8577. https://doi.org/10.1371/journal.pone.0008577

Park, C.-K., Xu, Z.-Z., Berta, T., Han, Q., Chen, G., Liu, X.-J., & Ji, R.-R. (2014). Extracellular microRNAs activate nociceptor neurons to elicit pain via TLR7 and TRPA1. *Neuron*, *82*, 47–54. https://doi.org/10.1016/j.neuron.2014.02.011

Perez-Gonzalez, R., Gauthier, S. A., Kumar, A., & Levy, E. (2012). The exosome secretory pathway transports amyloid precursor protein carboxyl-terminal fragments from the cell into the brain extracellular space. *Journal of Biological Chemistry*, *287*, 43108–43115. [pii] https://doi.org/10.1074/jbc.M112.404467

Pisitkun, T., Shen, R.-F., & Knepper, M. A. (2004). Identification and proteomic profiling of exosomes in human urine. *PNAS*, *101*, 13368–13373. https://doi.org/10.1073/pnas.0403453101

Potolicchio, I., Carven, G. J., Xu, X., Stipp, C., Riese, R. J., Stern, L. J., & Santambrogio, L. (2005). Proteomic analysis of microglia-derived exosomes: metabolic role of the aminopeptidase CD13 in neuropeptide catabolism. *Journal of Immunology*, *175*, 2237–2243. https://doi.org/10.4049/jimmunol.175.4.2237 [pii]

Prada, I., Furlan, R., Matteoli, M., & Verderio, C. (2013). Classical and unconventional pathways of vesicular release in microglia. *Glia*, *61*, 1003–1017. https://doi.org/10.1002/glia.22497

Pulliam, L., Sun, B., Mustapic, M., Chawla, S., & Kapogiannis, D. (2019). Plasma neuronal exosomes serve as biomarkers of cognitive impairment in HIV infection and Alzheimer's disease. *Journal of Neurovirology*, 702–709. https://doi.org/10.1007/s13365-018-0695-4

Raab-Traub, N., & Dittmer, D. P. (2017). Viral effects on the content and function of extracellular vesicles. *Nature Reviews Microbiology*, *15*, 559–572. https://doi.org/10.1038/nrmicro.2017.60

Ranganathan, P., Ngankeu, A., Zitzer, N. C., Leoncini, P., Yu, X., Casadei, L., Challagundla, K., Reichenbach, D. K., Garman, S., Ruppert, A. S., Volinia, S., Hofstetter, J., Efebera, Y. A., Devine, S. M., Blazar, B. R., Fabbri, M., & Garzon, R. (2017). Serum miR-29a is upregulated in acute graft-versus-host disease and activates dendritic cells through TLR binding. *Journal of Immunology*, *198*, 2500–2512. https://doi.org/10.4049/jimmunol.1601778

Rao, P. S. S., O'connell, K., & Finnerty, T. K. (2018). Potential role of extracellular vesicles in the pathophysiology of drug addiction. *Molecular Neurobiology*, *55*, 6906–6913. https://doi.org/10.1007/s12035-018-0912-4

Renneberg, H., Albrecht, M., Kurek, R., Krause, E., Lottspeich, F., Aumüller, G., & Wilhelm, B. (2001). Identification and characterization of neutral endopeptidase (EC 3. 4. 24. 11) from human prostasomes–localization in prostatic tissue and cell lines. *The Prostate*, *46*(3), 173–183. https://doi.org/10.1002/1097-0045(20010215)46:3⟨173::aid-pros1021⟩3.0.co;2-f

Renneberg, H., Konrad, L., Dammshauser, I., & Seitz, J., & Aumuller, G. (1997). Immunohistochemistry of prostasomes from human semen. *The Prostate*, *30*(2), 98–106. https://doi.org/10.1002/(sici)1097-0045(19970201)30:2⟨98::aid-pros5⟩3.0.co;2-g

Ronquist, G. K., Larsson, A., Stavreus-Evers, A., & Ronquist, G. (2012). Prostasomes are heterogeneous regarding size and appearance but affiliated to one DNA-containing exosome family. *The Prostate*, *72*, 1736–1745. https://doi.org/10.1002/pros.22526

Sacks, S., Ries, R. K., Ziedonis, D. M., & Center for Substance Abuse Treatment. (2005). Substance abuse treatment for persons with co-occurring disorders. *Treatment Improvement Protocol (TIP) Series, No. 42*, *42*.

Sahlén, G. E., Egevad, L., Ahlander, A., Norlén, B. J., Ronquist, G., & Nilsson, B. O. (2002). Ultrastructure of the secretion of prostasomes from benign and malignant epithelial cells in the prostate. *The Prostate*, *53*, 192–199. https://doi.org/10.1002/pros.10126

Salimi, L., Akbari, A., Jabbari, N., Mojarad, B., Vahhabi, A., Szafert, S., Kalashani, S. A., Soraya, H., Nawaz, M., & Rezaie, J. (2020). Synergies in exosomes and autophagy pathways for cellular homeostasis and metastasis of tumor cells. *Cell & Bioscience*, *10*, 64. https://doi.org/10.1186/s13578-020-00426-y

Sandau, U. S., Duggan, E., Shi, X., Smith, S. J., Huckans, M., Schutzer, W. E., Loftis, J. M., Janowsky, A., Nolan, J. P., & Saugstad, J. A. (2020). Methamphetamine use alters human plasma extracellular vesicles and their microRNA cargo: An exploratory study. *Journal of Extracellular Vesicles*, *10*, e12028. https://doi.org/10.1002/jev2.12028

Sander, H., Wallace, S., Plouse, R., Tiwari, S., & Gomes, A. V. (2019). Ponceau S waste: Ponceau S staining for total protein normalization. *Analytical Biochemistry*, *575*, 44–53. https://doi.org/10.1016/j.ab.2019.03.010

Santangelo, L., Giurato, G., Cicchini, C., Montaldo, C., Mancone, C., Tarallo, R., Battistelli, C., Alonzi, T., Weisz, A., & Tripodi, M. (2016). The RNA-binding protein SYNCRIP is a component of the hepatocyte exosomal machinery controlling MicroRNA sorting. *Cell Reports*, *17*, 799–808. https://doi.org/10.1016/j.celrep.2016.09.031

Schwenkgrub, J., Zaremba, M., Joniec-Maciejak, I., Cudna, A., Mirowska-Guzel, D., & Kurkowska-Jastrzębska, I. (2017). The phosphodiesterase inhibitor, ibudilast, attenuates neuroinflammation in the MPTP model of Parkinson's disease. *PLoS ONE*, *12*, e0182019. https://doi.org/10.1371/journal.pone.0182019

Sekine, Y., Minabe, Y., Ouchi, Y., Takei, N., Iyo, M., Nakamura, K., Suzuki, K., Tsukada, H., Okada, H., Yoshikawa, E., Futatsubashi, M., & Mori, N. (2003). Association of dopamine transporter loss in the orbitofrontal and dorsolateral prefrontal cortices with methamphetamine-related psychiatric symptoms. *American Journal of Psychiatry*, *160*, 1699–1701.

Sekine, Y., Ouchi, Y., Sugihara, G., Takei, N., Yoshikawa, E., Nakamura, K., Iwata, Y., Tsuchiya, K. J., Suda, S., Suzuki, K., Kawai, M., Takebayashi, K., Yamamoto, S., Matsuzaki, H., Ueki, T., Mori, N., Gold, M. S., & Cadet, J. L. (2008). Methamphetamine causes microglial activation in the brains of human abusers. *Journal of Neuroscience*, *28*, 5756–5761. https://doi.org/10.1523/JNEUROSCI.1179-08.2008

Shah, A., Silverstein, P. S., Singh, D. P., & Kumar, A. (2012). Involvement of metabotropic glutamate receptor 5, AKT/PI3K signaling and NF-kappaB pathway in methamphetamine-mediated increase in IL-6 and IL-8 expression in astrocytes. *Journal of Neuroinflammation*, *9*, 52. https://doi.org/10.1186/1742-2094-9-52

Shahjin, F., Guda, R. S., Schaal, V. L., Odegaard, K., Clark, A., Gowen, A., Xiao, P., Lisco, S. J., Pendyala, G., & Yelamanchili, S. V. (2019). Brain-derived extracellular vesicle microRNA signatures associated with in utero and postnatal oxycodone exposure. *Cells*, *9*, 21. https://doi.org/10.3390/cells9010021

Shastri, A., Bonifati, D. M. & Kishore, U. (2013). Innate immunity and neuroinflammation. *Mediators of Inflammation*, *2013*, 342931. https://doi.org/10.1155/2013/342931

Shurtleff, M. J., Temoche-Diaz, M. M., Karfilis, K. V., Ri, S., & Schekman, R. (2016). Y-box protein 1 is required to sort microRNAs into exosomes in cells and in a cell-free reaction. *Elife 5*. https://doi.org/10.7554/eLife.19276

Sioud, M. (2005). Induction of inflammatory cytokines and interferon responses by double-stranded and single-stranded siRNAs is sequence-dependent and requires endosomal localization. *Journal of Molecular Biology*, *348*, 1079–1090. https://doi.org/10.1016/j.jmb.2005.03.013

Skibinski, G., Kelly, R. W., & James, K. (1994). Expression of a common secretory granule specific protein as a marker for the extracellular organelles (prostasomes) in human semen. *Fertility and Sterility*, *61*, 755–759. https://doi.org/10.1016/s0015-0282(16)56658-8

Skog, J., Würdinger, T., Van Rijn, S., Meijer, D. H., Gainche, L., Curry, W. T., Carter, B. S., Krichevsky, A. M., & Breakefield, X. O. (2008). Glioblastoma microvesicles transport RNA and proteins that promote tumour growth and provide diagnostic biomarkers. *Nature Cell Biology*, *10*, 1470–1476. https://doi.org/10.1038/ncb1800

Sódar, B. W., Kittel, Á., Pálóczi, K., Vukman, K. V., Osteikoetxea, X., Szabó-Taylor, K., Németh, A., Sperlágh, B., Baranyai, T., Giricz, Z., Wiener, Z., Turiák, L., Drahos, L., Pállinger, É., Vékey, K., Ferdinandy, P., Falus, A., & Buzás, E. I. (2016). Low-density lipoprotein mimics blood plasma-derived exosomes and microvesicles during isolation and detection. *Scientific Reports*, *6*, 24316. https://doi.org/10.1038/srep24316

Sriram, K., Miller, D. B., & O'callaghan, J. P. (2006). Minocycline attenuates microglial activation but fails to mitigate striatal dopaminergic neurotoxicity: role of tumor necrosis factor-alpha. *Journal of Neurochemistry*, *96*, 706–718. https://doi.org/10.1111/j.1471-4159.2005.03566.x

Stephans, S. E., & Yamamoto, B. K. (1994). Methamphetamine-induced neurotoxicity: Roles for glutamate and dopamine efflux. *Synapse*, *17*, 203–209. https://doi.org/10.1002/syn.890170310

Stridsberg, M., Fabiani, R., & Lukinius, A., & Ronquist, G. (1996). Prostasomes are neuroendocrine-like vesicles in human semen. *The Prostate*, *29*, 287–295. https://doi.org/10.1002/(SICI)1097-0045(199611)29:5⟨287::AID-PROS3⟩3.0.CO;2-7

Stuffers, S., Sem Wegner, C., Stenmark, H., Brech, A. (2009). Multivesicular endosome biogenesis in the absence of ESCRTs. *Traffic (Copenhagen, Denmark)*, *10*, 925–937. https://doi.org/10.1111/j.1600-0854.2009.00920.x

Sullivan, R., Saez, F., Girouard, J., & Frenette, G. (2005). Role of exosomes in sperm maturation during the transit along the male reproductive tract. *Blood Cells, Molecules & Diseases*, *35*, 1–10. https://doi.org/10.1016/j.bcmd.2005.03.005

Suzumura, A., Ito, A., & Mizuno, T. (2003). Phosphodiesterase inhibitors suppress IL-12 production with microglia and T helper 1 development. *Multiple Sclerosis*, *9*, 574–578. https://doi.org/10.1191/1352458503ms970oa

Suzumura, A., Ito, A., Yoshikawa, M., & Sawada, M. (1999). Ibudilast suppresses TNFalpha production by glial cells functioning mainly as type III phosphodiesterase inhibitor in the CNS. *Brain Research*, *837*, 203–212. https://doi.org/10.1016/s0006-8993(99)01666-2

Takahashi, R.-U., Prieto-Vila, M., Hironaka, A., & Ochiya, T. (2017). The role of extracellular vesicle microRNAs in cancer biology. *Clinical Chemistry and Laboratory Medicine*, *55*, 648–656. https://doi.org/10.1515/cclm-2016-0708

Tallóczy, Z., Martinez, J., Joset, D., Ray, Y., Gácser, A., Toussi, S., Mizushima, N., Nosanchuk, J., Goldstein, H., Loike, J., Sulzer, D., & Santambrogio, L. (2008). Methamphetamine inhibits antigen processing, presentation, and phagocytosis. *Plos Pathogens*, *4*, e28. https://doi.org/10.1371/journal.ppat.0040028

Taylor, A. R., Robinson, M. B., Gifondorwa, D. J., Tytell, M., & Milligan, C. E. (2007). Regulation of heat shock protein 70 release in astrocytes: Role of signaling kinases. *Developmental Neurobiology*, *67*, 1815–1829. https://doi.org/10.1002/dneu.20559

Temoche-Diaz, M. M., Shurtleff, M. J., Nottingham, R. M., Yao, J., Fadadu, R. P., Lambowitz, A. M., & Schekman, R. (2019). Distinct mechanisms of microRNA sorting into cancer cell-derived extracellular vesicle subtypes. *Elife*, *8*. https://doi.org/10.7554/eLife.47544

Thomas, D. M., & Kuhn, D. M. (2005). MK-801 and dextromethorphan block microglial activation and protect against methamphetamine-induced neurotoxicity. *Brain Research*, *1050*, 190–198. https://doi.org/10.1016/j.brainres.2005.05.049

Thomas, D. M., Dowgiert, J., Geddes, T. J., Francescutti-Verbeem, D., Liu, X., & Kuhn, D. M. (2004). Microglial activation is a pharmacologically specific marker for the neurotoxic amphetamines. *Neuroscience Letters*, *367*, 349–354. https://doi.org/10.1016/j.neulet.2004.06.065

Tosar, J. P., Gambaro, F., Sanguinetti, J., Bonilla, B., Witwer, K. W., & Cayota, A. (2015). Assessment of small RNA sorting into different extracellular fractions revealed by high-throughput sequencing of breast cell lines. *Nucleic Acids Research*, *43*, 5601–5616. https://doi.org/10.1093/nar/gkv432

Trajkovic, K., Hsu, C., Chiantia, S., Rajendran, L., Wenzel, D., Wieland, F., Schwille, P., Brüger, B., & Simons, M. (2008). Ceramide triggers budding of exosome vesicles into multivesicular endosomes. *Science*, *319*, 1244–1247. https://doi.org/10.1126/science.1153124

Treiber, T., Treiber, N., Plessmann, U., Harlander, S., Daiß, J.-L., Eichner, N., Lehmann, G., Schall, K., Urlaub, H., & Meister, G. (2017). A compendium of RNA-binding proteins that regulate MicroRNA biogenesis. *Molecular Cell*, *66*, 270–284.e13 e213. https://doi.org/10.1016/j.molcel.2017.03.014

Tsai, S.-Y., Segovia, J. A., Chang, T.-H., Morris, I. R., Berton, M. T., Tessier, P. A., Tardif, M. R., Cesaro, A., & Bose, S. (2014). DAMP molecule S100A9 acts as a molecular pattern to enhance inflammation during influenza A virus infection: Role of DDX21-TRIF-TLR4-MyD88 pathway. *Plos Pathogens*, *10*, e1003848. https://doi.org/10.1371/journal.ppat.1003848

Valadi, H., Ekström, K., Bossios, A., Sjöstrand, M., Lee, J. J., & Lötvall, J. O. (2007). Exosome-mediated transfer of mRNAs and microRNAs is a novel mechanism of genetic exchange between cells. *Nature Cell Biology*, *9*, 654–659. https://doi.org/10.1038/ncb1596

Vandenbark, A. A., Meza-Romero, R., Benedek, G., & Offner, H. (2019). A novel neurotherapeutic for multiple sclerosis, ischemic injury, methamphetamine addiction, and traumatic brain injury. *Journal of Neuroinflammation*, *16*, 14. https://doi.org/10.1186/s12974-018-1393-0

Villarroya-Beltri, C., Gutiérrez-Vázquez, C., Sánchez-Cabo, F., Pérez-Hernández, D., Vázquez, J., Martin-Cofreces, N., Martinez-Herrera, D. J., Pascual-Montano, A., Mittelbrunn, M., & Sánchez-Madrid, F. (2013). Sumoylated hnRNPA2B1 controls the sorting of miRNAs into exosomes through binding to specific motifs. *Nature Communications*, *4*, 2980. https://doi.org/10.1038/ncomms3980

Vojtech, L., Woo, S., Hughes, S., Levy, C., Ballweber, L., Sauteraud, R. P., Strobl, J., Westerberg, K., Gottardo, R., Tewari, M., & Hladik, F. (2014). Exosomes in human semen carry a distinctive repertoire of small non-coding RNAs with potential regulatory functions. *Nucleic Acids Research*, *42*, 7290–7304. https://doi.org/10.1093/nar/gku347

Volkow, N. D., Chang, L., Wang, G.-J., Fowler, J. S., Ding, Y.-S, Sedler, M., Logan, J., Franceschi, D., Gatley, J., Hitzemann, R., Gifford, A., Wong, C., & Pappas, N. (2001). Low level of brain dopamine D2 receptors in methamphetamine abusers: Association with metabolism in the orbitofrontal cortex. *American Journal of Psychiatry*, *158*, 2015–2021.

Volkow, N. D., Chang, L., Wang, G.-J., Fowler, J. S., Franceschi, D., Sedler, M., Gatley, S. J., Miller, E., Hitzemann, R., Ding, Y.-S., & Logan, J. (2001). Loss of dopamine transporters in methamphetamine abusers recovers with protracted abstinence. *Journal of Neuroscience*, *21*, 9414–9418

Wei, Z., Liu, X., Feng, T., & Chang, Y. (2011). Novel and conserved micrornas in Dalian purple urchin (Strongylocentrotus nudus) identified by next generation sequencing. *International Journal of Biological Sciences*, *7*, 180–192.

Willem, J., ter Beest, M., Scherphof, G.& Hoekstra, D.(1990). A non-exchangeable fluorescent phospholipid analog as a membrane traffic marker of the endocytic pathway. *European Journal of Cell Biology*, *53*, 173–184

Winkler, C. W., Taylor, K. G., & Peterson, K. E. (2014). Location is everything: let-7b microRNA and TLR7 signaling results in a painful TRP. *Science Signaling*, *7*, pe14. https://doi.org/10.1126/scisignal.2005407

Xu, J., Camfield, R., & Gorski, S. M. (2018). The interplay between exosomes and autophagy - partners in crime. *Journal of Cell Science*, *131*. https://doi.org/10.1242/jcs.215210

Yamada, A., Cox, M. A., Gaffney, K. A., Moreland, A., Boland, C. R., & Goel, A. (2014). Technical factors involved in the measurement of circulating microRNA biomarkers for the detection of colorectal neoplasia. *Plos One*, *9*, e112481. https://doi.org/10.1371/journal.pone.0112481

Yamamoto, B. K., Moszczynska, A., & Gudelsky, G. A. (2010). Amphetamine toxicities: Classical and emerging mechanisms. *Annals of the New York Academy of Sciences*, *1187*, 101–121. https://doi.org/10.1111/j.1749-6632.2009.05141.x

Yelamanchili, S. V., Lamberty, B. G., Rennard, D. A., Morsey, B. M., Hochfelder, C. G., Meays, B. M., Levy, E., & Fox, H. S. (2015). MiR-21 in extracellular vesicles leads to neurotoxicity via TLR7 signaling in SIV neurological disease. *Plos Pathogens*, *11*, e1005032. https://doi.org/10.1371/journal.ppat.1005032

You, Y., & Ikezu, T. (2019). Emerging roles of extracellular vesicles in neurodegenerative disorders. *Neurobiology of Disease*, *130*, 104512. https://doi.org/10.1016/j.nbd.2019.104512

Zhang, H., Freitas, D., Kim, H. S., Fabijanic, K., Li, Z., Chen, H., Mark, M. T., Molina, H., Martin, A. B., Bojmar, L., Fang, J., Rampersaud, S., Hoshino, A., Matei, I., Kenific, C. M., Nakajima, M., Mutvei, A. P., Sansone, P., Buehring, W., Wang, H., … Lyden, D. (2018). Identification of distinct nanoparticles and subsets of extracellular vesicles by asymmetric flow field-flow fractionation. *Nature Cell Biology*, *20*, 332–343. https://doi.org/10.1038/s41556-018-0040-4

Zhang, Q., Higginbotham, J. N., Jeppesen, D. K., Yang, Yu-P, Li, W., Mckinley, E. T., Graves-Deal, R., Ping, J., Britain, C. M., Dorsett, K. A., Hartman, C. L., Ford, D. A., Allen, R. M., Vickers, K. C., Liu, Qi, Franklin, J. L., Bellis, S. L., & Coffey, R. J. (2019). Transfer of functional cargo in exomeres. *Cell Reports*, *27*, 940–954.e6 e946. https://doi.org/10.1016/j.celrep.2019.01.009

SUPPORTING INFORMATION

Additional supporting information may be found in the online version of the article at the publisher's website.

How to cite this article: Chand, S., Gowen, A., Savine, M., Moore, D., Clark, A., Huynh, W., Wu, N., Odegaard, K., Weyrich, L., Bevins, R. A., Fox, H. S., Pendyala, G., & Yelamanchili, S. V. (2021). A comprehensive study to delineate the role of an extracellular vesicle-associated microRNA-29a in chronic methamphetamine use disorder. *Journal of Extracellular Vesicles*, *10,* e12177. https://doi.org/10.1002/jev2.12177